Dissecting the mechanism of nuclear restitution in *Arabidopsis* male meiosis

Dissertation

zur Erlangung des

Doktorgrades der Naturwissenschaften (Dr. rer. nat.)

der

Naturwissenschaftlichen Fakultät III

-Agrarwissenschaften-

der Martin-Luther-Universität Halle-Wittenberg

vorgelegt von

Frau Yingrui Ma

Gutachter/Reviewer:

1. Prof. Dr. Andreas Houben (Martin-Luther-Universität Halle-Wittenberg/ Leibniz Institut für Pflanzengentik und Kulturpflanzenforschung (IPK))
2. Prof. Dr. Nico de Storme (KU Leuven)

Chair of the doctorate committee/ Vorsitzender der Promotionskommission:
Prof. Dr. Klaus Pillen

Date of the Disputation/ Tag der Verteidigung: 13. Januar 2025

Acknowledgement

This project was funded by the Deutsche Forschungsgemeinschaft in the facilities of the Leibniz Institute of Plant Genetics and Crop Plant Research in Gatersleben.

First of all, I would like to thank my supervisor Dr. Hua Jiang for offering this opportunity to study and work as a PhD candidate in IPK. From the experience of working with him, I learned more in my scientific career and became firm in my work. He also offered me a chance to monitor master's students, which is also a precious experience in my future career. Great thanks also to my lab members Dr. Ewa Piskorz Dr. Jingping Chen, and Dr. Linhao Xu who have taught me most of the lab skills used in this study. I would like to also acknowledge the contribution of our lab technicians Leane Gottschalk, and master students who once worked with me, Isha Bhansali.

In addition to the daily work, I also got help from different groups in and outside of IPK. I would like to thank Dr. Stephen Heckmann for sharing his lab resources and sincerely giving advice. I would like to thank Dr. Amanda Souza Camara for teaching me Alphafold tools, Dr. Inna Lermontova and her lab for sharing seeds that are important for my experiment, Dr. Saravanakumar Somasundaram (IPK. CSF) for teaching me the Golden Gate cloning method which is crucial to improve my vesicle marker result, Dr. Chao Fen (IPK, ME) and Dr. Stephanie Durand (MPIPZ) for teaching and providing support for my 3D-immunostaining experiment, Dr. Joerg Fuchs for teaching me flow cytometry, and Dr. Maria Cuacos to help me do the live imaging. And also, the PZB group in IPK for sharing their confocal microscope. Supports also come from outside of IPK. Thanks to Dr. Yazhong Wang from Max Planck Institute for Plant Breeding Research to teach me the key points to design CRISPR-CAS9 mutants.

The life of PhD in a non-native environment is full of challenges. I would like to thank Dr. Jiaying Zhu for her mental support as a pioneer in scientific research. The Club team and PhD board as warm communities. And all my friends in IPK for accompanying and exploring new life in Gatersleben. Last but not least, I need to mention Ms. Bianka Jacobi and Dr. Britt Leps, without their support in the administration, I would not be able to start my life and research easily in Gatersleben and process the graduation.

I would like to dedicate all my efforts to my old friends, teachers and families, who gave me endless support throughout my PhD time. Especially when I was depressed, they always showed me the broader world and the positive side of life.

Thank you!

Contents

1. Introduction

1.1 Meiotic cell cycle and gamete development

Meiosis is a unique cell division process for sexual reproduction in plants, fungi, and animals. In the meiotic cell cycle, a single round of DNA replication is followed by two rounds of nuclear division: meiosis I and meiosis II. During meiosis I, homologous chromosomes separate, and ploidy is reduced by half (De Storme & Geelen, 2013a, 2013b). In comparison, meiosis II segregates sister chromatids (De Storme & Geelen, 2013a, 2013b). In general, meiosis I and meiosis II can be further divided into interphase, prophase, metaphase, anaphase, and telophase by the cell cycle events that occur inside.

1.1.1 General Meiosis process

Prophase I is where homologous chromosome pairing, synapsis, and recombination occur (Morgan et al., 2021; Zickler & Kleckner, 2015). Based on different chromosome features, prophase I can be further divided into leptotene, zygotene, pachytene, diplotene, and diakinesis. Chromosome threads first appear at leptotene, followed by chromosome synapsis during zygotene and pachytene. When chromosomes fully synapse, crossovers take place at the end of pachytene. The crossover point, called chiasmata, is important to set up spindle tension for further division and increase genetic diversity for the next generation (Hirose et al., 2011; Ma, 2005). As the synaptonemal complex begins to degrade and homologous chromosomes lose connection except at chiasmata, the cells enter diplotene. Finally, chromosomes condense to form bivalent pairs at diakinesis and are ready for chromosome segregation. At metaphase I, homologous chromosomes connected by chiasmata align at the equational plate. Cohesion along the chromosome arm was removed, while the centromeric cohesion remains until the second division (Wassmann, 2013). This is followed by the segregation of crossover points and the separation of homologous chromosomes at anaphase I (Hughes & Hawley, 2020). Telophase I is the last phase of meiosis I, where chromosomes de-condense and are separated by either a cell plate or organelle band(Brownfield et al., 2015; De Storme & Geelen, 2013a). As a result, meiosis I can reduce the ploidy by half; thus, meiosis I is also called the reductional division.

After meiosis I, chromosomes re-condense, and the nuclear envelope is rebuilt at prophase II. The following steps of meiosis II are similar to mitosis (d'Erfurth et al., 2009). Sister chromatids connected by centromere align at the equatorial plate at

metaphase II (Figure 1C). Sister chromosomes then separate into four directions (Figure 1C). After anaphase, a phragmoplast-like structure consisting of microtubules is formed between the divided nuclei to maintain a proper distance (Brownfield et al., 2015; De Storme & Geelen, 2013a). After the secondary division, chromosomes de-condense to form haploid nuclei. Since the ploidy will not change during the second division, meiosis II is also called the equational division.

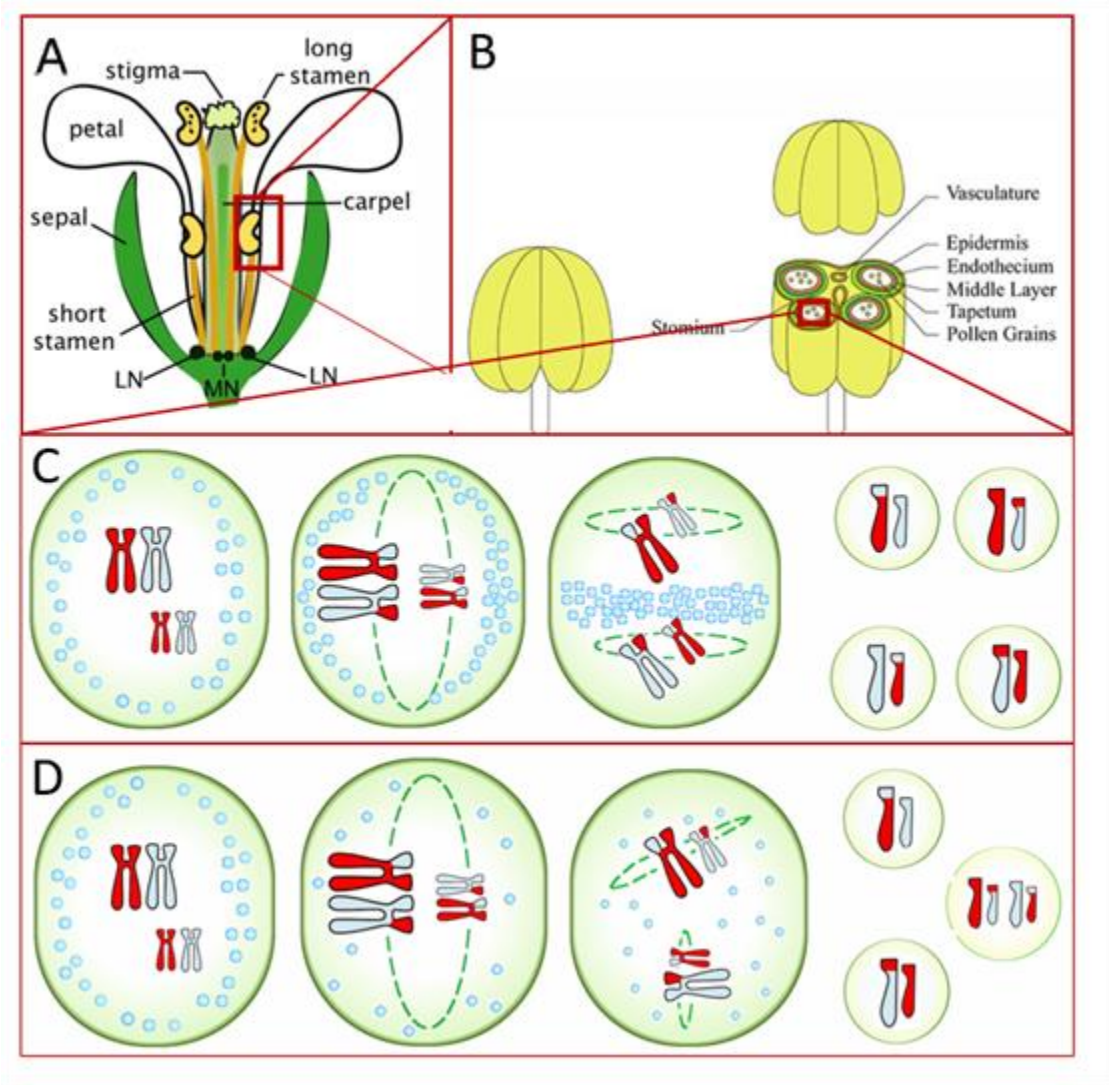

Figure 1. Male gamete development and meiotic cell cycle. A)Arabidopsis flower structure. B) Male meiotic cells in anthers. C) Meiotic cell cycle and organelle band formation in WT. D) Meiotic cell cycle in organelle band disordered mutants jas.

1.1.2 Male and female gamete development

In angiosperms, like *Arabidopsis*, male and female gametes share the same meiotic stages, but the division occurs in different organs, and the divided cells have different cell fates. Female meiosis occurs in ovules, where only one cell in each ovule can undergo meiosis. Male meiosis occurs in anthers (Figure 1A, 1B) (Mauch & Schoenwolf, 2001), with more microspores and ease of manipulation, making them good research material for meiosis study. After the meiotic cell cycle, the products of male and female meiosis have different fates. In female meiosis, only one cell survives, while the other three become polar bodies and degrade(Mauch & Schoenwolf, 2001). The surviving meiocyte undergoes three mitotic divisions and develops into a mature female gametophyte with seven cells (Mauch & Schoenwolf, 2001; Yadegari & Drews, 2004). In contrast, in male meiosis, all four microspores can survive and enter the microspore stage (Figure 1B) (Mauch & Schoenwolf, 2001). During the microspore stage, the four divided nuclei are surrounded by callose and form what is called a tetrad (Mauch & Schoenwolf, 2001). If errors occur during the meiotic cell cycle and nuclei fuse, there are only two or three nuclei in one cell, called dyad or triad respectively (Brownfield et al., 2015; Calvo-Baltanás et al., 2022). The microspore stage cell is commonly used to characterise the meiotic phenotype in this study, as it represents the meiotic products and is relatively easy to observe. After the microspore stage, the four gametes enter mitotic division to form a vegetative and a generative cell. In most plants, the generative cell undergoes mitotic division before or during pollen tube germination, generating two sperm cells (Borg et al., 2009). During fertilisation, organelles from the vegetative cell form the pollen tube which delivers sperm cells to the female gametophyte (Moscatelli & Idilli, 2009; Sato & Maeshima, 2019). The study of the meiotic cell cycle can deeply influence plant breeding technology.

1.2 The reduced and unreduced gametes formation

The most important feature of meiosis is the “reduction of genome size”, where gametes with half ploidy of the mother cell are produced, called reduced gametes. Fertilisation between the male and female reduced gametes can maintain the ploidy stability between generations. The whole process of meiotic division takes around 34 hours. In this period, prophase takes around 30 hours, and the cell division (from metaphase I to telophase II) takes around 3 to 4 hours (Armstrong et al., 2003). Because of the relatively short division time, most of the meiosis errors happened at the division phase.

1.2.1 Nuclear restitution produces unreduced gametes

Unreduced gametes were produced when errors happened during meiotic division. Delicate mechanisms are enrolled in the meiotic division stages to ensure the proper heritage of the chromosome number. The process in which more than one set of chromosomes is divided into one nuclear is called nuclear restitution. Nuclear restitution is a mechanism occurring in the meiotic cell cycle. The First Division Restitution (FDR) always causes errors in homologous segregation, producing unreduced gametes genetically retaining parental heterozygous (De Storme & Geelen, 2013b). The Second Division Restitution (SDR) leads to errors in sister chromatid segregation, producing homozygous chromosomes from the centromere to the first crossover point (De Storme & Geelen, 2013b).

Restitution can be induced by the meiotic error during the first division, second division and cytokinesis. Here are some examples of nuclear restitution (Table 1). One well-studied defect in first division restitution of chromosome division is *switch1* (*swi1*)/*dyad*, a WINGS APART-LIKE antagonist that maintains sister chromatid cohesion (Yang et al., 2019). A mutation of *swi1/dyad* can prevent cohesion degradation at metaphase I, blocking meiosis I chromosome segregation and giving rise to FDR unreduced gametes. Similarly, the mutation of *omission of the second division* (*osd1*) can inhibit the anaphase-promoting factor to promote cell entry into anaphase II, thus causing second-division failure and the production of SDR unreduced gametes(Cromer et al., 2012). These distinct mechanisms produce different types of unreduced gametes: the *swi1/dyad* mutant bypasses meiosis I, producing gametes that remain homogeneity with the pollen mother cell. While the *osd1* mutation skips meiosis II, producing gametes that remain heterogeneous to the pollen mother cell.

Table 1. Examples of nuclear restitution mutants

Function	Name	Species	Reference(s)
FDR	*swi1*/*dyad*	Arabidopsis	(Agashe et al., 2002; Yang et al., 2019)
		Rckcress	(Sezer et al., 2016)
	ago104	Maize	(Singh et al., 2011)
	Jas	Arabidopsis	(Brownfield et al., 2015)
	Ps	Arabidopsis	(d'Erfurth et al., 2008)
		Carnation	(Zhou et al., 2015)
SDR	*osd1*	Arabidopsis	(Cromer et al., 2012)
		rice	(Mieulet et al., 2016; Wang et al., 2019)
	tam1	Tomato	(Wang et al., 2024)
		Arabidopsis	(d'Erfurth et al., 2010)

1.2.2 *jas* induced unreduced gametes

This study focused on the *jason* (*jas*)-*induced* nuclear restitution. In *jas*, Meiotic nuclei can undergo both meiotic divisions, but the divided genetic material that should form future nuclei regrouped before cytokinesis. This process relies on the special process of meiotic division in dicots. Unlike in monocots, where a cell wall forms at the end of meiosis I before the next division occurs, dicots form a structure consisting of organelle vesicles between separated chromosomes to prevent the regrouping of homologous chromosomes (Brownfield et al., 2015; Koc & Storme, 2022)(Figure 1C). Compared to the real cell wall, this vesicle structure is less stable, especially under stress (De Storme & Geelen, 2013a; Wang et al., 2020; Zhou et al., 2015). Consequently, dyads and triads are formed when the organelle band is disordered after the meiotic cell cycle.

The *jason* (*jas*) was reported by Erilova in 2009 through screening the *Arabidopsis* mutants which produced unreduced male gametes (Erilova et al., 2009). *jas* produces unreduced male gametes through first-division restitution, resulting in unreduced pollen grains (De Storme & Geelen 2011). Microscopic analysis revealed that *jas* undergoes both the first and second meiotic divisions. However, because of the precocious disappearance of the organelle band at metaphase II, the homologous chromosomes regroup into one nucleus after the cell cycle (Brownfield et al., 2015) (Figure 2). Consequently, *jas* produces 75% of dyads and triads after meiosis. Fertilization between unreduced male gametes and female gametes results in triploid seeds. This phenotype suggests that *jas* influences male meiosis but not female meiosis (Brownfield et al., 2015). This discrepancy may be due to the asymmetric division of female meiosis (Almonacid et al., 2014; Halet & Carroll, 2007).

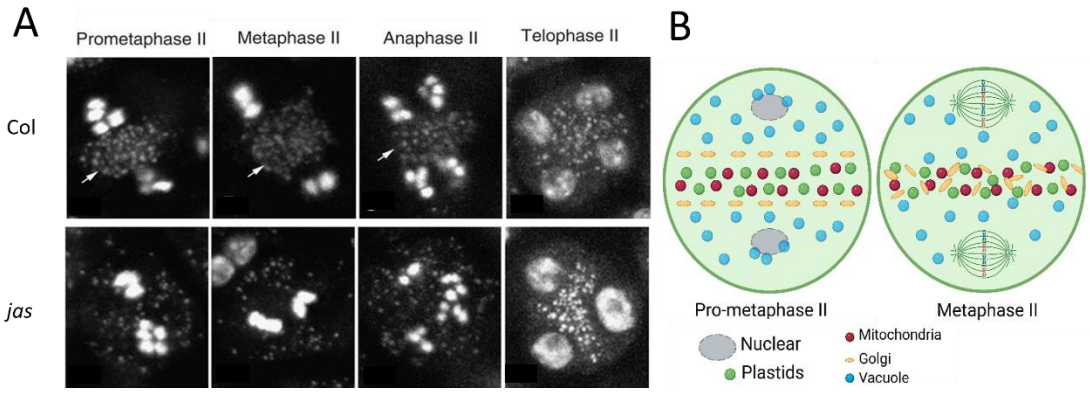

Figure 2. The organization of vesicles during cell division and growth.

A) The assembly and maintenance of organelle bands during male meiosis in WT and *jas* (signal stained by DAPI)(Brownfield et al., 2015)). B) The organization of vesicles derived from different organelles during metaphase II (Koc & Storme, 2022).

Previous studies have tried to understand the mechanism behind the *jas* mutant. By comparing the meiotic cell in WT and *jas*, the major difference was found at metaphase II. The spindle orientation is found to be abnormal in *jas*. Some research attribute the phenotype to the mis-orientated spindles (De Storme & Geelen, 2011; De Storme & Geelen, 2013a, 2013b). Parallel, tripolar and fused spindles occurred in *jas,* and the misoriented spindle will lead to abnormal phragmoplast in telophase II. However, the abnormal spindles continue to increase at metaphase II. At the beginning of metaphase II, there is nearly no abnormal meiosis, but at the end of metaphase II, around 80% of cells showed abnormal spindles (Figure 3).

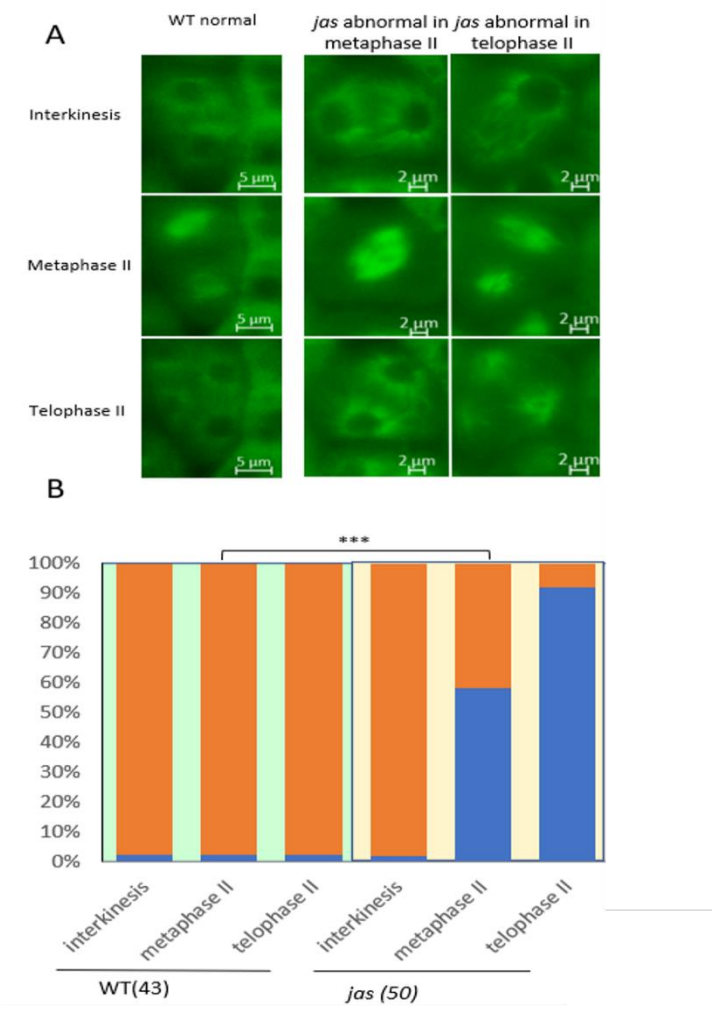

Figure 3. Spindle misorientation during metaphase II is gradually enhanced in *jas* (original data from Piskorz et al., 2022).

A) The spindle dynamics at the prometaphase II, metaphase II and anaphase II. B) The percentage of spindle position abnormality was gradually increased in the *jas* phenotype. The yellow color represents the cell with normal spindles, and the blue color represents the cell with abnormal spindles.

Meanwhile, the phragmoplasts do not show any difference between WT and *jas*, suggesting that the organization of microtubules is normal, but the regulation of spindle location is different. Spindle location and orientation were regulated by the microtubule organization centre (MTOC) in plants, animals, and fungi. In animals, fungi, and lower plants, the centrosome or spindle pole body was formed to organise spindle location and orientation (Nabais et al., 2020; Sanchez & Feldman, 2017). But higher plants don't have such structure (Lüders & Stearns, 2007). The cell wall or organelle band should be partially involved in spindle positioning and orientation. Previous studies also found that the *jas* mutation disrupts the organelle band. Therefore, the organelle band can also perform an important role in separating spindles and maintaining chromosome distance during meiosis II. However, our understanding of this process is limited. How this restitution process occurs and its significance in terms of this special mechanism remains a mystery.

1.3 The organelle band in plant meiosis

The organelle band is a specialized structure unique to metaphase II in dicotyledonous plants. The organelle band is considered a physical barrier between the divided chromosomes during simultaneous cytokinesis (Figure 2A). One piece of evidence is that the organelle band disorder mutant *jas* exhibits chromosome restitution and produces unreduced gametes (Figure 2A). The organelle band is a relatively variable structure. It is also recognized as a precursor of the cell plate (Brown et al., 1996; Brownfield et al., 2015). Unfortunately, the organelle band during meiosis is very less studied. Since the organelle band is recognized as a precursor of the cell wall, some common knowledge from cell wall formation in cytokinesis potential can be used to explain the basis of the organelle band structure.

1.3.1 Organelle band consists of endomembrane vesicles.

Within plant cells, various organelles, including mitochondria, endoplasmic reticulum, the Golgi apparatus, lysosomes, vacuoles, peroxisomes, and plastids, collaborate to execute essential cellular functions. Smooth trafficking between these organelles is a prerequisite for quick and diverse responses under different conditions. Endomembrane trafficking is essential for the transport of proteins and other macromolecules both inside and outside of the cell. In plant cells, there are three major pathways of endomembrane trafficking: (i) the biosynthetic secretory pathway, (ii) the endocytic pathway. (iii) the vacuole transport pathway or sorting pathway (Figure 4).

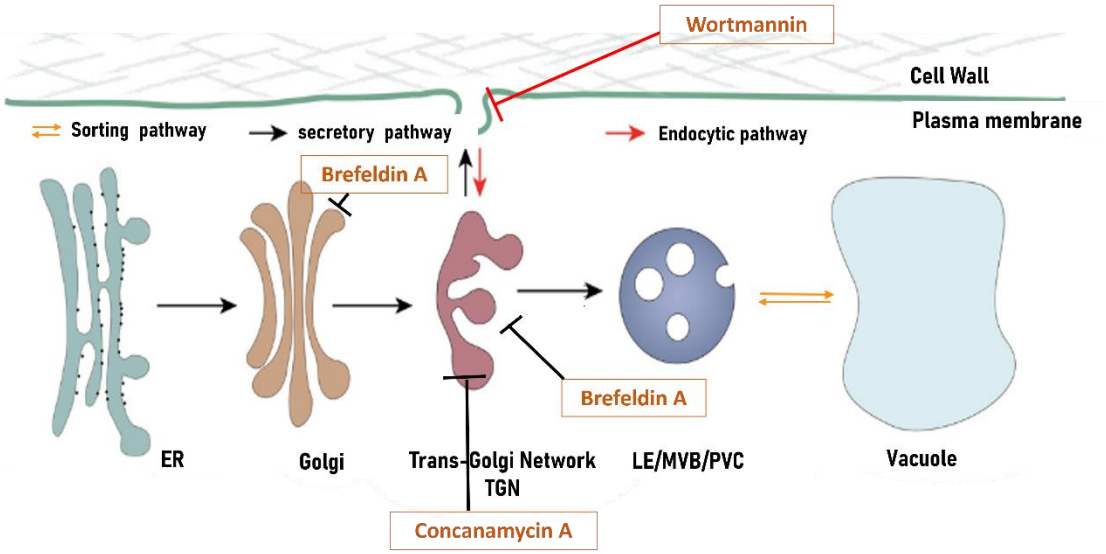

Figure 4. The vesicle trafficking pathways and their specific inhibitors.

The secretory pathway (exocytic), endocytic pathway, and the vacuolar transport pathway (sorting pathway) are showed here. The corresponding vesicle trafficking inhibitors are also showed in the image.

The secretory pathway

The secretory pathway transfers newly synthesized proteins from the endoplasmic reticulum (ER) through the Golgi apparatus and finally to the plasma membrane or the extracellular space (Figure 4). In the secretory pathway, previous research has mainly focused on two steps: ER–Golgi trafficking and post-Golgi trafficking.

ER–Golgi trafficking is the most well-studied step. Key proteins like COPI and COPII have been identified. COPII proteins identify the ER exit sites and mediate ER to Golgi trafficking with the help of the tubulin network (Weigel et al., 2021). COPI mediates Golgi to ER trafficking, controlling the quality of the biosynthesized product (Arakel & Schwappach, 2018). Brefeldin A (BFA) inhibits the GDP/GTP exchange reaction on adenosine ribosylation factors (ARFs), thus preventing the association of COPI vesicles (Bonifacino & Jackson, 2003; Zeeh et al., 2006). BFA treatment can inhibit protein trafficking from the ER to the Golgi complex (Figure 4), and generate a fragmented Golgi structure.

The post-Golgi trafficking is essentially for cell division. The Trans-Golgi Network (TGN) acts as a sorting hub for post-Golgi trafficking. The TGN can deliver vesicles to the plasma membrane (for secretion) or the vacuole (for degradation and reuse) in non-division cells. In mitotic cells, the TGN can deliver vesicles to the cell plate during

cytokinesis and form the new cell wall (Van Damme & Geelen, 2008). Concanamycin A can inhibit vesicle trafficking exiting from the TGN and inhibit both the secretory and endocytic pathways (Reichardt et al., 2007).

The endocytic pathways

The endocytic pathways can internalize protein or other biochemical factors from the plasma membrane to organelles. In plants, clathrin-dependent pathway is the most well-studied model (Aniento et al., 2021), where endocytic accessory proteins, like Adaptor Protein complex-2 (AP-2), bind phosphatidylinositol kinesis to initiate the endocytosis pathways. Wortmannin can inhibit phosphatidylinositol 3-kinase (PI3K) family proteins (Leshem et al., 2007). PI3K is required for macroautophagy, whereas the product of PI3K, Phosphatidylinositol 3-phosphate (PI3P), is required for vesicle trafficking to the late endosome (Leshem et al., 2007)(Figure 4). External materials are imported into the cell through membrane-coated endosomes (Boucrot & Kirchhausen, 2007; Gautreau et al., 2014). Endosomes can either be recruited to the TGN or targeted to the vacuole for delivering material to the required organelle (Gautreau et al., 2014). Endosome enters TGN delivers the material to the TGN, and then transfers through the secretory pathways (Gautreau et al., 2014). The endosome fussed with vacuoles can be delivered to other organelles through the sorting pathway (Boucrot & Kirchhausen, 2007; Gautreau et al., 2014).

The vacuolar transport pathway (sorting pathway)

The vacuolar transport pathway is similar to the secretory pathway but involves further sorting to endosomes and vacuoles. Vacuole is the starch storage organelle, and starch is the most important material to build the cell wall (Noguchi, 2014). In the mitotic cell cycle, this pathway delivers biosynthesized materials to build up the new cell wall, suggesting that it is potentially related to *de novo* cell well formation (Noguchi, 2014). The vacuolar transport pathway cross-talks with the other two vesicle trafficking pathways (Frémont & Echard, 2018; Šamaj et al., 2006; Shintani et al., 2002). The major feature of this pathway is the involvement of the vacuole (Figure 4). Up to four pathways delivering vesicles to vacuoles have been reported (Frémont & Echard, 2018; Shintani et al., 2002). Due to the complexity of this pathway in different tissues and stages, it is still not very clear which vesicles are sorted and recruited to where. Another interesting point is that in plant cytokinesis, vesicle trafficking to the new cell wall is not classified into vacuolar transport pathways, but predominantly included in secretory pathways (Frémont & Echard, 2018).

1.3.2 Vesicle trafficking during cytokinesis

During plant cell cytokinesis, a microtubule and actin-based structure known as the phragmoplast is assembled and acts as a path for trafficking vesicles to the cell plate (De Storme & Geelen, 2013a). Vesicles derived from the Golgi apparatus and other organelles can transfer through the cytoskeleton path to the mid-zone of the cell. These vesicles originate predominantly from the secretory pathway and partially from the endocytic pathway, as the spatial localization of the Golgi apparatus is close to the phragmoplast during telophase (De Storme & Geelen, 2013a; Neto et al., 2011). Many of the post-Golgi trafficking proteins mentioned above are also involved in cytokinesis (Jürgens, 2004). Accordingly, cell plate formation is sensitive to BFA treatment.

The organelle band acts as a precursor of the cell plate and could be potentially regulated by pathways similar to those in the mitotic cell cycle (Brown et al., 1996; Brownfield et al., 2015). While there are still differences between the cell wall in mitosis and the organelle band in meiosis. In mitosis, once the vesicles are delivered and fused at the cell wall area, vesicles stay at the mid-zone and form the new cell well from the middle to the peripheral. However, the organelle band is a highly dynamic structure. After the first meiotic division, the vesicles comprising the organelle band redistribute during the secondary division. And disruption of organelle band remains a small proportion of cells undergo the meiotic cell cycle normally (Brownfield et al., 2015). The organelle band provides more flexibility for plants.

1.3.3 Dynamics of organelles during plant meiosis

Compared to the study of chromosome behaviour and cytoskeleton organization during mitosis, the study of organelles during the meiotic cell cycle is relatively limited. However, organelles play crucial roles and interact during meiotic division. In meiosis I, vesicles gather around the spindle and provide ATP for the high-energy demanding processes of spindle formation and chromosome segregation (Fan & Li, 2001; Koc & Storme, 2022). After metaphase I, organelles move towards the midzone to form the organelle band, which contains plastids, the Golgi apparatus, mitochondria, and other small organelles (Figure 2).

Following telophase I and before meiosis II, organelles are grouped and ordered linearly (Koc & Storme, 2022). This linear ordering is quickly disturbed before metaphase II, likely due to cytoplasmic streaming resulting from the biogenesis and activity of the spindles (Koc & Storme, 2022)(Figure 2B). The distinct organelle band is maintained at the central midzone until telophase II. After cytokinesis, all types of

organelles are released from the central organelle band and repositioned in the daughter cells. In mitosis, the precursor of the cell wall is only present from prometaphase to anaphase and does not need to be maintained as long as in meiosis (Brownfield et al., 2015; Jürgens, 2004; Sinclair et al., 2022). Therefore, researchers are only concerned about the establishment and recruitment of organelles in mitosis but not maintaining the position of organelles.

The meiotic mutant *jas* shows a clear, linearly ordered organelle band until prophase II, but this structure is quickly disrupted, leading to the inability to maintain the organelle band and resulting in the restitution of divided nuclei. Observing the organelle band from telophase I to prophase II in *jas* showed that the organelle band does not show any difference with wild type (Brownfield et al., 2015), suggesting that the establishment of the organelle band at telophase I and the maintenance of the organelle band at metaphase II are two different processes. The study of JAS-related pathways reveals the mechanism of organelle band maintenance during meiosis II.

1.4 Cytoskeleton dynamic during cell division

In monocotyledonous plants, meiosis after the first division can build up a cell plate between separated chromatids. However, two rounds of cytokinesis occur simultaneously at the end of meiosis II in dicotyledonous plants. The establishment of the cell wall in cytokinesis and the maintenance of the organelle band at metaphase II are interconnected but separate processes. Previous research on vesicle trafficking during cytokinesis suggests that cytoskeletal structures, such as spindle microtubules and actin filaments, serve as the "path" for trafficking vesicles (Khoso et al., 2023; Kim et al., 2005).

1.4.1 Microtubule function during cytokinesis

Chromosome segregation is orchestrated by the dynamics of spindle microtubules during cell cycle progression. Microtubules are polar polymers consisting of α and β tubulin dimers. The dynamic instability of microtubules, where α and β tubulin dimers polymerize at the plus end and depolymerize at the minus end, plays a crucial role in this process (Mitchison & Kirschner, 1984). When the spindle attaches to the condensed chromosomes, the phragmoplast structure forms. In the phragmoplast, microtubules have their plus end at the chromosome and the minus end at both poles, which are attached to the chromosome and pull into two poles. Correct chromosome segregation depends on the bipolar orientation of the spindle and the dynamic instability of microtubules (Gregan et al., 2011). The assembly of phragmoplast from

anaphase to telophase guides the vesicles that transfer the material to build the cell wall to the mid-zone in the mitotic cell cycle (Khoso et al., 2023; Weigel et al., 2021). There are very less studies about the microtubule organization in the meiotic cell cycle. There is some discussion of whether phragmoplast still exists. The phragmoplast-like structure is formed twice before metaphase I and II to recruit organelles and facilitate the organelle band assembly (Esseling-Ozdoba et al., 2009; Smertenko et al., 2018).

In WT, meiotic tubulin behaves similarly to mitosis. The spindle microtubule is first built during metaphase I, pulling chromosomes to both poles. During and after anaphase I, the phragmoplast is established between the divided nuclei. Until metaphase II, phragmoplast disappeared and tubulin again was associated with the spindle to facilitate sister chromatid division (Brownfield et al., 2015). Live imaging of TUA-GFP suggests normal phragmoplast-like structures before secondary division in WT, *jas*, and *jas pel,* but abnormal location and orientation of spindles in jas (De Storme & Geelen, 2011; De Storme & Geelen, 2013a; Piskorz et al., 2022). The presence of a fussed spindle does not positively correlate with the mutant genotype (Piskorz et al., 2022). These data suggest that the fused spindle is not the causative reason but the consequence of the *jas* phenotype. Therefore, other factors or pathways, like actin and vesicle organization, may be responsible for disrupting the organelle band phenotype observed in the *jas* mutant.

1.4.2 Actin dynamic during the cell cycle.

Similar to microtubules, actin serves as a dynamic cytoskeletal structure during the cell cycle. The actin monomer (G-actin) can assemble to form filamentous structures (F-actin) while aiding in the delivery of vesicles to target membranes. Actin filament formation at the intermembrane system drives various cellular processes, such as endosome sorting and recycling, exocytosis, and autophagy (Gautreau et al., 2014). Many organelles have been reported to be involved in actin organization. For instance, an ER-specific myosin organizes vesicle positioning and F-actin orientation (Ueda et al., 2010), while a tonoplast-specific protein can reorganize actin filaments during stomatal closure induced by plant immunity (Hawkins et al., 2021). Previous studies of actin dynamics in the cell cycle provide insight into the function of actin in male meiosis.

Actin filament in the mitotic cell cycle

The actin network determines cell shape and is tightly regulated during the mitotic cell cycle. When cells enter mitosis, the actin network forming the cytoskeleton is disassembled and reorganized to allow changes in cell shape (Gibieža & Petrikaitė,

2021). In later metaphase, actin assembles with microtubules to facilitate vesicle trafficking. Interestingly, an actin-free region appears during this stage to indicate the future division plate (Gibieža & Petrikaitė, 2021; Hoshino et al., 2003). During cytokinesis, a phragmoplast consisting of actin and microtubules is established and surrounded by vesicles. These vesicles will transport materials needed for the formation of the new cell wall. The new cell wall is formed from the middle to the periphery at the actin-free region (Gibieža & Petrikaitė, 2021).

Actin filament in female meiosis

The research of actin filament in male meiosis is rare, but actin is crucial for nuclear positioning in mammalian oocytes. During metaphase I, the spindle of mammalian oocytes was pushed to one side of the cell by actin to undergo asymmetry division. The organization of actin structures involves nucleation and elongation processes. The nucleation process initiates the assembly of actin filaments, while the elongation process dynamically adds G-actin to the plus end of F-actin. By regulating the nucleation and speed of F-actin assembly at one side of the spindle, the spindle can be pushed to the other side of the cell to achieve asymmetry division. An actin motor protein, formin 2, is believed to act as an actin nucleator, generating the force necessary to maintain nuclear position (Duan & Sun, 2018; Romero et al., 2004). Actin nucleators normally located on vesicle membranes, leading to vesicle assembly and extension of the actin network (Schuh, 2011). The metaphase I cell of mammalian oocytes also showed ER and Golgi derived vesicles clustered with the actin network.(Halet & Carroll, 2007) The movement of vesicles bearing actin is facilitated by motor proteins like Myosin (Duan & Sun, 2018; Schuh, 2011). Although the situation of male and female meiosis cell cycle is different, the research in female meiosis indicates the function of actin filament in maintaining the nuclear position.

1.5 Screening of *jas* suppressor

To investigate the genetic factors influencing unreduced gamete formation, forward genetic screening was employed to identify suppressors of *jas* (Yi et al., 2023). In this screen, a mutant named *pel* was identified. Under the *jas* background, *pel* can reverse the *jas* phenotype, producing over 80% 1n pollen (Piskorz et al., 2022). The pollen of *jas pel* can fertilize with the female gametes, producing normal 2n seeds. The *pel* single mutant does not influence chromosome behaviour during the meiotic cell cycle. Analysing the organelle band of *jas pel* suggests that the organelle band is presented between homologous chromosomes to act as a physical barrier (Figure *5*B). Accordingly, *jas pel* showed a bigger chromosome distance and fewer 2n pollen compared to *jas* (Figure *5*A, 3D). The chromosome distance was defined by the

shortest distance between two sets of chromosomes at metaphase II. Using a confocal microscope to observe the meiocyte in the whole anther of *jas pel* also indicates around 60% of the meiotic cells have recovered the organelle band (Figure 5C). Compared with over 80% absent organelle band in the *jas* and nearly 100% normal organelle band in WT, the *jas pel* showed a partially recovered organelle band that recovers the *jas* phenotype. The criteria of normal, partial, and absent organelle band has already been defined in the previous study (Brownfield et al., 2015; Piskorz et al., 2022).

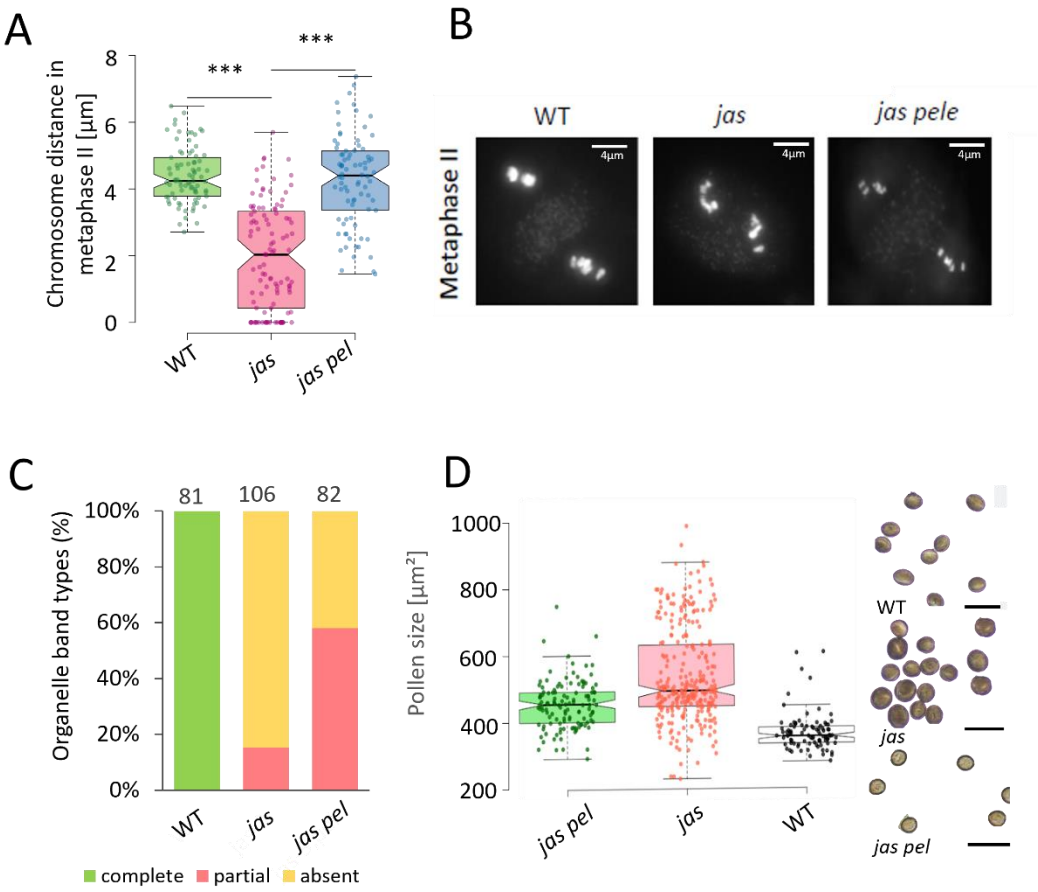

Figure 5. The phenotype analysis of the *jas pel* mutant.

A) jas pel showed a larger chromosome distance at metaphase II in male meiosis. The chromosome distance was defined by the shortest distance between two set of chromosome in metaphase II. B) *jas pel* partially recovered the organelle band. The organelle band in WT is the normal organelle band, and the organelle band in *jas* is the distoried organelle band. The organelle band in *jas pel* can separate chromosme but not as clearly as WT C) The percentage of absent organelle band is dramatically reduced from 80% to 40% in *jas* and *jas pel* respectively. D) *jas pel* produces less unreduced gametes.

Although these recovered organelle bands appear not as condensed as the organelle band in WT, the partial organelle band is functional in recovering the *jas* phenotype. This study aims to dissect the function of PEL, thus revealing the possible mechanisms of the organelle band regulation in male meiosis.

1.6 Application and biological significance of unreduced gametes.

1.6.1 Unreduced gametes during evolution

Unreduced gametes are widely used in breeding applications. Fertilisation of unreduced gametes normally produces polyploids. Polyploidy is characterised by an organism containing more than two sets of genetic material. Polyploidy is commonly observed in plant species (Wood et al., 2009). However, the formation of polyploidy in nature has been a question for a long time. In the early 1930s, scientists induced whole-genome duplication in maize and other cereal plants under heat stress (DORSEY, 1936; Randolph, 1932). Asexual reproduction was thought to be the main path of somatic polyploidization in plants. In 1975, Harlan and deWet realized that polyploidy also arises from unreduced gametes (Harlan & deWet, 1975). Since then, naturally occurring unreduced gametes have been observed in different species (Mason et al., 2011; Pécrix et al., 2011). It is now believed that sexual polyploidy can naturally occur through the fertilization of unreduced gametes.

Fertilization of unreduced gametes produces polyploids that have extra sets of genetic material. Polyploids have a general increase in cell size, known as the "gigas" effect. Compared to diploid counterparts, polyploids typically exhibit an increase in organ size (Sattler et al., 2016). Additionally, the extra sets of genomes provide redundancy, masking deleterious mutations with extra copies of normal alleles, thereby offering a “buffering effect” to the genome. Polyploidy is divided into allopolyploid and autopolyploid based on its formation process. Allopolyploids arise from the hybridization of two different species, creating a new genome that is absent in the parent species. Allopolyploidy can occur naturally. For example, Triticum aestivum (Genome composition AABBDD) arises from hybridization between *Triticum turgidum* (AABB) and *Aegilops tauschii* (DD) (Matsuoka, 2011). The new combination of genotypes can increase heterozygosity and bring stronger resistance. Autopolyploids possess extra sets of chromosomes from one parent. Compared with allopolyploidy, autopolyploidy cannot create a new genome. However, the duplication of genetic material can also cause alterations in transcription and expression, producing new genes and enhancing resistance (Adams & Wendel, 2005; Calvo-Baltanás et al., 2022).

The extra set of genome brings benefits as well as challenges to plants. One obvious problem is how the plant deals with the extra copies of genes. In the long-term evolution, polyploids adapt to the environment by evolving or silencing functional genes (Adams & Wendel, 2005). During the domestication and polyploidization of wheat, alternative splicing of transcription occurs frequently (around 21% of genes undergo alternative splicing) to increase genetic diversity (Yu et al., 2020) . These alternative splicing are proven to be a response to abiotic stress (Liu et al., 2018). Genome sequencing has shown that most of the modern plant genomes have evidence of multiple polyploidizations (Seoighe & Gehring, 2004). Therefore, in application polyploids not essentially show improved quality. In addition to the polyploid breeding, unreduced gametes can also be used for double haploid induction.

1.6.2 Application of unreduced gametes

There are two major methods of inducing polyploidy in applications: *in vivo* and *in vitro* genomic duplication. *in vitro* genomic duplication can be induced by disrupting chromosome segregation by chemicals like colchicine, oryzalin, and trifluralin. These chemicals can disrupt the spindle formation and inhibit chromosome duplication Successful cases in cotton and *Jatropha curcas* obtained higher yields compared to diploid plants (Gotmare, 2010; Niu et al., 2016). However, the preferred features may not pass to the next generation since crossovers among multiple homologous chromosomes occur during reproduction*in vitro* genomic duplication produces unreduced gametes as a result of meiotic defect, which then form polyploids upon fertilization. In potatoes, the omission of *secondary division mutation (osd1)* generating tetraploids shows stronger resistance to pathogens (Calvo-Baltanás et al., 2022). Many of the FDR mutant can also inhibit crossovers in parents (Table 1), but the application of GMO plant is still an ethnic issue.

Nowadays, unreduced gametes can also be used to produce double haploid plant. The double haploid plants are formed when one set of the chromosomes from normal gametes are duplicated without fertilization (Clarke et al., 2012). The double haploid breeding method produce homozygous in 2 generations, while the traditional breeding method produce homozygous over 7 generations (Clarke et al., 2012). In Arabidopsis and rice, *MiMe* (*Mitosis instead of Meiosis*) generated by the combination of *osd1, rec8,* and *spo11-1* mutations, can change meiosis to mitosis (Isabelle d'Erfurth et al., 2009; Mieulet et al., 2016). Therefore, the *MiMe* mutations produce unreduced gametes that have the same genetic material as vegetative cells (I. d'Erfurth et al., 2009; Mieulet et al., 2016). Cultivation of the gametes from *MiMe* mutants solved the

problem that the preferred phenotype would be lost in the next generation because of crossovers. The table below summarized current in vivo double haploid induction mutants (
). The Unreduced gamete formation studies have shown potential in the breeding industry. Understanding the mechanism of unreduced gametes can be used to generate new cultivars.

Table 2. in vivo double haploid induction mutants

Name	**Function**	**Species**	**Reference(s)**
MATRILINEAL (MTL)/ ZmPLA1/ NOT LIKE DAD (NLD)	Sperm-specific phospholipase triggers maize haploid induction	Maize	Kelliher *et al*. (2017), Liu *et al*. (2017), Gilles *et al*. (2017)
indeterminate gametophyte (*ig*)	An LOB domain protein affects haploid induction	Maize	Evans (2007)
haploid initiator gene (*hap*)	Prevents fertilization of the egg cell and not affecting fertilization of the polar nuclei and development of the endosperm	Barley	Hagberg and Hagberg (1980), Hagberg and Hagberg, (1981), Mogensen (1982)
CENH3	Haploid induction through centromere-mediated chromosome elimination	Arabidopsis	Ravi and Chan (2010)
first division restitution 1 (fdr1)	Restores haploid male fertility attributable to first division restitution and produce diploid kernels	Maize	Sugihara *et al*. (2013)
MiMe genotype (*osd1/spo11-1/rec8*)	Transfers meiosis into mitosis	Arabidopsis	Cifuentes *et al*. (2013)

2 Research Aims

Meiosis is a unique cell division process for sexual reproduction in plants and animals. In the meiotic cell cycle, a single round of DNA replication is followed by two rounds of chromosome division, called meiosis I and meiosis II. Both rounds of the meiotic cell cycle contain prophase, metaphase, anaphase, and telophase. Homologous chromosomes segregate at metaphase I and form two cells after a new cell wall is built during telophase I. In dicotyledons, instead of a real cell wall, a band structure consisting of vesicles derived from different organelles acts as a physical barrier between homologous chromosomes until the end of telophase II. JASON (JAS) maintains the organelle band to separate spindles (Brownfield et al. 2015). To understand the consistent and maintaining mechanism of organelle band, a forward genetic screen is applied to obtain a *jas* suppressor called *pel*. This study analyses the structure and function of PEL to understand the mechanism of organelle band organization during metaphase II.

1) **Identifying the component vesicles in the organelle band.**
   Vesicle trafficking markers are used to visualize the vesicles derived from different organelles in WT *jas,* and *jas pel*. By comparing the marker signals in different mutants, the important organelle band component can be identified. Additionally, inhibitors that can block specific vesicle trafficking pathways are applied in different mutants to observe the phenotype during meiosis II. The functional vesicles will show different phenotypes when inhibited by corresponding inhibitors.

2) **Screening the interaction protein of PEL.**
   PEL is a protein that does not have clear known functions, how *pel* influence the vesicle trafficking and cell cycle is still unclear. Microscopic, genetic and proteomic analyses are performed to understand the localization and function of PEL. Through Y2H screening and database searching, two different PEL interactors are found. Using Y2H to express the functional domain and identify possible interaction protein. The identified protein was then confirmed by Y2H, BiFC, or mutagenesis.

3) **Exploring the mechanism of PEL during meiosis**
   According to the previous study of PEL interactors, different working models were hypothesized. Based on the hypothesis, inhibitor treatment and Y2H are applied to identify the possible functional pathway of PEL through PEL interactors.

4) **The function of cytoskeletal structures in organelle band organization.**

Vesicles are trafficked through cytoskeletons during many biological processes. PEL-regulated vesicle trafficking is related to cytoskeleton dynamics without exception. Actin filament can be regulated by vesicle-located proteins during cell division. Actin dye was used to visualize the structure of actin in WT, *jas*, and *jas pel* backgrounds. Inhibitor treatment and dominant negative mutant were applied to further confirm the function of filament actin.

3 Materials and methods

3.1 Plant materials and growth conditions

This study uses the Arabidopsis thaliana accession Columbia as the wild type of reference. The mutant plants, transformed plants, and “wave” line marker (Geldner et al., 2009) plants used in this study are listed in Appendix 3. Seeds were treated at 4°C, in a humid chamber without light for 2 days before the experiment. The treated seeds can either grow on ½MS plates (½MS, 1% sucrose, 0.8% plant agar) or directly into the Peat-Based soil. When grown on ½MS plates, seeds are sterilized in 70% (v/v) ethanol for 10 minutes and rinsed twice with ethanol absolute. Air-dried seeds were then placed on ½MS plates. Antibiotics can be added depending on the selection genes on the transformed plasmid (Table S2). Seeds were kept on a plate for 2 weeks, and the selected plant was transferred to soil. When growing plants directly on the soil, using spray can keep the surface of the soil moist. Put 1-2 seeds per pot, and grow the seeds in a short day culturing room for 2 weeks (day : night = 8 hrs : 16 hrs, 22°C). Then move the tray to the long day culturing room (day : night = 16 hrs : 8 hrs 22°C) for rapid growth.

3.2 Plant genotyping

DNA for genotyping was extracted from 0.1g of fresh plant leaves using the Edwards method (Edwards et al.,1991). Plant material was homogenized using polypropylene pestles in a 1.5ml Eppendorf tube. Then, DNA was extracted by Edwards’ method (Edwards et al.,1991). Upon dissolving in water, DNA pellets were stored at -20°C for long-term storage.

For ordinary genotyping PCR, 2 × Taq Master Mix kits (P211, Vazyme)(Buzard et al., 2012) were used for PCR. The PCR system and reaction process were set based on the protocol from Vazyme. Primers used for different mutants are listed in Appendix 3. For dCAPS genotyping, the PCR process follows the same protocol. After the PCR reaction, 10µl corresponding restriction enzyme (Thermo scientific or New England Biolabs) mix (2µl 10Xbuffer, 0.3ul enzyme, 7.7 µl H_2O) for every 10 µl PCR product was prepared and added to the PCR reaction system, then incubate for 3 hours in recommended temperature for digestion.

PCR results were viewed and recorded from the gel electrophoresis method. Ultra GelRed (GR501, Vazyme) was diluted and added to DNA samples before loading. After loading the sample in the gel, the DNA band were separated by electrophoresis at 130V for 20 minutes, and visualized with the SynGene Gel Doc system.

3.3 Plant phenotyping

Pollen size analysis

After 5-6 weeks, 2-3 open flowers per plant were dipped in a drop of 1x PBS on slides. The pollen images were observed and captured under the optical microscope (SMZ1500 Nikon). The projection of pollen size in images was measured using ImageJ.

Microspore analysis

After 5-6 weeks of culturing, the whole inflorescence was fixed in Carnoy's solution (Carnoy, 1887) (Puchtler et al., 1968) for a minimum of 4 hours and then washed away twice with 1X PBS buffer. Open flowers normally are removed before dissecting the closed buds. Dissection was done under a stereoscope (Zeiss). The biggest two closed buds (around 1.0-1.5 nm in diameter) were selected and the rest buds were discarded. Using a blade cut the selected buds to release the developing pollen grains from the anthers and stained nuclei with 0.1% (w/v) toluidine blue solution (Sigma-Aldrich, dissolved in H_2O). The slide can be kept in a humid environment for a week.

Chromosome distance and organelle band analysis

The Chromosome distance and organelle band analysis need to visualize meiotic cells in one anther. The chromosome distance can be measured from the whole anther analysis images and do statistical analysis. Like the microspore analysis, the meiotic cells were fixed by the same method as the microspore analysis. When dissecting the meiotic buds, the third and fourth biggest buds were selected (0.5 nm to 1 nm). The flower panels were removed by a needle, keeping anthers on the slide. 10 µl 4',6-diamidino-2-phenylindole (DAPI) dye (0.4 ug/ml in 10X PBS) was added to each slide (Rossig et al., 2021). Z-stack images were taken under a confocal microscope (LSM788 Zeiss). Selecting the Z-stack images that showed the divided homologous chromosome in the same layers. The line Measurement tool from ZEN 2.0 was used to measure the chromosome distance. The cells with clear organelle bands were used for organelle band type analysis.

3.4 Molecular cloning methods

Gateway plasmid construction

The Gateway method was applied for all the BiFC plasmids and some of the fluorescent protein expressions. The fragments cloned from genomic sequence or CDS were ligated to the TSK108 entry vector. Then Gateway™ LR Clonase™ II Enzym-Mix (Invitrogen) clones the fragment in the corresponding expression vector (Table S3). The constructed plasmid was transferred into *E.coli* and selected on the corresponding

selection medium (Table S3). The selected colony plasmid was extracted through GeneJET Plasmid Miniprep Kit (Thermo Scientific™), and sequenced by LGC Genomics (https://shop.lgcgenomics.com/).

In-fusion cloning method for plasmid construction

In-fusion cloning method was applied for all yeast plasmid construction. The desired fragment was directly cloned to the expression vector by ClonExpress UItra One Step Cloning Kit (C115 Vazyme) (Liu et al., 2023). And the selection and sequencing steps were exactly the same as the description before.

The Golden Gate cloning method for plasmid construction.

The Golden Gate method was applied for most of the marker protein expression. MoClo Toolkit (Addgene) plasmids are used for modulating construction. The MoClo Toolkit is a set of empty standardized modules plasmids that can be used for hierarchical assembly based on the Golden Gate cloning technique. The plant selection module and bacterial selection module Level 1 plasmid are kindly provided by Saravanakumar Somasundaram (Ag. CSF, IPK). The plasmid construction followed the methods from the MoClo Toolkit (Weber et al., 2011). And the selection and sequencing steps were the same as the description before.

Site mutagenesis in plasmid construction

In dominant negative mutants, the E272 to K272 site mutant on *ACT8* was generated by Mut Express II Fast Mutagenesis Kit V2 (Vazyme). In this method, the primer (designed following the kit manual) containing the mutation site amplified the whole constructed plasmid, and then Dpn1 was used to digest the PCR products to allow homologous recombination to form the mutated plasmid. The *DMC1* promoter fragment (template provided by Chao Feng, Ag.ME, IPK) and *ACTIN8 (ACT8)* fragment from the cDNA library were firstly cloned to the TSK108 plasmid. Using primers that contain mutant sites to generate mutation on the *ACT8* sequence through the PCR process (Table S3), then using the Gateway method to clone the promoter and mutated gene to the PGWB501 terminal vector.

3.5 Plasmid expression and transformation

***E.coli* transformation**

The plasmid was replicated or selected using different commercial strains of *E.coli.* For the plasmid that does not contain the *CCDB* sequence, NEB® 10-beta Competent *E. coli* (NEB) cells were used for replication and selection. The 1 X 10^9 cells/µL Competent cell was prepared with the Mix & Go! *E.coli* Transformation Kit and Buffer Set (ZYMO

RESEARCH). In every 100µl competent cell, up to 100ng DNA was added for transformation. The cells were placed on ice for 30 minutes after adding the DNA. Then heat shocked at 42°C for 1 min. After the heat shock transformation, the tube was immediately chilled on ice and cooled for 3 min. After the temperature was reduced, ice-cold LB medium was added and the cells were recovered at 37°C 200rpm for 1 hr before plating on the corresponding antibiotic selection medium (the selection antibiotics of different plasmid are shown in Table S3). For the plasmid that contains the *CCDB* sequence, the DB3.1™ Competent Cells was used for transformation. The transformation protocol was the same with 10-beta Competent cells.

Agrobacterium-mediated plant expression plasmid transformation

The plant expression plasmid was firstly transferred to Agrobacterium and then inoculated Agrobacterium to *Arabidopsis* or *Nicotiana benthamiana*. Agrobacterium competent cell (GV3101) was prepared with the standard protocol (Weigel & Glazebrook, 2002) and stored at -80°C. During Agrobacterium transformation, up to 100ng DNA was added in every 100µl GV3101 agrobacterium and incubated on ice until the agrobacterium defrosted. Then the agrobacterium was dropped at -80°C for 3 min, in 37°C, and immediately chilled on ice for 3 min. The LB medium was added in the transformed agrobacterium and incubated under 25°C for 3 hours. Then the recovered cells were plated on a selective medium that contains Rif and Gen for GV3101 and terminal vector selection antibiotics. The terminal vector selection antibiotics are shown in Table S3.

Flower-dip transformation methods were applied to transfer the expression vector into *Arabidopsis* plants (Zhang et al., 2006). The transferred plants were continuously grown in the long day culturing room and collected the seeds 4 weeks after transformation. Seeds with insertion of the gene of interest were selected in ½MS plates with the selection antibiotics (Table S3).

Agrobacterium-mediated Infiltration of *Nicotiana Benthamiana* was applied by the published method from our lab (Xu et al., 2024). Infiltration buffer was used as a blank control.

Yeast transformation and Y2H

Yeast transformation for Yeast-two-Hybrid experiments was applied based on the standard protocol from Dualsystems Biotech (DUALmembrane starter kits User Manual). The bait and pray plasmids were constructed following the plasmid construction protocol from Dualsystems Biotech. The plasmids were then co-transformed to the NMY51 yeast with positive and negative control plasmids following the yeast co-transformation protocol from Dualsystems Biotech. The transformed plasmids are selected on the SD/-Leu -Trp -His plate, SD/-Leu -Trp -His -Ade plate, and

SD/+IPTG +X-Gal plate (Matchmaker Gold Yeast Two-Hybrid System, Takara). The plasmid that can be grown on the SD/-Leu -Trp -His -Ade plate after transformation was the properly expressed plasmid. The properly expressed plasmids were used for Y2H screening. The Bait plasmid contains the target protein sequence and the pray plasmid contains the cDNA library fragment from the flower bud are co-transferred to a large volume of yeast and plate on SD/ -Leu -Trp -His -Ade plate. After 4 days under 28°C, the positive colonies were selected in liquid culture for two more days to extract the Pray plasmid. The plasmids from positive colonies selected from Y2H screening were lysis and extracted through a published method (Singh & Weil, 2002) with the GeneJET Plasmid Miniprep Kit (ThermoFisher Scientific). Afterwards, the extracted plasmid was directly transferred into *E.coli* as described before. The transformed cells were selected on the LB medium with ampicillin. Two colonies from each plate were selected and grown in liquid culture for plasmid purification. The purified plasmids were then sequenced by LGC genomics. Yeast Minimal Media (SD) (Takara) set and YPDA rich media (Takara) were prepared before use.

3.6 Cytological analysis

Cytopainter staining

The live cell staining method was applied to visualize organelle dynamics during the meiotic cell cycle. F-actin (ab112127), ER (ab139481, data not shown), and Mitochondria (ab138897, data not shown) staining kits were used from the Abcam Cytopainter. The F-actin Cytopainter kit is based on the traditional phalloidin staining method. The actin stain is maximised with the kit, The fresh flower buds were fixed in 4% Paraformaldehyde (v/v dissolved in H_2O) 10 min to stop the cell division. Rinsed the fixed sample with room temperature F-actin staining kit working buffer 3 times. The flower bud that had a diameter of around 0.5-1.0 nm was selected and dissected under a microscope. Used a blade or a sharp needle to cut the anther and release the meiotic cells. The cells on the slides were stained following the kit protocol. The coverslip was added. Meiotic cells were observed under a confocal microscope (LSM780 Zeiss).

Fluorescent protein signal observation

The transformed plants that contained fluorescent expression vectors were checked for the root signal at 4-6 days after sowing on the selection plate. Only plants with observable signals were transferred into the soil. Plants were grown as the standard plant growing protocol. After 6 weeks of sowing, the flower buds were fixed by 100% methanol in -20℃ for 10 min. The meiotic anthers were carefully dissected and kept in the dark to avoid signal bleaching. In each slide, 10 µl DAPI-PBS solution (0.02 ug/ml

DAPI dissolved in 1XPBS) was added and stained for 10 mins in dark and cold. Later the cover slip was carefully added without breaking the anthers. Until the slides were observed under a microscope, the anther was broken by squeezing the cover slip.

Immunostaining

The sample fixation, dissection, and slide preparation are done following the published method (Morgan et al., 2021). 1st antibody of (Rabbit anti Mouse) PIP1;4, Syp32, and VAMP711 were prepared and obtained from Biointron. The antibodies were diluted 1:100 and 1:500 separately to test which concentration is more suitable. 2nd antibody with the fluorescent label was diluted 1:2000 in 1XPBS solutions to stain the slides. 10 µl DAPI-1XPBS solution (0.02ug/ml DAPI dissolved in 1XPBS) was added and stained for 10 mins before observing under a microscope. For tubulin immunostaining, the PBS solution in the protocol above was changed into a microtubule-stabilizing buffer (Heckmann et al., 2014).

3.7 Inhibitor treatment by inflorescence culture

The flowers from the main stems of 6-week-old *Arabidopsis* inflorescence were used for the experiment. The medium for inflorescence culture is made of 200ml 1X MS salt, 3% sucrose (w/v), and 1X vitamins (Feldmann & Marks, 1987), and adjusting pH to 6.0 with KOH. Inhibitors are prepared in a Master mix. Concanamycin A (ChemCruz) powder is dissolved in DMSO to make a 200uM stock solution. Wortmannin (Abcam) powder is also dissolved in DMSO to make the stock solution at 3 mM. Both solutions are stored at -20°C and fully dissolved before the experiment. Brefeldin A Solution 1000X (BioLegend) is freshly diluted in 9 volumes of DMSO to make Master Mix before use. The treatment medium is prepared by adding the master mix to the inflorescence culture medium in the ratio of 1:100 to final concentration of 2 µM Concanamycin A, 30 µM Wortmannin, and 2 µg/mL Brefeldin A. Prepared treatment culture is aliquoted to 0.5 ml Eppendorf tubes and sealed by a piece of adhesive foil to prevent contamination. Used a tip to poke a hole in the middle of each tube. Selecting inflorescence with good condition to cut with a blade and immediately insert the inflorescence into the hole on the 0.5 ml Eppendorf tube. The stem of the inflorescence should get into the treatment culture. Bring the culture system to the Arabidopsis long-day culturing room and culture at the standard condition for 24 hrs. After 24 hrs, the treated inflorescence can be fixed and analyzed by the phenotyping methods described in session 3.3. The Fixed sample can be stored at 4°C maximum for 1 week.

3.8 Bioinformatic and statistical analysis

Building Phylogenetic Tree

The gene of interest, *PEL*, was found on the TAIR website (https://www.arabidopsis.org/). The protein sequence of PEL is used to find the homologous sequence by Blast (Altschul et al., 1997). Meanwhile, homologous sequence is also acquired on the TAIR website. Comparing the species from Blast and TAIR, the sequence used to generate the Phylogenetic tree is defined. The sequences were then aligned by MEGA5 using the MUSCLE method (Hall, 2013). Also, in the MEGA5 software, the Neighbor Joining method is used to estimate the tree. The reliability of the tree is tested by the "Bootstrap Method" (Hall, 2013).

Functional domain analysis and protein structure prediction

The functional domain of the protein of interest is analyzed by the Interpro website (https://www.ebi.ac.uk/interpro/) and the function of each domain is predicted by the string website (https://string-db.org/). Transmembrane domain structure is predicted by Interpro and TMHMM 2.0 tools (https://services.healthtech.dtu.dk/services/TMHMM-2.0/). The 3-dimensional structure was analyzed by the Alphafold 2.0 tool (Monomer script was provided by Dr. Amanda Souza Camara. Github link: https://github.com/amandascamara/Protein-Structure-Workshop/tree/main). Using the pyMOL software (https://pymol.org/) to visualize the predicted structure and label the interaction site.

Protein-protein interaction prediction

Similar to the prediction of one protein structure, the Alphafold 2.0 tool is also used for the prediction of protein-protein interaction. In this case, a different model is used (called multimer predictions). Using pyMOL V2.X software to visualize the protein structure and predict the interaction site. In this study, interaction was defined by the distance of interaction residue. Normally, the contacts that are less than 3 Å can be recognized as interaction residue (Headd et al., 2007). The protein residue can be either a polar-bound interaction or a nonpolar-bound interaction. Polar-bond is a special type of residue interaction that unevenly distributes electron density. Since polar bonds played a crucial role in protein structure maintenance, chemical reaction, and maintaining solvent properties, the polar-bound between the residues were labelled in pyMOL by selecting the polar-bound interaction. In this study, the interactions (except special disclaimed) are polar-bound interactions.

Statistical analysis

The Chi-square test was used for the microspore analysis data and BiFC analysis data. R languages tools were applied to perform the analysis. The analysis script can be found in Appendix 4. The analyzed data were then plotted by Microsoft Excel or R Studio. The significance of data was manually added to all Figures. * represents p value< 0.5, ** represents p value<0.01, *** represents p value<0.001, n.s represent no significant different. One-way ANOVA tests were applied to all the pollen size analyses. Graphpad 7.0 was used to do the one-way ANOVA test. * represents p value< 0.5, ** represents p value<0.01, *** represents p value<0.001, n.s represent no significant different.

4 Results

4.1 *pel* rescues the organelle band defect in *jas* via vesicle trafficking

4.1.1 *pel* rescues the vesicles derived from vacuoles to the organelle band.

The organelle band is a structure that is studied rarely in male meiosis II. Based on previous publications, organelles and vesicles derived from organelles move to the organelle band area, suggesting that the organelle band consists of different organelles and vesicles. In previous publications (Brownfield et al., 2015), the organelle band was visualized by 4',6-diamidino-2-phenylindole (DAPI), a fluorescent dye that specifically stains DNA. However, the DAPI staining result doesn't represent all organelles. Many non-DNA-containing organelles cannot be stained by DAPI. Therefore, I used multiple types of organelle maker lines (Geldner et al., 2009) to visualize the localization of organelles in meiosis II.

There were two different methods tested to visualize the vesicles derived from different organelles: the immunostaining using the antibody of vesicle-specific protein and the fluorescent protein-tagged vesicle-specific protein. ZYP1 can label the chromosome at prophase. SYP32 can label the Golgi apparatus, and VAMP711 can label the vacuole membrane (tonoplast). After many attempts with both methods, The Immunostaining does not work properly for the meiotic organelle-specific proteins. Even though the concentration of the 1st antibody was increased to 1:100 with the incubation buffer, no signals showed in meiosis (Figure 6). The DAPI-stained vesicles also disappear after the immunostaining process, because of the long-time digestion and antibody incubation. Thus, this method cannot be used for further study (Figure 6).

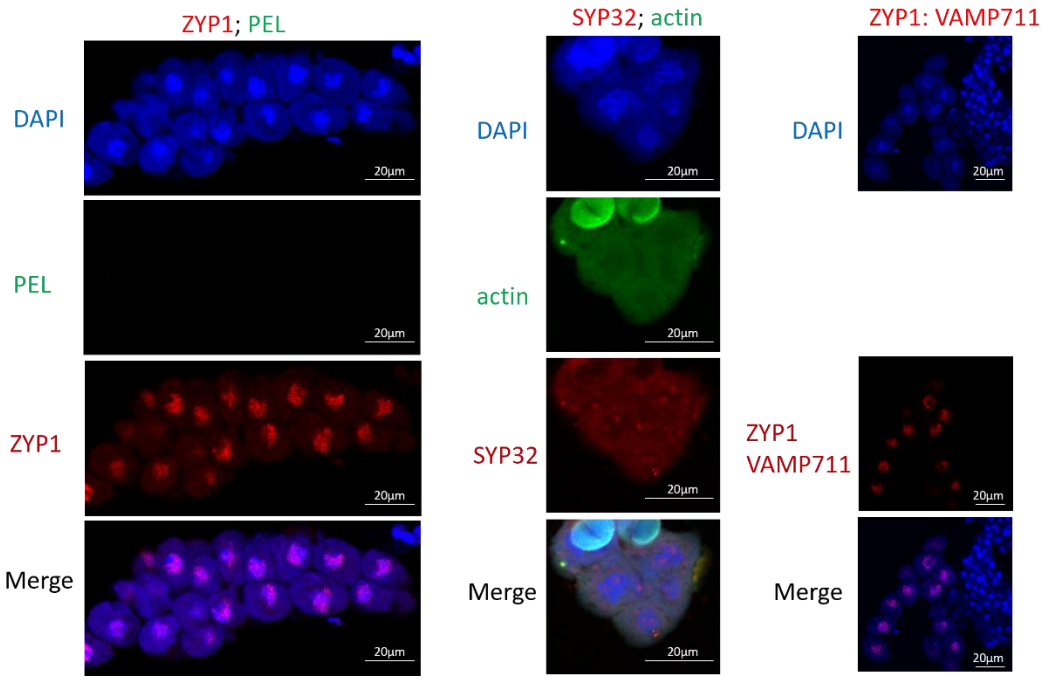

Figure 6. Immunostaining of vesicles in meiotic cell.

1st antibody: rabbit anti ZYP1 (1:2000 dilution), mouse anti PEL (1:100 dilution), rabbit anti SYP32 (1:100 dilution), rabbit anti VAMP711 (1:100 dilution) and actin cytopainter (Ab112127) show green fluorescent. 2nd antibody: goat-anti rabbit (red signal 1:2000 dilution) and goat-anti-mouse (green signal 1:2000 dilution). The PEL SYP32, and VAMP711 antibodies do not show a clear detectable signal, while the ZYP1 antibody in the same cell showed a good signal.

The wave lines (Geldner et al., 2009) are marker lines of membrane compartments in *Arabidopsis*. The wave lines were used to visualize the localization of different organelles in meiosis II. The marker is tagged with mCherry, driven by a *UBQ10* promoter that is active in multiple tissues and developmental stages. In this study, multiple markers in meiosis II are expressed in the wild-type (WT) background to select the markers with clear signals. PIP1;4, VTI-12, VAMP711 and SYP32, which labelling the plasma membrane, trans-Golgi network, vacuole, and Golgi apparatus respectively was used in this study. These marker lines showed very strong signals in the organelle band in meiosis II (Figure 7,8,9), implying that fluorescently labelled proteins are also organelle band compartments. VAMP711 is a vacuolar marker that was shown to be co-localized with the PEL-GFP signal in root cells (Piskorz et al., 2022). Afterward, the tested marker lines in the WT background were then crossed with *jas* and *jas pel* to observe the subcellular localization in the mutant.

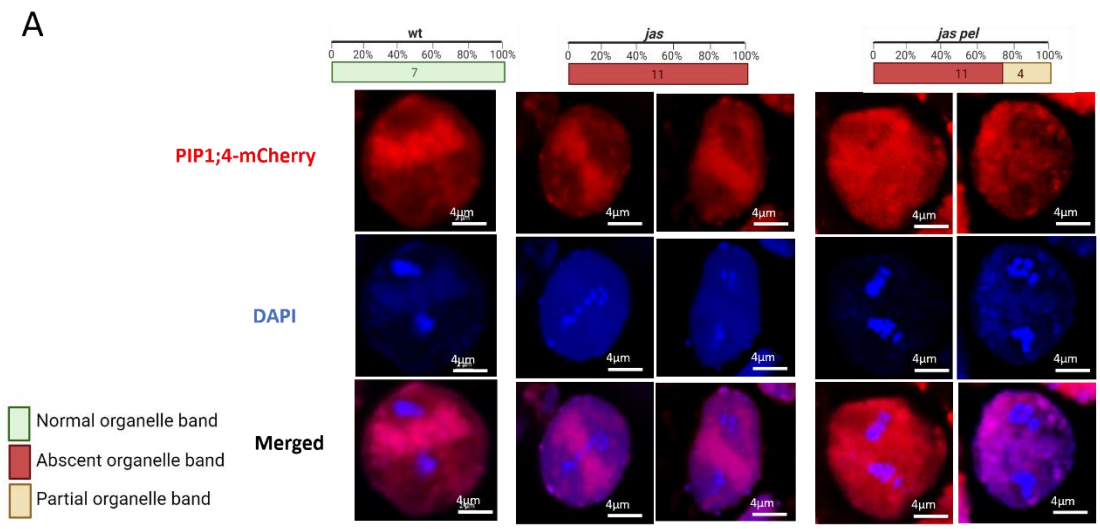

Figure 7. Reorganization of PM marker during meiosis in WT, *jas*, and *jas pel* plant.

PIP1;4 markers counted 7, 11, and 15 metaphase II cells in WT, *jas,* and *jas pel* background separately. All of the WT cells showed normal complete organelle bands, all of the *jas* cells showed absent organelle bands, although the absent organelle can still show 20% separated chromosomes. *jas pel* showed both absent organelle band and partial organelle band and has 70% separated chromosomes.

The F2 generation of the marker lines crossed with *jas* and *jas pel* was genotyped and selected based on the root signals. DAPI staining was applied to meiotic cells to figure out the meiotic stages. The differential patterns were observed in different marker lines (Figure 8,9). The signal of PIP1;4 in *jas* was similar to WT, the PIP1;4-mCherry signal was observed in the middle zone in the *jas* cells with very close chromosome distance and disordered organelle band (Figure 7). Suggesting the PM organelle at the middle zone is not sufficient to maintain the organelle band. The pattern is different for the other markers in *jas*. Both VTI-12 and Vamp711 cannot maintain their localization on the organelle band, showing an asymmetrical signal (Figure 9)(Figure 8). The disorder of TGN and vacuole marker is the potential regulation element of chromosome distance. The SYP32 marker in homologous plants expresses a weak mCherry signal all around the cells (Figure S1), Thus, the SYP32 was not tested further in *jas pel*. The organelle band type in *jas* mutants is counted, and almost all of the cells showed abnormal organelle band, which is same as the phenotype described in *jas* (Brownfield et al., 2015).

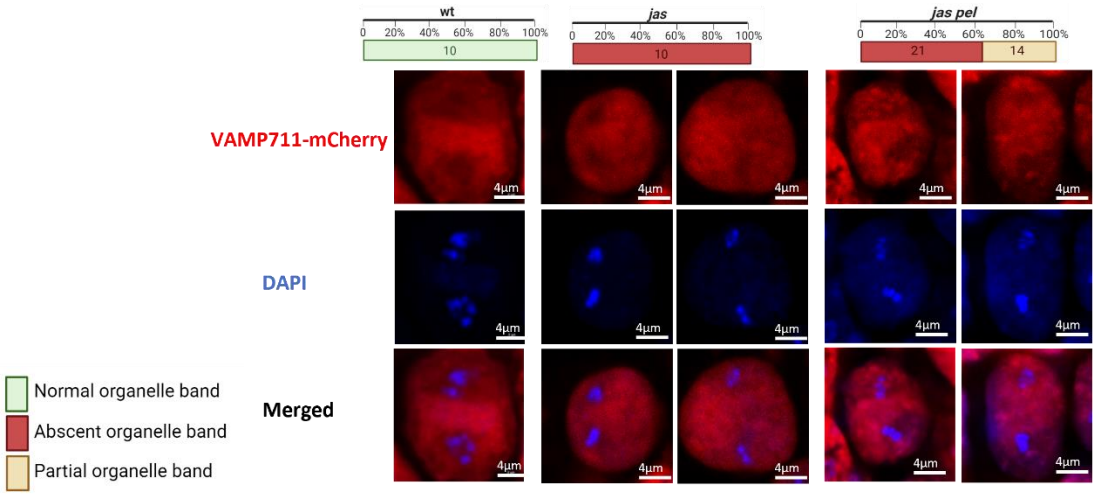

Figure 8. Reorganization of vacuole marker during meiosis in WT, *jas*, and *jas pel* plant.

VAMP711 marker counted 10, 10, and 35 metaphase II cells in WT, *jas*, and *jas pel* background separately. All of the WT cells showed normal complete organelle bands. All of the *jas* cells showed absent organelle bands, although the absent organelle can still show 20% separated chromosomes. *jas pel* showed both absent organelle band and partial organelle band and has 70% separated chromosomes.

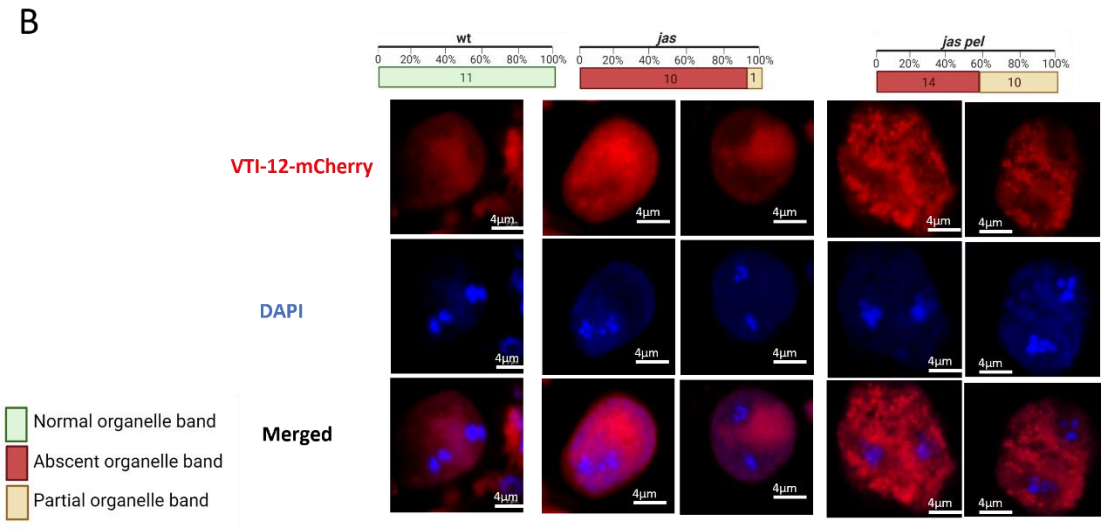

Figure 9. Reorganization of TGN marker during meiosis in WT, *jas*, and *jas pel* plant.

VTI-12 marker courted 11, 11, and 24 metaphase II cells in WT, *jas*, and *jas pel* background separately. All of the WT cells showed normal complete organelle bands. Over 90% of the *jas* cells showed absent organelle bands, although the absent organelle can still show 20% separated chromosomes. *jas pel* showed both absent organelle band and partial organelle band and has 70% separated chromosomes.

The signal of markers under the *jas pel* background is again different from the *jas* background. The VAMP711 (vacuole) marker showed a cluster of signals in the recovered organelle band area. Even in cells that lost the organelle band, a thin layer of VAMP711 signal is observed in the mid-center zone (Figure 8). Compared with the wild-type organelle band, the recovered organelle band is wider in size and not as condensed as the wild-type organelle band. The recovered vacuole membrane potentially separates spindles. Vacuole-derived vesicles depend on the *pel* to move to the organelle band. The VTI-12 (TGN) marker is not always recovered to the mid-center area. In cells with an absent organelle band, the VTI-12 marker signal is spread all around the cell, while in cells with a partially recovered organelle band, the VTI-12 marker is partially recruited to the organelle band area, with some signals remaining around the spindle (Figure 9). Trans-Golgi network (TGN)-derived vesicles partially depend on *pel* to recruit to the organelle band. Surprisingly, PIP1;4 (plasma membrane) maker signal is not specifically located at the mid-centre area in the *jas pel* background (Figure 7), suggesting that the recovered organelle band is irrelevant to plasma membrane-derived vesicles.

Overall, the recovered organelle band in *jas pel* contains vacuoles and TGN-derived vesicles during meiosis but not plasma membrane-derived vesicles. The recovered vacuole membranes are sufficient to separate the spindles during metaphase II. Referring to current knowledge, vacuoles, and TGN are involved in the exocytosis and sorting vesicle trafficking pathway(Aniento et al., 2021; Jiang et al., 2021), while the plasma membrane is involved in the endocytosis pathway (Aniento et al., 2021). In the next step, inhibitors that specifically inhibit different pathways are used to further test which pathway is sensitive in *jas pel*.

4.1.2 *pel* phenotype depends on specific vesicle trafficking pathways.

Based on the image of different marker lines, *pel* should be functionally related to specific vesicle trafficking pathways. If such an association occurs, inhibiting the corresponding trafficking route will decrease the efficiency of recovering the organelle band in *jas pel*. Therefore, inflorescence treatments with vesicle trafficking inhibitors can convert *jas pel* phenotype to *jas*. Inhibitor, as well as DMSO controls, are applied on *jas pel* flower buds for 24 hours. Concanamycin A blocks both endocytosis and exocytosis, increasing the percentage of dyads and triads from 30% to 70% compared with DMSO treatment in *jas pel* (Figure 10), suggesting that Concanamycin A suppresses the rescued phenotype in the *jas pel* background. To dissect the effect of *pel* on endocytosis or exocytosis, the inflorescences are treated with Wortmannin and

BFA that inhibit endocytosis and exocytosis respectively. As a result, Wortmannin did not significantly influence the phenotype of the *pel*, while BFA treatment significantly increased the percentage of triads and dyads from 30% to 60% (Figure 10). The chi-square test showed a significant difference between untreated *jas pel* plant and Concanamycin A, as well as BFA, treated *jas pel* plant.

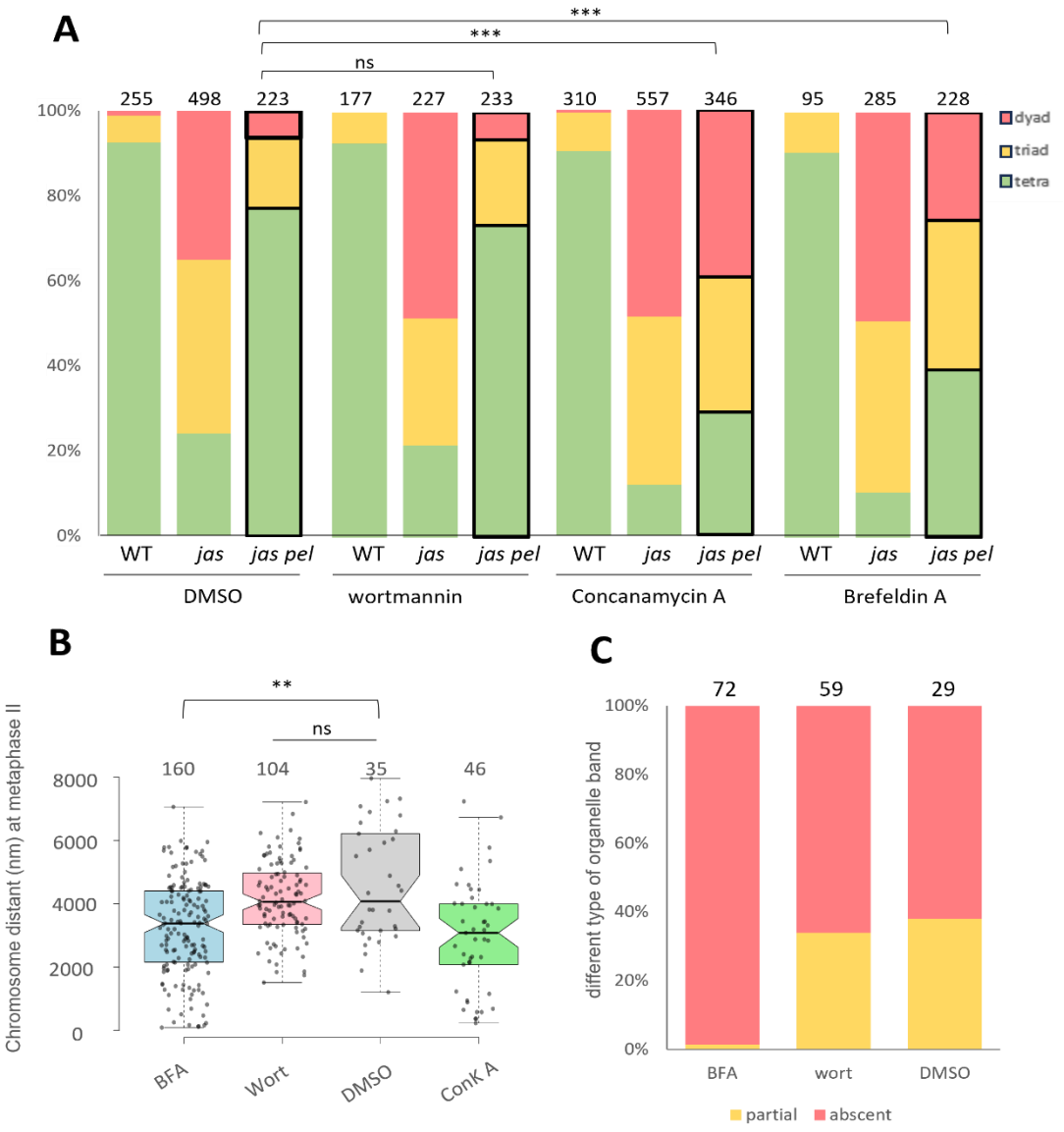

Figure 10. Different inhibitor treatments influence meiotic division under *jas pel*

A) The *jas pel* phenotype depends on the exocytotic pathway. ConKa and BFA can dramatically change the ratio of dyad : triad : tetrad ($p<0.001$, Chi-Square test) B) BFA and ConK A treated jas pel male meiotic cells showed a shorted chromosome distance. C) The partially recovered organelle band in *jas pel* is disturbed by BFA (from 40% to less than 1%), but not influenced by wortmannin (40% to 35%).

The WT and *jas* inflorescence are also treated with inhibitors. WT doesn't show a dramatic difference after three different treatments. This is because of the negative regulation role of *PEL*. *jas pel* rebuilt the organelle band, thus, PEL negatively facilitates organelle band construction. The rebuilding of the organelle band happened only when the organelle band was disordered. In WT, the organelle band is maintained by JAS, thus, the whole *PEL*-related pathway is not active. In *jas*, the number of abnormal meiosis was increased to different extents after three different treatments. Compared with the wortmannin treatment, Concanamycin A and BFA showed more abnormal meiosis, suggesting the inhibitor-inhibited pathway also contributed to form normal meiotic products in *jas*. From this data, I hypothesised that the Concanamycin A and BFA-inhibited vesicle trafficking pathways are essential during organelle band to rebuild in *jas*.

To further test whether inhibitor treatment influences the organelle band at metaphase II, the distance between chromosomes is measured at metaphase II in inhibitor-treated male meiosis. In line with the results of the tetrad analysis, organelle band type and chromosome distance are also examined in the treated cells. Almost all of the cells after BFA treatment showed an absent organelle band (Figure 10), but Wortmannin treatment did not change the proportion of partially recovered organelle band versus absent organelle band (Figure 10). Meanwhile, BFA but not Wortmannin significantly decreased the distance between two groups of chromosomes at metaphase II (Figure 10), suggesting that BFA inhibited pathway is required for separating chromosomes at meiosis II in *jas pel*. The ConK A treatment strongly inhibits the cell cycle, and I cannot find Metaphase II cell images that are sufficient for analysis. However, like what was revealed in the introduction, the classification of vesicle trafficking pathways has not had a slandered criterion. The current result implies the importance of exocytic and sorting pathways, but there is still not enough evidence to prove the specific biochemistry pathways. Concanamycin A and BFA-inhibited vesicle trafficking pathways positively consist of the organelle band, while PEL negatively regulates the organelle band.

4.2 Characterization of PEL

4.2.1 Localization of PEL in WT and *jas*

In *Arabidopsis*, the *PEL* gene (AT5G11700) is annotated as an ephrin type-B receptor gene, but no further functional studies have been conducted in plant cells. The screened EMS mutant of *pel* will generate a stop codon at 3015 bp of the coding sequence. PEL has a relatively high expression level in meiotic stage cells but is not tissue-specific (Piskorz et al., 2022). Expression of the genetic PEL sequence tagged with GFP suggests that PEL is located at the tonoplast in root cells (Piskorz et al., 2022). Since all the organelles are reorganized during meiosis, the PEL-GFP plasmid was introduced into WT and *jas pel* to visualize the PEL localization in meiosis. During metaphase II, PEL-GFP is always located in the cytoplasm (Figure 11). *PEL* is a gene that has not been functionally studied, and the *pel* alone does not show an observable phenotype (Piskorz et al., 2022), complementation analysis of PEL-GFP transformed into *jas pel* is necessary to confirm the functional sequence of PEL. The analysis of meiotic products showed that the transformed plasmid complements the phenotype of gamete size in *jas pel*, resulting in unreduced gamete in *jas* (Figure 11). The complementation result confirmed the expressed PEL-GFP is functional. In WT, PEL-GFP was localized in the cytoplasm outside of the spindle at metaphase II (Figure 11), and PEL remains in the same position of cytoplasm in both WT and *jas* background.

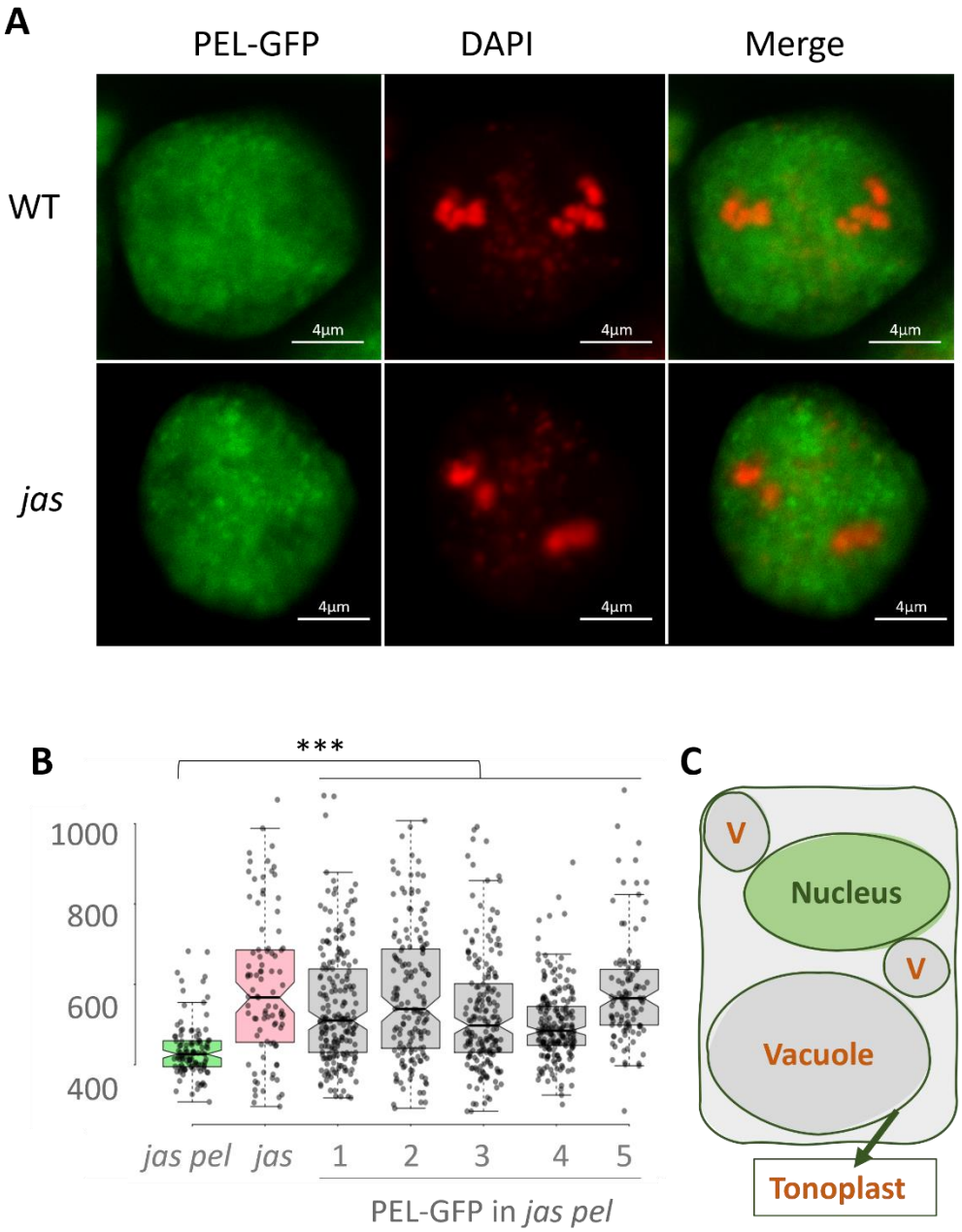

Figure 11. PEL-GFP location in WT and *jas* during metaphase II.

A） PEL-GFP is located at the cytoplasm predominantly outside of the nuclear and organelle band, and the location does not change in the *jas* background. B) Transfering PEL-GFP into *jas pel* can complement jas pel phenotype, and produce unreduced pollen. C) The vacuole and tonoplast structure.

PEL was annotated to be a tonoplast-located protein in Arabidopsis. The tonoplast is the membrane around vacuoles (Figure 11). The tonoplast is also involved in the vesicle trafficking pathways. The location images of meiosis showed that PEL is not

only located at the tonoplast but also located in the cytoplasm. While the PEL in root cells showed colocalization with the tonoplast marker (Piskorz et al., 2022). The location of PEL in meiosis and vegetative cells implies a special function of the pel in meiosis.

4.2.2 Structure analysis and phylogeny tree of Arabidopsis PEL

The Arabidopsis PEL protein consists of 1,453 amino acids and lacks known domains that could suggest its biological function. The phylogeny tree of Arabidopsis *PEL* (*AtPEL*) suggests a relatively conserved sequence in angiosperms, especially dicotyledonous plants. There are 2 paralogs of PEL in *Arabidopsis*. The phylogeny tree of the *AtPEL* sequence compared *AtPEL* and two of the *AtPEL* paralogs to other 18 species (Figure 12). The *AtPEL* sequence is conserved within the Brassica and has similarities to other angiosperm species in the phylogeny tree. While the two paralogs of *AtPEL* have evolved in a different direction. The *AtPEL* paralogs are more similar to the gymnosperms or early angiosperms species, suggesting these two versions evolved to have a different function with PEL. Among angiosperms, PEL is also found to be more conserved in dicotyledons rather than monocotyledons. The dicotyledons normally undergo a simultaneous type of meiotic cytokinesis (Brownfield et al., 2015; De Storme & Geelen, 2013a). This means the cell wall does not form after the first division but only forms after the second division. While the monocotyledon undergoes successive types of meiotic cytokinesis, in which the cell wall forms after the first and second meiotic division(De Storme & Geelen, 2013a). The organelle band structure that is destroyed in *jas* during metaphase II only appears in a simultaneous type of meiotic cytokinesis. These findings support that PEL performs its function in plants that undergo a simultaneous type of meiotic cytokinesis. The pathway involved in PEL is related to cytokinesis. The Organelle band is a potential precursor of the cell wall(Brownfield et al., 2015).

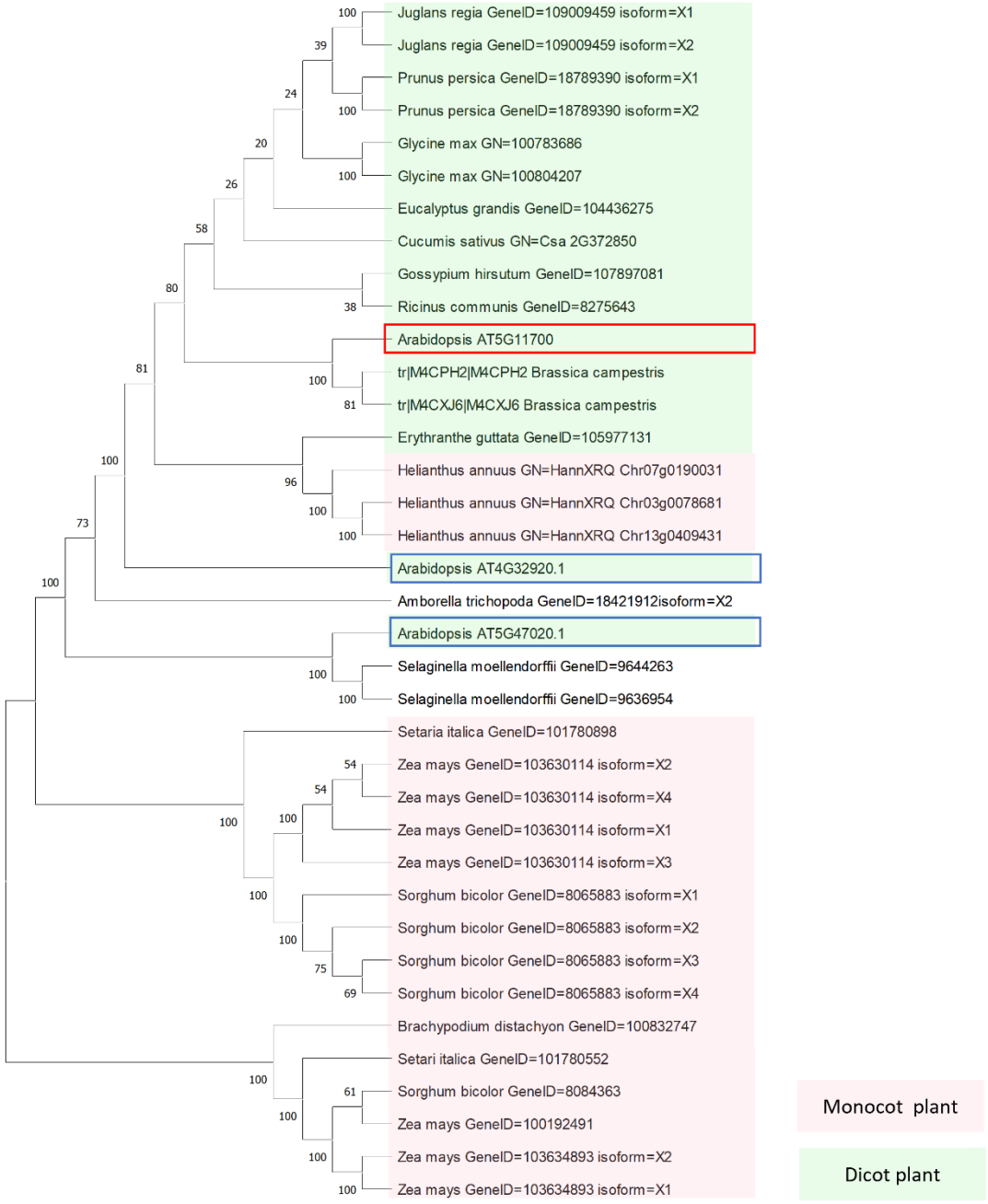

Figure 12. Phylogeny tree of PEL protein sequence.

(Note: PEL is labelled in red color and PEL paralogous are labelled in blue). *PEL* is conserved in dicot plants, especially Brassica. While the other two paralogs of *PEL* are more conserved to gymnosperm and dicot plants separately.

Prediction of functional domains of PEL by online tools (InterPro: https://www.ebi.ac.uk/interpro/) showed that PEL contains a signal peptide, a non-cytoplasmic domain, several transmembrane domains, and one undefined domain at the C-terminal (Figure 13). The transmembrane domain of PEL indicates that PEL is a

membrane-bound protein (Figure 13). Previous studies annotated PEL as a putative multi-transmembrane tonoplast protein of unknown function (Shimaoka et al., 2004). Alignment between *AtPEL* and *AtPEL* paralog sequences found that *AtPEL* has a special N-terminal sequence (including a signal peptide), a non-cytoplasmic domain, a cytoplasmic domain, and an unknown C-terminal domain (Figure 13). The identity of PEL protein sequence between different species is low (less than 40%). The C terminal of PEL shared a relatively higher identity (around 60-90%). In summary, the PEL protein have a conserved C terminal domain and variable N terminal signal domain. EMS-generated mutant is located on the cytoplasmic domain, and the domain after the stop code cannot be expressed (Figure 13). The mutation site suggests that the cytoplasm and C terminal domain might be important for the PEL function.

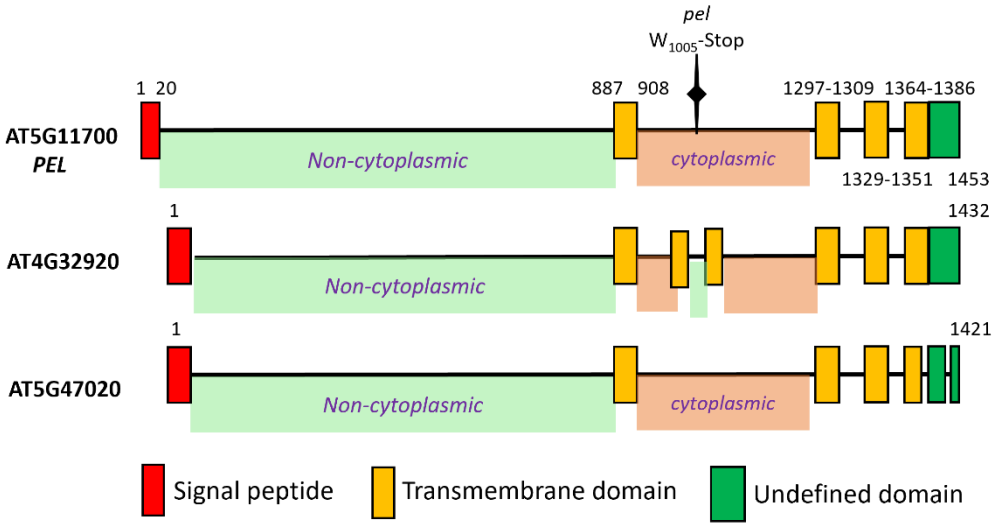

Figure 13. PEL structure and predicted function.

AT2G11700: *PEL*. AT4G32920 and AT5G47020: *PEL* paralogous. The EMS *pel* mutant changed W1005 to a stop code and terminated the translation at cytoplasm domain

4.2.3 The C terminal domain is important for PEL function.

From analysing the PEL sequence, The N and C terminal was found to be important n PEL function. Thus, PEL with the N and C terminal truncation was constructed and transferred into *jas pel* to test the complementation function respectively. As a result, neither the truncation of the N-terminal nor the C-terminal of PEL could complement the *jas pel* phenotype (Figure 14). Both the N and C terminals are essential in the PEL structure, but the two parts perform different functions. Microscopy images showed that the N-terminal truncated PEL is mis-located during the meiotic cell cycle and degraded at metaphase II (Figure 14). The signal peptide is a structure that can guide

the protein to a specific functional organelle. Since the N-terminal signal peptide is different between paralogs, the specific N-terminal sequence will guide PEL to distinctive membranes to perform its function. The C-terminal truncated PEL maintained the same localization as the full-length PEL but still could not recover the phenotype (Figure 14). However, different from the N terminal truncation, the C terminal truncation can maintain its cellular location during meiosis (Figure 14). Therefore, the C-terminal PEL is important for bioreaction, like protein-protein interaction and biochemical processes, during meiosis.

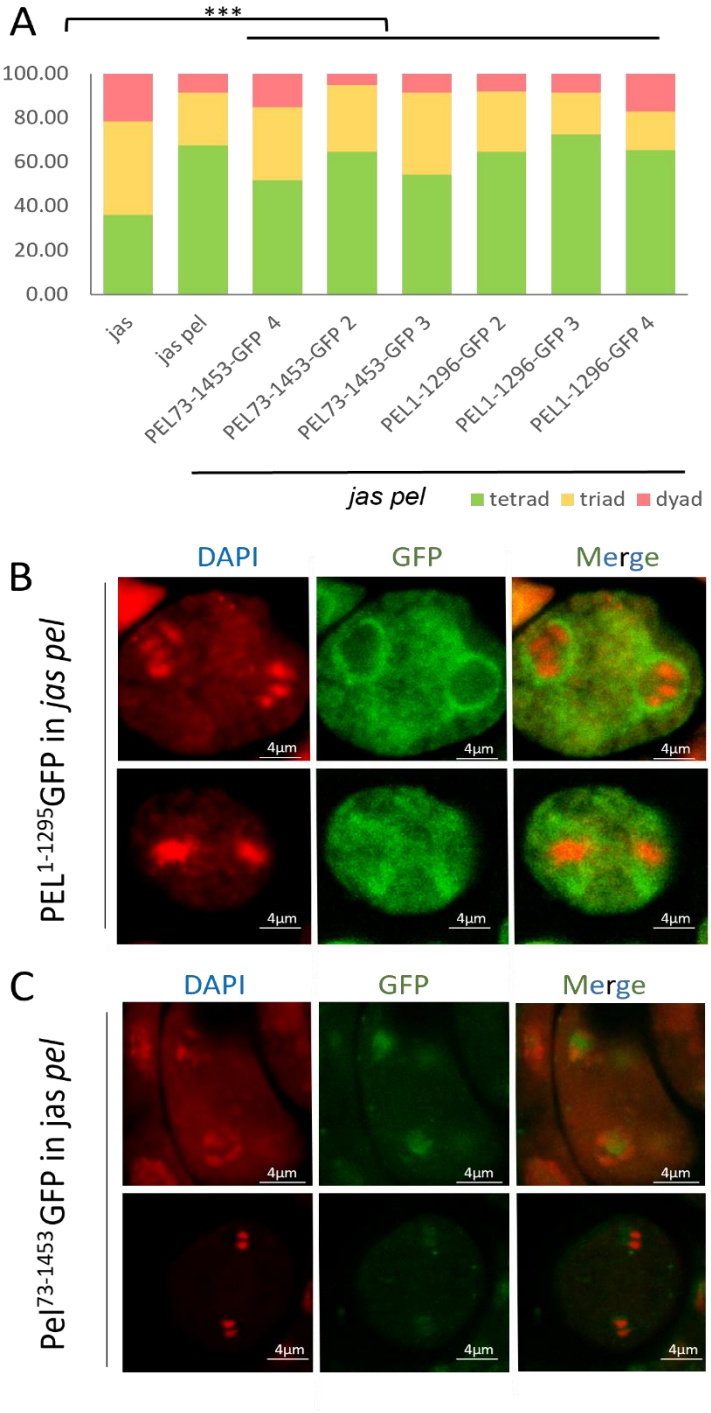

Figure 14. Truncation of the N and C terminals of PEL abolishes the PEL function.

*A) N and C terminal truncated PEL cannot recover the pel phenotype. (***p<0.001, using the Chi-square test). B) C terminal truncated PEL has the same subcellular localization as PEL1-1453 during meiosis. C) N terminal truncated PEL will be degraded during meiosis II.*

4.3 PEL$^{1295-1453}$ interacts with photosystem complex subunit protein.

4.3.1 Screening of the PEL$^{1295-1453}$ interaction proteins

A ubiquitin-split Yeast two-hybrid (Y2H) system was used to screen for possible interacting proteins of PEL. In this system, the ubiquitin sequence is split into two parts and ligated with the Bait and Prey plasmids sequence separately. When the Bait and Prey parts of the ubiquitin interact, a full ubiquitin protein is recognized by ubiquitin-specific proteases, releasing the transcription factor that activates resistant genes transcription (Figure 15).

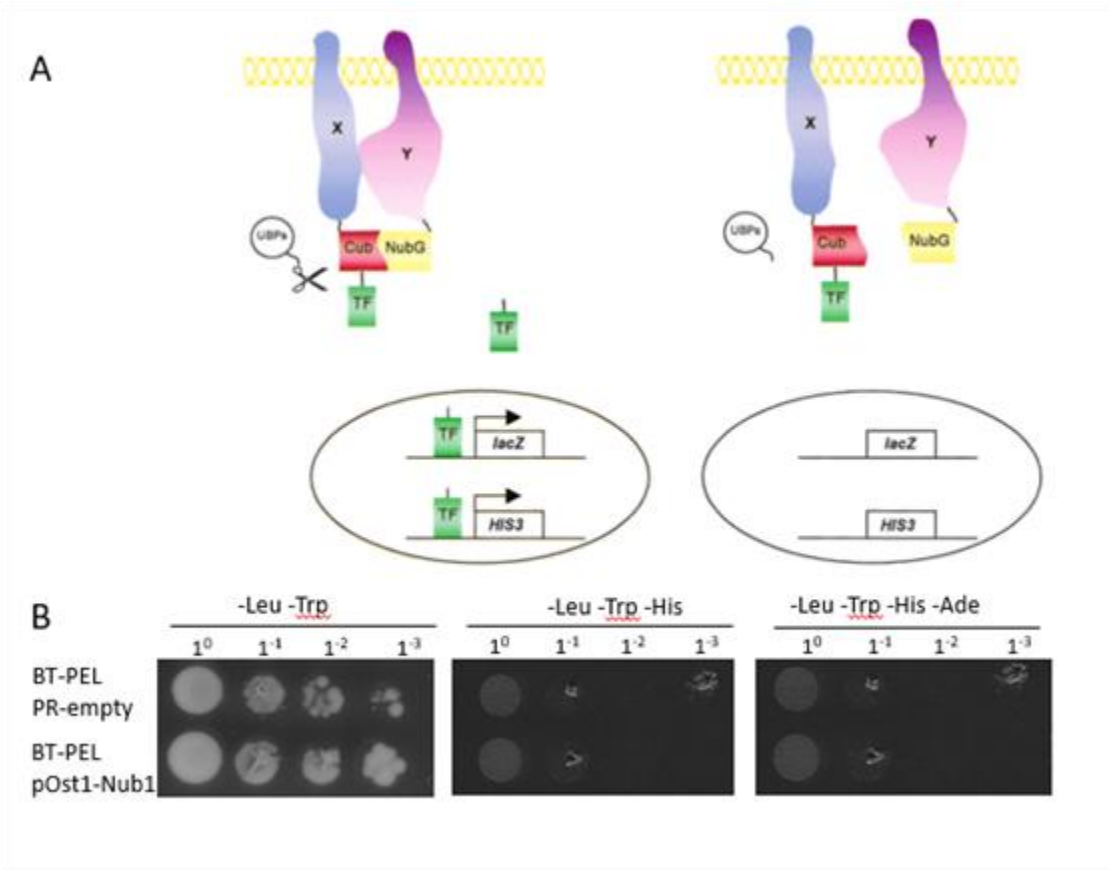

Figure 15. The ubiquitin-split Y2H system and functional assay in the Y2H system

A) When the tested protein X from the bait plasmid and protein Y from the prey plasmid interact with each other, the C and N parts of the ubiquitin protein are brought together. The ubiquitin protein performs its degradation function to release the transcription factor from the membrane. The transcription factor then enters the nucleus to activate *HIS3* gene transcription. Expression of *LacZ* and *HIS3* enables survival in histidine-deficient medium. the LacZ expression can show blue color in X-gal containing medium. The LacZ gene can be the second selection marker. B) *PEL*-BAIT cannot be functionally expressed in the Y2H system.

The transcription of the HIS3 gene will allow the yeast colony to grow on a selection medium (yeast SD medium -Leu -Trp -His) and strict selection medium (yeast SD medium -Leu -Trp -His -Ade). To ensure an accurate selection of interaction proteins, site mutation was applied on the N terminal of the Ubiquitin protein to reduce the affinity of N and C terminals interaction. On the other hand, the original version of N terminal ubiquitin protein (represented by NubI) can be used as a positive control. Due to the strong interaction affinity between NubI and Cub, the selection gene will remain active as long as the Bait and Prey proteins are positioned on the same side of the membrane.

To ensure correct folding and function of the PEL protein, the N-ubiquitin (NubI) plasmid, which encodes the ubiquitin protein sequence and has a high-affinity interaction with the C-ubiquitin (Cub) sequence, is co-transferred with the PEL bait plasmid. When PEL is properly folded, the C-ubiquitin and N-ubiquitin should be located on the same side of the membrane, activating selection marker genes and allowing robust growth. However, the transformation of the PEL Bait with the NubI plasmid yielded results similar to the negative control (Figure 15), suggesting that the Bait construction cannot express PEL properly in the yeast system. This is because of the special feature of transmembrane protein. The transmembrane proteins need to be folded and located correctly at different organelle membranes, which are regulated by complicated structures and pathways, like the signal peptide (Hong et al., 2022). The yeast and plant have different signal peptide systems, thus, the protein sequence from the plant might not be able to be properly folded on the endomembrane system (Hong et al., 2022).

Since the C-terminal domain has already been proven as an important functional domain of PEL, the C-terminal of PEL is used for Y2H screening (Figure 14). the C-terminal of PEL is tested to be properly expressed in the yeast system. Using the new constructs for interaction protein screening. The cDNA-library for screening is prepared from the closed flower buds. The constructed C terminal PEL Bait plasmid was also tested with the negative and positive control, and the co-transferred yeasts showed robust growth in the selection medium. The C terminal PEL bait plasmid can be used for further screening.

The Yeast hybrid screening was applied by co-transferring the bait and Prey plasmid and selecting positive colonies from the Strick selection medium. The positive colonies (around 200 colonies) from strick selection plates were then selected for a colony PCR to eliminate colonies that contain multiple DNA insertions or DNA insertion fragments less than 250bp. The plasmid DNA from remaining colonies (around 60 colonies) were

then cultured, extracted, amplified, and sequenced. Out of the sequenced 48 colonies, 20 colonies containing plasmids encoding in-frame DNA sequences were selected and shown in Table 1. Photosystem II subunit R (AT1G79040) appeared 5 times among the selected 20 colonies. Additionally, AT1G77030 and AT2G24765 are annotated as gamete development-related proteins and Golgi vesicle trafficking proteins, respectively (Table 3), and are interested in vesicle trafficking research.

Table 3. PELC terminal Y2H screening result

Colony ID	Gene	Annotation
5a	AT1G09210	Calreticulin 1b
8b	AT1G20693	NUCLEOSOME/CHROMATIN ASSEMBLY FACTOR GROUP
8c-2	AT1G29930	LIGHT-HARVESTING CHLOROPHYLL A/B-PROTEIN 1.3
8c	AT1G29930	LIGHT-HARVESTING CHLOROPHYLL A/B-PROTEIN
11g	AT1G77030	Required for functional maturation of male and female gametophytes. (CRT1)
1b	AT1G79040	photosystem II subunit (PsbR)
3D	AT1G79040	photosystem II subunit (PsbR)
11a	AT1G79040	photosystem II subunit (PsbR)
5d	AT1G79040	photosystem II subunit (PsbR)
3a	AT1G79040	photosystem II subunit (PsbR)
6d	AT2G21160	Translocon-associated protein
7a	AT2G21660	Encodes a small glycine-rich RNA binding protein
4c	AT2G24765	GTPase required for Golgi targeting of GRIP domain proteins (ARF3)
7d	AT2G35635	RELATED TO UBIQUITIN 2, RUB2, UBIQUITIN 7 (UBQ7)
8c	AT2G41840	Ribosomal protein S5 family protein
7c	AT2G43550	Defensin-like (DEFL) family protein
1C	AT3G23730	xyloglucan endotransglucosylase/hydrolase 16
4B	AT4G20150	excitatory amino acid transporter
4d	AT4G31290	Gamman glutamyl acyltransferase
5c	AT5G18230.4	NOT3

These 3 selected prey plasmids were transformed back into yeast with the bait plasmid to confirm the interaction between the C-terminal PEL and the selected fragments. Consequently, all 3 fragments showed positive results for the Bait-Prey interaction (Figure 16). Since the purified plasmid contains fragments of the corresponding gene, the Prey plasmid with the corresponding CDS sequence was constructed and transformed into yeast again. Interestingly, only AT1G79040 still showed a strong interaction (Figure 16). This result could be due to variations in protein folding. Many protein sequences can form non-covalent bonds to stabilize the functional structure of the protein. Missing a large fragment of the sequence disrupts the functional structure. Thus, the interaction between fragments may be altered in the full-length

protein. The reason why fragmented PEL is used in this experiment depends on our previous study of PEL structure. The C terminal PEL was found to be important in the complementary experiment. Meanwhile, the fragment used in this experiment contains several transmembrane domains. The membrane physically separates the expressed part from the other parts of the sequence.

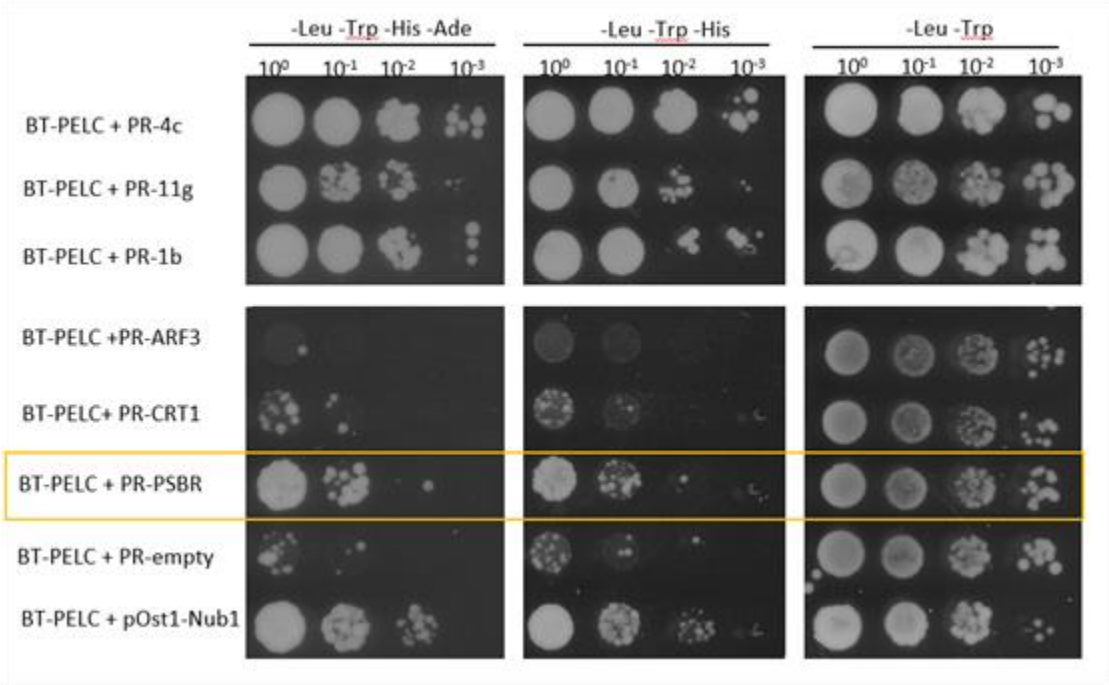

Figure 16. Yeast confirmation of interaction between identified candidate proteins and *PELC* terminal sequence

BT: bait plasmid background, PR: pray plasmid background. 4c, 11g,1b represent *ARF3*, *CRT1*, *PsbR* fragment separately. BT-*PELC*+PR-empty as the negative control. BT-*PELC*+pOst1-*Nub1* as the positive control

4.3.2 Photosystem II subunit R (PsbR) interacts with PEL C terminal domain.

PsbR is one of the subunit proteins in the photosystem II complex. The photosystem II complex is a group of proteins localized on the chloroplast thylakoid membrane in green plants, where it catalyzes light-induced electron transfer. PsbR has been suggested to be associated with the oxygen-evolving complex and is crucial for oxygen production and quinone reoxidation (Allahverdiyeva et al., 2013; Suorsa et al., 2006). Previous studies have shown that *psbr* leads to reduced light-harvesting efficiency without observable phenotypic effects on plant growth and organ development (Allahverdiyeva et al., 2013; Suorsa et al., 2006). Functional PsbR in leaf cells is observed to be located on the chloroplast, and post-translational modification is

required to maintain the stability of the PsbR protein (Zheng et al., 2022). PsbR requires SUMOylation modification under heat stress and is transferred into the chloroplast by TIC-TOC complexes. Mutation of both K51 and K48 SUMOylation sites (2KR) of PsbR prevents its entry into the chloroplast under high-temperature stress (Zheng et al., 2022). So far, no research has been carried out on PsbR localization in non-pigment plastids. Considering that PsbR protein is synthesized outside of the chloroplast and transferred through post-translational modification and membrane-located translocons, PsbR has a chance to encounter other vesicle membrane-located proteins before entering the chloroplast.

Bimolecular fluorescence complementation (BiFC) enables the direct visualization of protein-protein interactions in live cells without chemical or antibody staining. In this method, the reporter protein sequence (normally a fluorescent protein like YFP) is split into N- and C-terminal parts and tagged with the tested two proteins, respectively. Interaction between the tested molecules brings the reporter fragments into proximity, allowing the reporter fragments to reform the native three-dimensional structure and exhibit fluorescence. To confirm the interaction between $PEL^{1295-1453}$ and PsbR, BiFC is used to check the interaction in tobacco. Before the experiment, the CDS sequences of PEL, $PEL^{1295-1453}$, and PsbR tagged with GFP expression were tested individually. PEL didn't show any detectable GFP signal in this system and cannot be used for further experiments (Figure S2). $PEL^{1295-1453}$-GFP is predominantly located in the cytoplasm, while the PsbR-GFP protein is associated with organelles (Figure S2). Hence, $PEL^{1295-1453}$ and PsbR were expressed in the BiFC experiment. The N- and C-terminal fragments of YFP tagged at the N- and C-ends of $PEL^{1295-1453}$ were tested separately with corresponding PsbR vectors (Data not shown). As a result, NYFP-PsbR+$PEL^{1295-1453}$-CYFP showed the best interaction signal in organelles (Figure 17). Interaction signals were not observed in the cytoplasm and chloroplast, but in small organelles that might be peripheral vacuoles or lysosomes (Figure 17). Quantitative analysis also supports the microscopy results. The T1 combination (NYFP-PsbR + $PEL^{1295-1450}$-CYFP) showed dramatically higher interaction signals, while the other combinations do not show dramatic difference with the negative control (Chi-square test, $p<0.01$). $PEL^{1295-1453}$ can interact with PsbR. In dividing cells, the interaction signal between PsbR and PEL is found in the newly formed cell wall (Figure 18). Both organelle-located proteins contribute to vesicle trafficking during cell wall formation. Although the BiFC might have a false positive result, this data indicates the potential function of PEL-PsbR interaction.

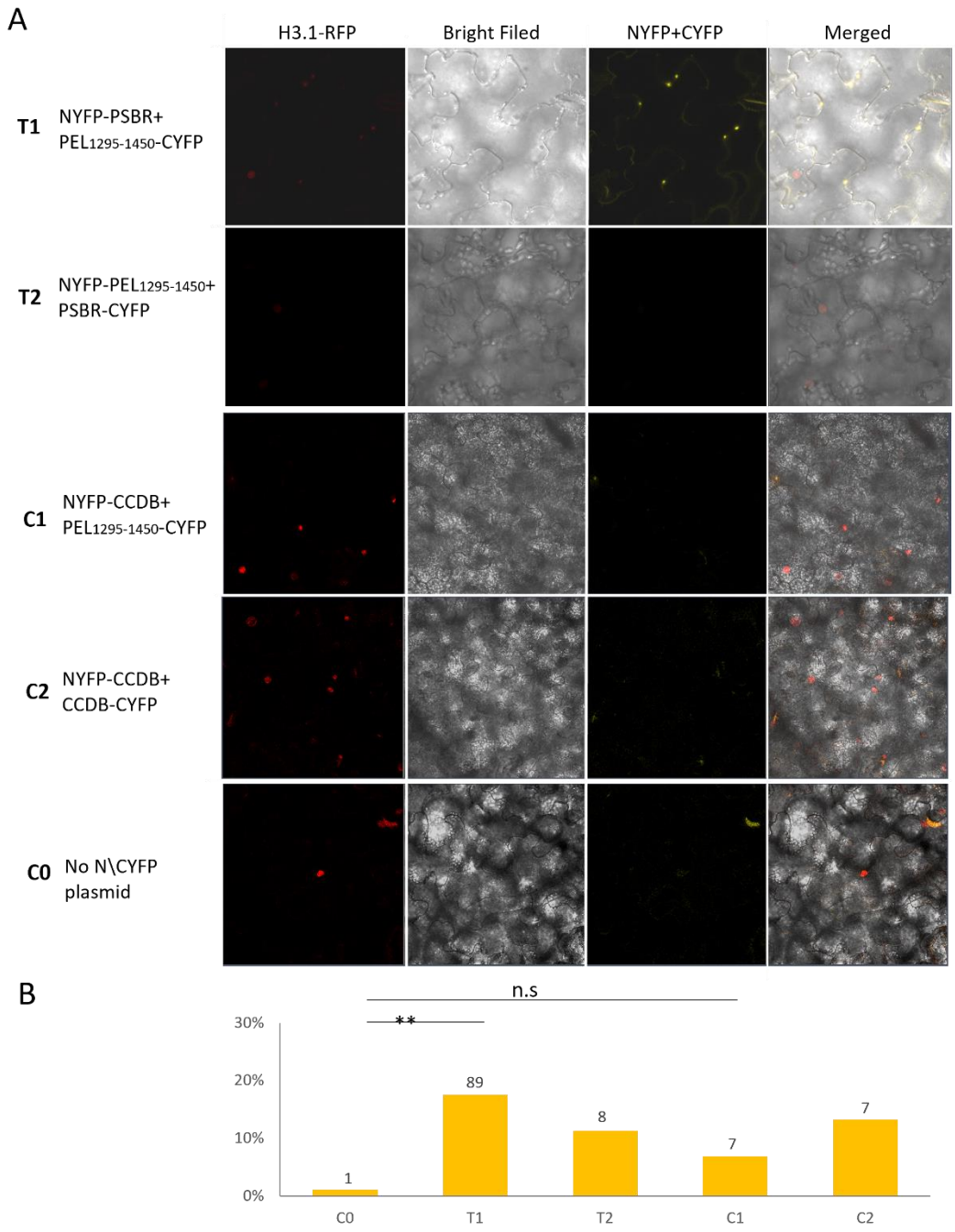

Figure 17. BiFC of PsbR and PEL interaction.

A) BiFC showed PEL$^{1295\text{-}1453}$ interact with PsbR in cell organelles. H3.1-RFP represent the nuclear in vivo. B) Quantitative analysis suggests a dramatically high level of interaction signal in *NYFP-PsbR+PEL$^{1295\text{-}1450}$-CYFP*. **p<0.01, n.s no significant. Using Chi-Square test. C0: No N\C YFP plasmid control. T1 have 89 positive cells counted: *NYFP-PsbR + PEL$^{1295\text{-}1450}$-CYFP*, T2 have 8 positive cells counted: *NYFP-PEL$^{1295\text{-}1450}$ + PsbR-CYFP*, C1 have 7 positive cells counted: *NYFP-CCDB + PEL$^{1295\text{-}1450}$-CYFP*, C2 have 7 positive cells counted: *NYFP-CCDB + CCDB-CYFP*.

T1
Dividing
cell

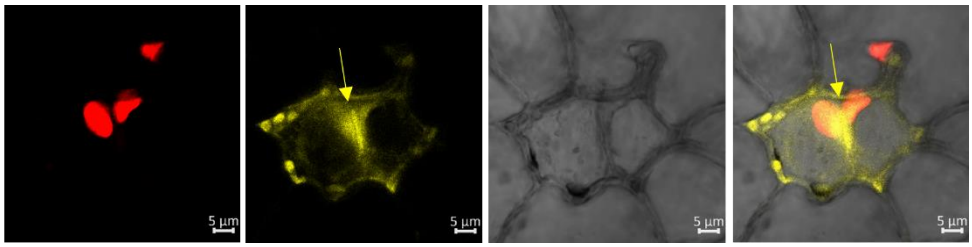

Figure 18. BiFC showed PsbR and PEL interaction at the new cell wall.

In the T1 combination*(NYFP-PSBR+PEL$^{1295-1450}$-CYFP*), the interaction signal is also found around the new cell well (see yellow arrow). The vacuole structure next to the nuclear is also visualized with weak interaction signal (yellow circle).

Since membrane trafficking pathways can vary among species and organs, the constructed overexpression plasmids of PEL$^{1295-1453}$-GFP and PsbR-RFP were also transformed into Arabidopsis plants to observe their co-localization in leaf protoplasts. After 3 days of dark treatment, the co-localization signal was observed in protoplasts. Strong signals were observed in peripheral vacuoles or tonoplast suggesting that PEL$^{1295-1453}$ also interacts with PsbR in Arabidopsis (Figure S3). The interaction in leaf cells further confirmed that the two proteins can encounter and interact within the cytoplasm.

Alphafold prediction was also utilized to confirm the interaction. The script and database resources were kindly provided by Dr. Amanda Souza Camara. Alphafold analysis of the interaction protein structure revealed that L1324 and K1395 from PEL interact with D105 and Y107 from PsbR, respectively (Figure 19).

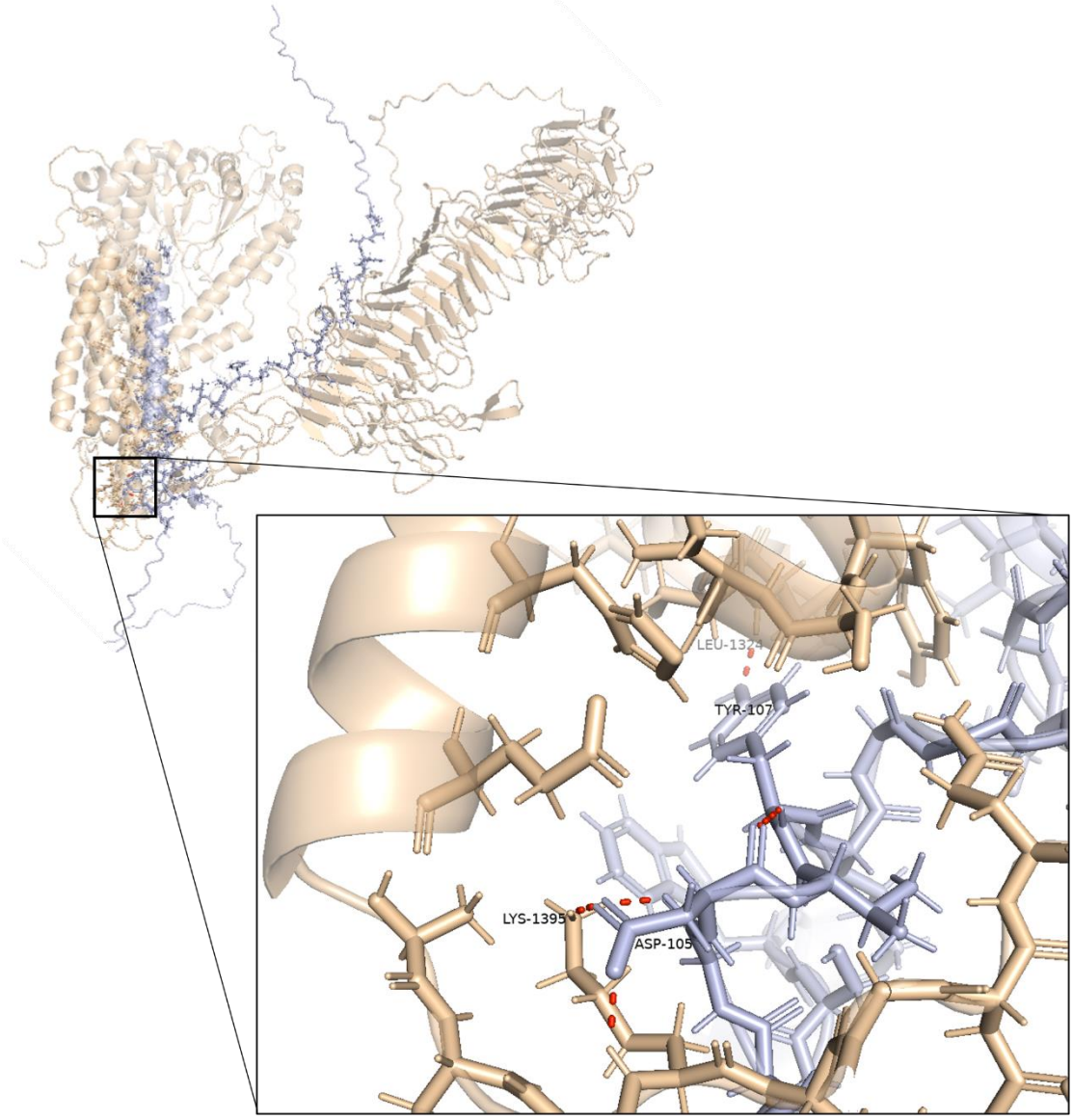

Figure 19. Alphafold 2.0 predicted the interaction of PEL$^{1295\text{-}1453}$ and PsbR

Gold color represents the PEL structure, blue color represents the PsbR structure. PEL and PsbR form non-polar bound at the transmembrane region and form polar bound between LYS1395-ASP105 and LEU1342-TYR107

These interaction sites have distances less than 3 Å, which is the criteria for strong interaction (Headd et al., 2007). Additionally, the transmembrane domain of both proteins (the helix structure at the upper left side of the interaction surface) showed non-polar bound interaction with a molecular distance of less than 4 Å. The predicted interaction residue suggests a closed molecular position between PEL and PsbR as well as the potential interaction site. Both *PEL* and *PsbR* are plant-specific genes, the interaction between these two proteins might suggest a plant-specific process during development. To understand the specific function of the interaction between *PEL* and *PsbR*, mutagenesis can be applied to the predicted sites in further study.

4.4 Ubiquitin-like superfamily protein (UBQL) interacts with PEL

In addition to the Y2H screening, existing databases also suggest that a Ubiquitin-Like superfamily protein (AT5G42220) can interact with PEL (BioGRID: https://thebiogrid.org/). UBQL protein consists of 879 amino acids, with a ubiquitin domain predicted at the N-terminal of UBQL. The rest of UBQL does not have a clear predicted structure but is shown to be a large proline-rich intrinsic disordered protein, a feature that often appears in chaperone proteins (Theillet et al., 2013) (Figure 20). The Large Proline-Rich family protein predominantly aids in inserting synthesized membrane proteins into the ER membrane to perform their function. It can also initiate degradation pathways to eliminate misfolded proteins. The intrinsically disordered region often appears in non-soluble proteins, suggesting that UBQL is located between the soluble phase and the non-soluble phase.

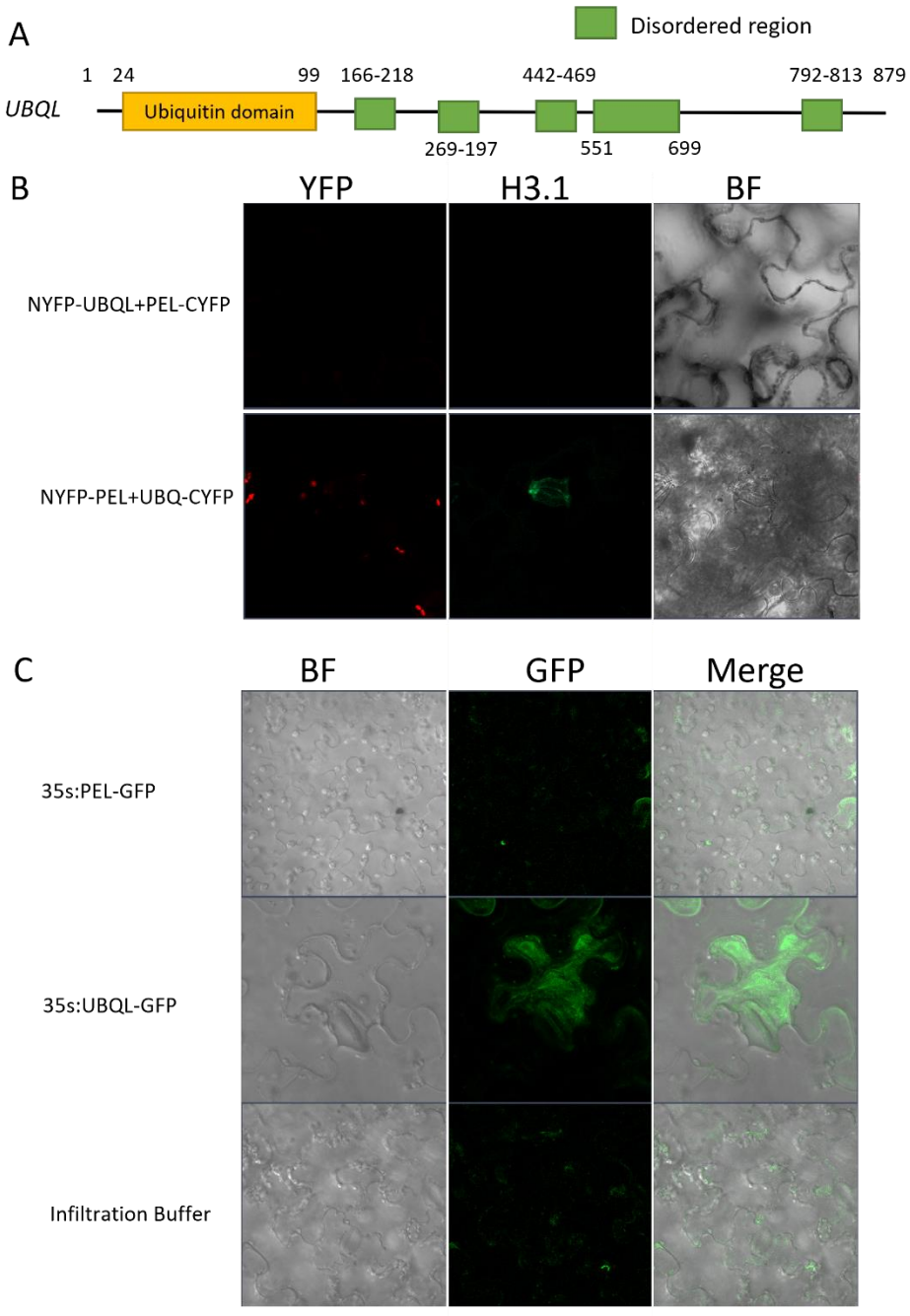

Figure 20. UBQL structure and interaction with PEL.

A) UBQL protein domains. B) Testing of PEL and UBQL interaction in the BiFC system. No positive interaction was observed C) PEL-GFP cannot properly expressed in tobacco cells but the UBQL-GFP can be expressed and assembled with cytoskeleton.

4.4.1 Confirming the interaction between UBQL and PEL

The database information from BioGRID is based on Y2H data. However, in the Ubiquitin-split Y2H system, PEL full length cannot be properly expressed. Therefore, I

tested the interaction with the same BiFC system used before. N and C terminal fragments of YFP are fused to the N and C ends of the PEL full-length sequence separately, and the corresponding UBQL plasmid is co-transferred with PEL constructs. The interaction between UBQL and PEL does not show clear co-localization in all tested groups (Figure 20). To confirm that technical issues do not cause negative results, a control plasmid that can express H3.1-RFP driven by the same promoter with the BiFC is transferred and checked. The expression of H3.1-RFP is very strong on the 3rd day after infiltration (Figure 20). Meanwhile, PEL-GFP and UBQL-GFP driven by the 35s promoter were also transferred and checked to eliminate the problem of plasmid construction (Figure 20). No clear signal was observed after infiltration of the PEL-GFP plasmid, suggesting that the expression of the full-length PEL protein is very low or degraded in *Nicotiana benthamiana*. In contrast, UBQL-GFP showed a strong signal on the cytoplasm. According to the shape and distribution of the Signal of UBQL-GFP, UBQL colocalized with cytoskeleton filaments. This result matched the previous findings that ubiquitin-related or ubiquitinated proteins are mainly enriched in the actin cytoskeleton and endomembrane organelles (Hitchcock et al., 2003).

4.4.2 *ubql* genetically inhibits *jas pel* phenotype.

Although the BiFC interaction between PEL and UBQL in tobacco was not successful, *ubql* shows a significant difference in phenotype in the *jas pel* background. The phenotype of *jas pel ubql* is different from *jas pel* in meiosis II, microspore stage, and pollen. *jas pel ubql* produced larger pollens that represent 2n pollen compared with *jas pel*. The microspore stage of *jas pel ubql* produced 70% dyads and triads, similar to the *jas* mutant (Figure 21). When zooming into meiosis, the mutant also showed different phenotypes in metaphase II. Chromosome distance measurements also suggest that the triple mutant has a dramatically closer chromosome distance at metaphase II compared to *jas pel* (Figure 22). The recovered phenotype in the *jas pel* is abolished in the *jas pel ubql* mutant. Meanwhile, the metaphase II stage images of *jas pel ubql* also showed disturbed organelle bands and very closed chromosomes. The chromosome distance measurements showed a dramatic difference compared with *jas pel ubql* (Figure 22). Taken together, the *jas pel ubql* showed a phenotype very similar to *jas*, the *ubql* inhibit *pel* phenotype. The UBQL acts as a counter-effect regulator of PEL.

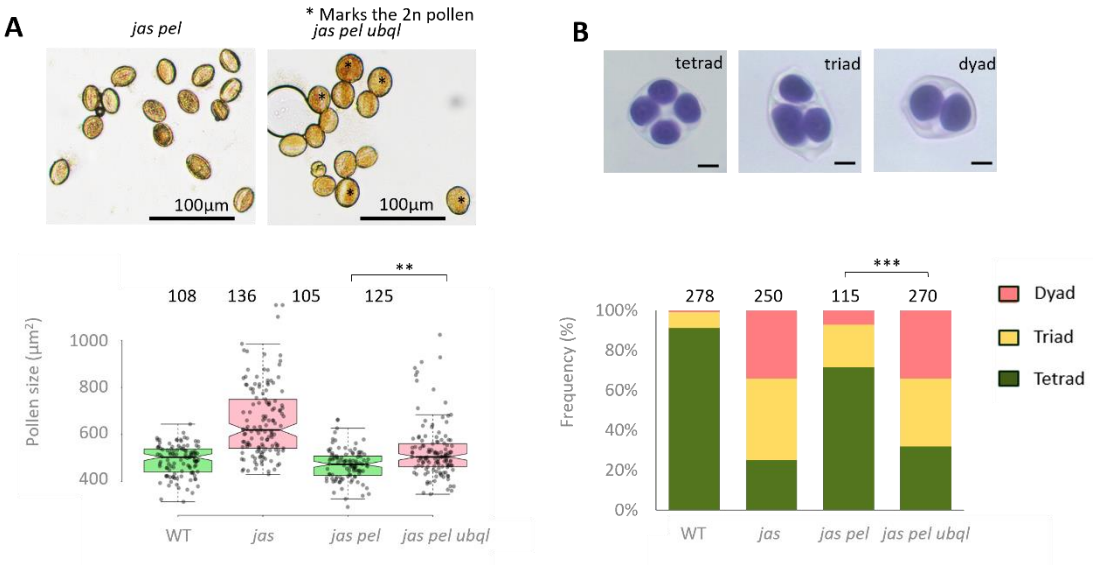

Figure 21. *jas pel ubql* have a diferent phenotype of *jas pel.*

A) The *jas pel ubql* produces more unreduced pollen compared with *jas pel*. *** p<0.001, n.s no significant difference. Using the one-way ANOVA test. B) The *jas pel ubql* produces more dyad and triad in the microspore stage. *** p<0.001. Using the Chi-square test.

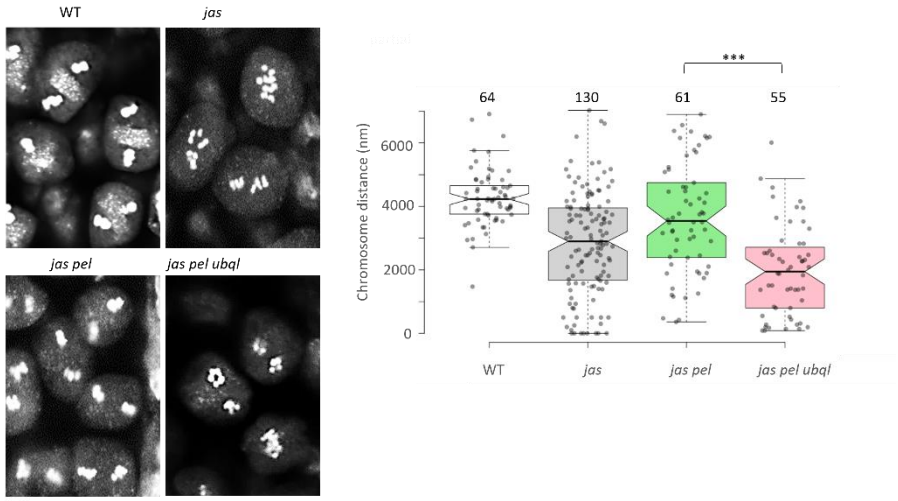

Figure 22. The chromosome distance is shorter in *jas pel ubql*

A) The organelle band in *jas pel ubql* is disappeared in the Metaphase II cell. B) The chromosome distance is shorter in *jas pel ubql*. *** p<0.001. Using one-way ANOVA test.

4.4.3 PEL-UBQL protein-protein interaction and functional prediction.

Since the PEL-UBQL interaction cannot be detected through the Y2H and BiFC. It is possible that PEL expression *in vitro* is misfolded and cannot perform native function. Therefore, the Alphafold tool was used to find possible interaction sites between PEL and UBQL (Figure 23). There are two interaction regions predicted, the ubiquitin domain of UBQL can interact with the non-cytoplasmic domain of PEL, while near C terminal of UBQL can interact with the cytoplasmic domain of PEL (Figure 23). There are 3 major groups of interaction bound found between PEL and UBQL. On the cytoplasmic domain of PEL, the W1028, R1029, and K1031 of PEL interact with E758, Q753, and G766 of UBQL separately through polar bound (Figure 23). The E758, Q753, and G766 are located at the soluble part of UBQL, which made it possible to form stable polar bonds with another protein. Between the transmembrane domains of PEL, the R862 of PEL interacts with H799 of UBQL. In the non-cytoplasmic domain of PEL, the Q365 interact with N26, T88 and G86 of UBQL. The EMS mutagenesis can disrupt PEL function with a stop code at W1005, suggesting that the cytoplasmic domain is also important in PEL function.

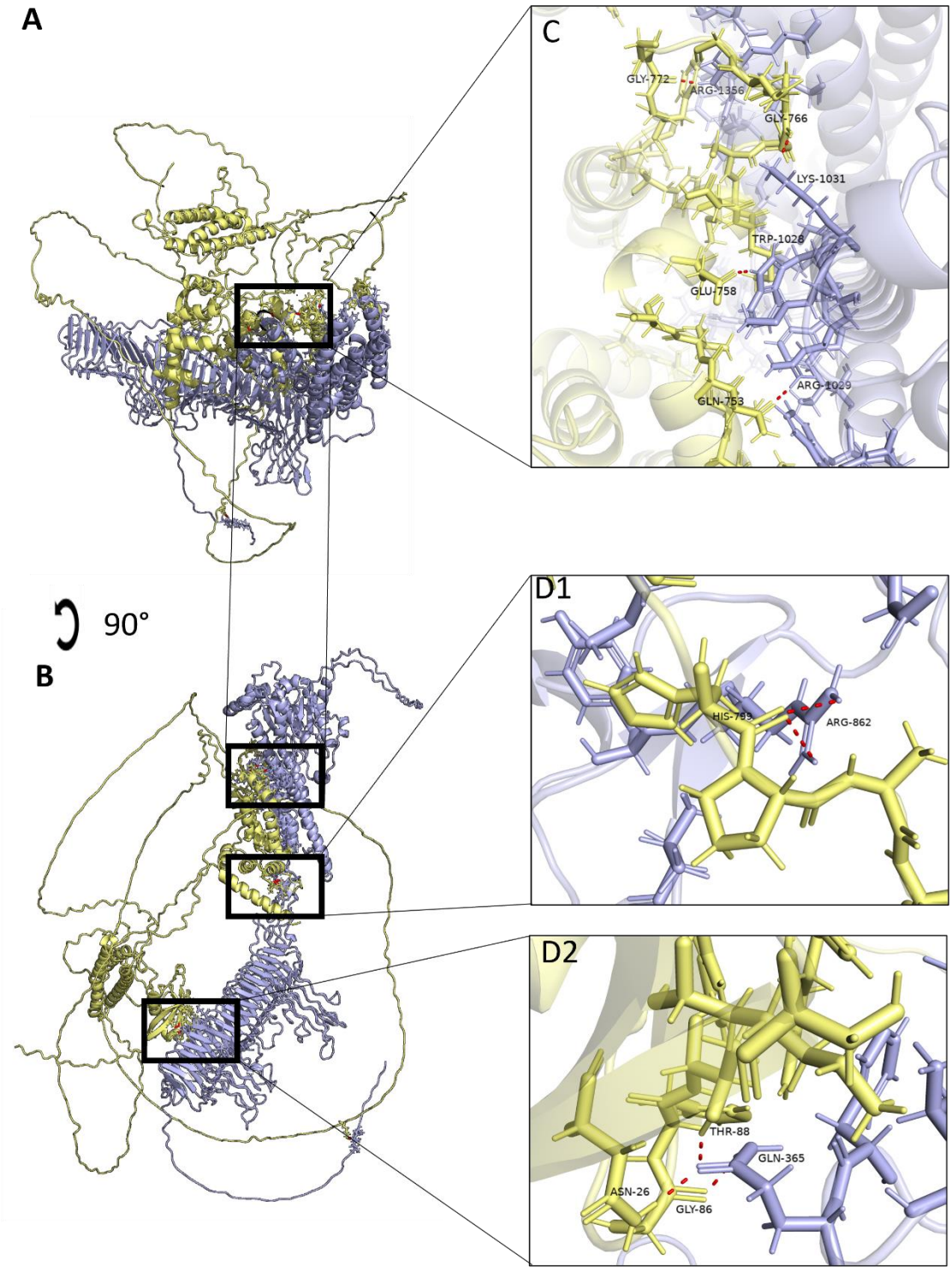

Figure 23. Predicted interaction model of PEL and UBQL.

The yellow colour represents UBQL, purple colour represents the PEL. The polar bound is labelled in a red dotted line. A) Top view of the interaction protein. B) side view of the interaction protein. C) interaction site in the cytoplasmic domain. D1 and D2) interaction site in Non-cytoplasmic domain.

According to the proteomic data of ubiquitin-like superfamily protein, the ubiquitin superfamily protein family can act as a chaperon protein to stabilize the transmembrane protein and degrade useless protein. UBQL belongs to the BAG6 complex, but the real function is not well studied in meiosis. There are two major models to describe the function of the BAG6 complex protein including the ubiquitin superfamily protein family (Figure 24). BAG6 complex can activate vesicle trafficking through stabilizing small GTPase (Miyauchi et al., 2023) (Figure 24). The ubiquitination-initiated degradation also requires signal cascades to active ubiquitination sites, hence, presenting the ubiquitin-like domain does not essentially indicate ubiquitination-initiated degradation (Takahashi et al., 2019) (Figure 24).

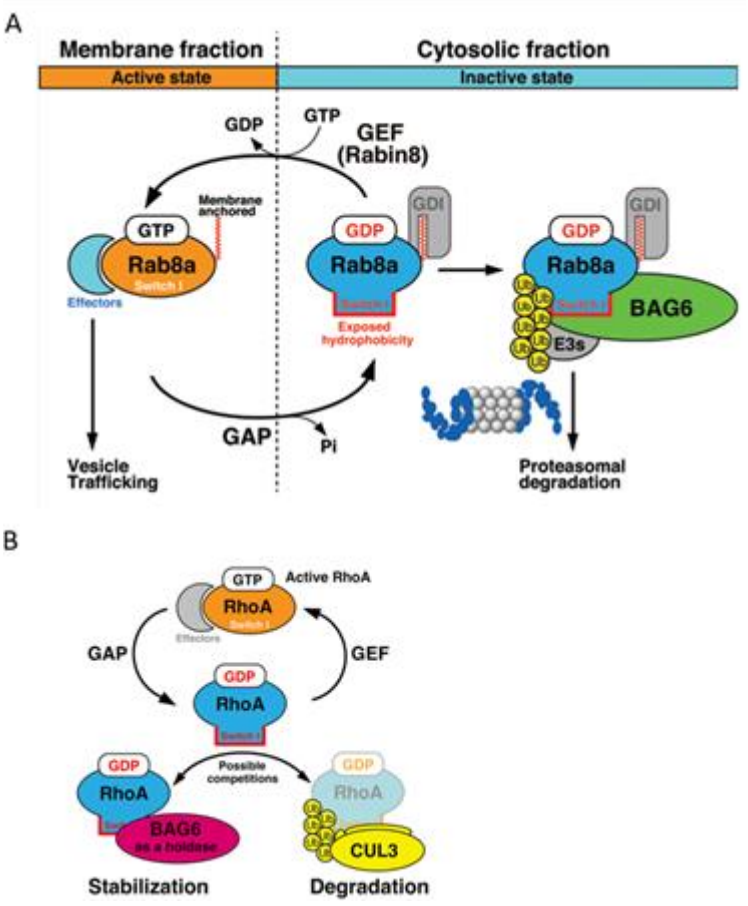

Figure 24. Two existing models of the ubql-related vesicle trafficking pathways

The degradation model of BAG6. BAG6 interacts with inactive Rab8a to degrade the Rab8a GDPase and prevent vesicle trafficking indirectly (Takahashi et al., 2019). B) The protection model of BAG6. BAG6 complex protects Rho GDP during stress fibre formation and maintains the integrity of actin fibre (Miyauchi et al., 2023).

According to the research in animals and yeast, there are two possible functions of UBQL. i) If the PEL non-cytoplasmic domain interacts with the UBQL ubiquitin domain, PEL can inhibit the ubiquitin-initiated degradation reactions through interaction with UBQL. ii) if the PEL cytoplasmic domain interacts with the UBQL C terminal area, the UBQL and BAG6 complex can insert PEL protein into the ER membrane. Experiments were carried out according to different hypotheses.

4.4.4 The *pel* phenotype is independent of ubiquitin-initiated proteasome degradation

To further confirm that Ubiquitinated protein degradation is not active by the ubiquitin domain in UBQL. Proteasome inhibitors, like MG115, were applied to treat *jas pel* meiotic cells. MG115 is a type of short peptide consisting of Z-LL(Nva)-CHO, often used as a specific and reversible inhibitor for the proteasome. If the interaction happened, *jas pel* should show *jas pel ubql* phenotype after MG115 treatment. If PEL inhibits the degradation function through interaction at the non-cytoplasmic domain, the MG115 treatment on *jas* pel should show *jas pel ubql* phenotype. After 24 hours treatment of MG115, the chromosome distance during metaphase II is measured in non-treated and treated groups. Compared with the nontreated group, the proteasome inhibitor does not show any significant difference (Figure 25). Since MG115 is a relatively large molecule, and the absorption rate of the meiosis cell is not well studied, it is possible that the MG115 cannot be transferred through the cells outside of meiosis. The KNL2-GFP plant is used as a positive control to further confirm if MG115 entered the male meiosis.

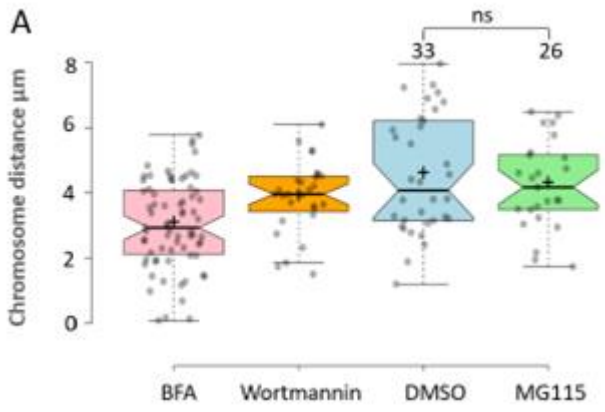

Figure 25. Proteasome inhibitor does not influence jas pel phenotype

MG115 treatment does not influence meiotic division in *jas pel* (n.s. No significant difference. Using one-way ANOVA test).

4.4.5 The PEL$^{909-1296}$ interacts with UBQL

According to the protein structure analysis and functional analysis, the cytoplasmic domain is highly possible to interact with UBQL. PEL contains several transmembrane domains and UBQL only contains disordered domains but not transmembrane. The PEL protein penetrates the membrane through the transmembrane α helix, leaving some parts inside of the membrane and some parts outside of the membrane (Alberts B, 2002). While the UBQL is potentially located between the lipid phase and soluble phase and is embedded in only one side of the membrane. A Y2H experiment was carried out to test which part of PEL can interact with UBQL. As the Full Length of PEL cannot be properly expressed in the yeast system (Figure 15). PEL fragments from different domains were expressed in the Y2H system to test the interaction. The PEL$^{1297-1543}$ are also tested since deletion of this part cannot recover the *jas pel* phenotype (Figure 14). The PEL$^{1297-1543}$ are properly expressed in bait plasmid but cannot interact with the UBQL protein in prey plasmid (Figure 26).

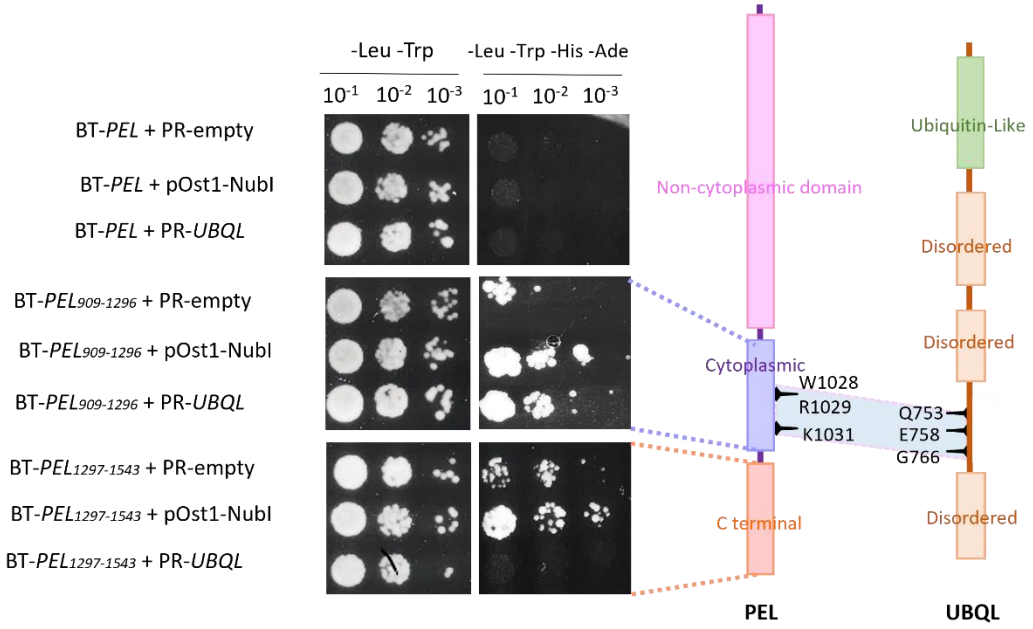

Figure 26. The confirmation of interaction domains between PEL and UBQL

The predicted interaction site between PEL and UBQL was located on the C terminal domain and the cytoplasmic domain. The C terminal domains and cytoplasmic domains are expressed separately in yeast to test the interaction. The PEL cytoplasmic domain-bait and UBQL-prey plasmid showed strong interaction compared to the negative controls, while the C-terminal domain of PEL do not show interaction compared to the negative controls.

In the same Y2H system, $PEL^{909-1296}$ is functionally expressed in yeast. Co-transformation with the *UBQL* sequence on the prey plasmid showed a robust growth in selection medium, suggesting that PEL interacts with UBQL through the cytoplasmic domain (Figure 26). UBQL potentially acts as a chaperone protein to protect PEL in the ER membrane and finally ships to the vacuole to perform its function.

4.5 Function of the actin filaments in organizing the organelle band

In the first part of the results (Chapter 4.1), this study uncovered the relationship between PEL and vesicle trafficking pathways. However, the later-defined interaction protein cannot explain how PEL influences exocytotic vesicles. The cytoskeleton, as an important structure for organizing vesicle trafficking and chromosome division, can regulate vesicle trafficking during the cell cycle. In plant cells, vesicles that transfer within cells are part of the endomembrane trafficking system. Many organelles have been reported to interact with actin organizations. For instance, an ER-specific myosin organizes vesicle positioning and F-actin orientation (Ueda et al., 2010), while a tonoplast-specific marker can reorganize actin filaments during stomatal closure induced by plant immunity (Hawkins et al., 2021). Actin filaments also provide the forces necessary for the dynamics of organelles and vesicles. Myosin, a group of motors protein, can generate pulling forces to move vesicle along the actin filaments (Duan & Sun, 2018; Schuh, 2011) Actin filament formation at the intermembrane system can drive several cellular processes, such as endosome sorting and recycling, exocytosis, and autophagy (Rottner et al., 2017) (Romero et al., 2004). Overall, actin filaments act as the "pathway" guiding trafficking vesicles in plant mitotically dividing cells. Therefore, I hypothesized that actin performed a similar role in meiotic cells.

The actin filament is a highly dynamic structure in live cells. Actin monomers assemble from the + end and disassemble from the – end during various biological activities. To investigate the organization of actin filaments, several methods are tested to visualize actin structure. Lifeact is a 17 amino acid peptide that can specifically stain F-actin in eukaryotes (Riedl et al., 2008). By tagging the lifeact sequence with a fluorescent protein, the F-actin signal can be visualized *in vivo*. The constructs were made based on the published sequence and transferred to *Arabidopsis*. But the T1 plants do not show observable signal in meiosis (Figure 27). Observing the signal of lifeact-RFP signal in the root cell under the microscope is impossible. The RFP signal is expressed in all layers of cells, identifying the focused cell is very difficult without an additional marker. Considering the difficulty of the lifeact method, another method seems to be a better choice. Phalloidin staining is a traditional method for actin staining (Romani et al., 2021), a fluorescent dye conjugated with phalloidin was used to stain actin in different

mutant backgrounds.

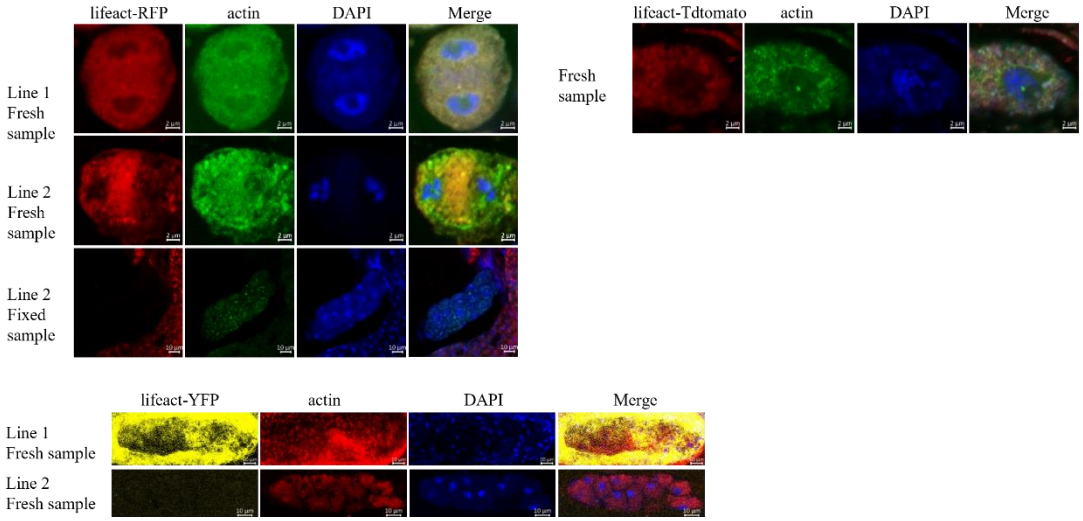

Figure 27. Lifeact-fluorescent protein signal location during meiosis.

Three different constructs of lifeact was tested in this study. A) lifeact-RFP constructed by our group. It showed good signal in the fresh sample. But the actin kept degrading as time goes. The general signal of actin is very weak. During metaphase II, the RFP signal did not match the phalloidin staining signal. The RFP signal is assembled at the middle zone, but the phalloidin staining signal is largely degreed and does not have a clear location area. We have also tried low concentration formaldehyde fixation, the phalloidin staining quality have a dramatic improvement after the fixation, but the RFP signal is totally lost. B) The lifeact-YFP construct from Prof. Marie-Cécile Caillaud was tested in fresh sample. The plant have strong signal in root but no fluorescent in meiosis. The image of one lobe showed that the signal is strong in somatic cells, but dark at the meiosis cell in the middle. Removing of the somatic cell clearly showed no signal of meiosis cell. C) The lifeact-Tdtomato constructs from Prof. Arp Schnittger's lab were tested in the fresh sample. The plant have a good meiosis signal, but similar to the lifeact-RFP construct, the lifeact signal did not match the Phalloidin stain result. In prophase, the actin signal in the nuclear envelope is missing in Tdtomato signal.

The Phalloidin staining result showed that actin forms a filament structure around the nuclear envelope and plasma membrane before metaphase I. At metaphase I, spindle microtubules are established and assist chromosome separation, and actin filament structures are associated with the spindle structure. From anaphase I until telophase I, a phragmoplast-like structure is formed between two nuclei, and actin is recruited to the microtubule (Figure S4). During meiosis I, actin is largely co-located with tubulin, but the condition changes at metaphase II (Figure 28) (Figure S4). The actin filament was located outside the DAPI-stained vesicles at metaphase II (Figure 28). In other

dicot plants like Magnoliaceae, actin also have a similar location (Dinis & Mesquita, 1993). When *jas* disrupts the organelle band, the actin filament structure invades the disrupted organelle band (Figure 28). In contrast, actin loses its filament structure and shows dot shape signals in the *jas pel* during metaphase II (Figure 28), suggesting that the actin filament was disassembled in the *jas pel*. According to research in female meiosis, the actin filament is organized as a network in the cytoplasm. In WT male meiosis, the presence of JAS and the organelle band separate the actin network into two parts to maintain nuclei position on both sides of the organelle band. When JAS is depleted, the organelle band is disordered. The disordered organelle band cannot limit the actin filament anymore. Assembly of the actin network towards the organelle band will bring nuclei to the middle area, causing closer chromosome distance. While in *jas pel*, the polymerization of actin is inhibited and the actin network is defective to move nuclei.

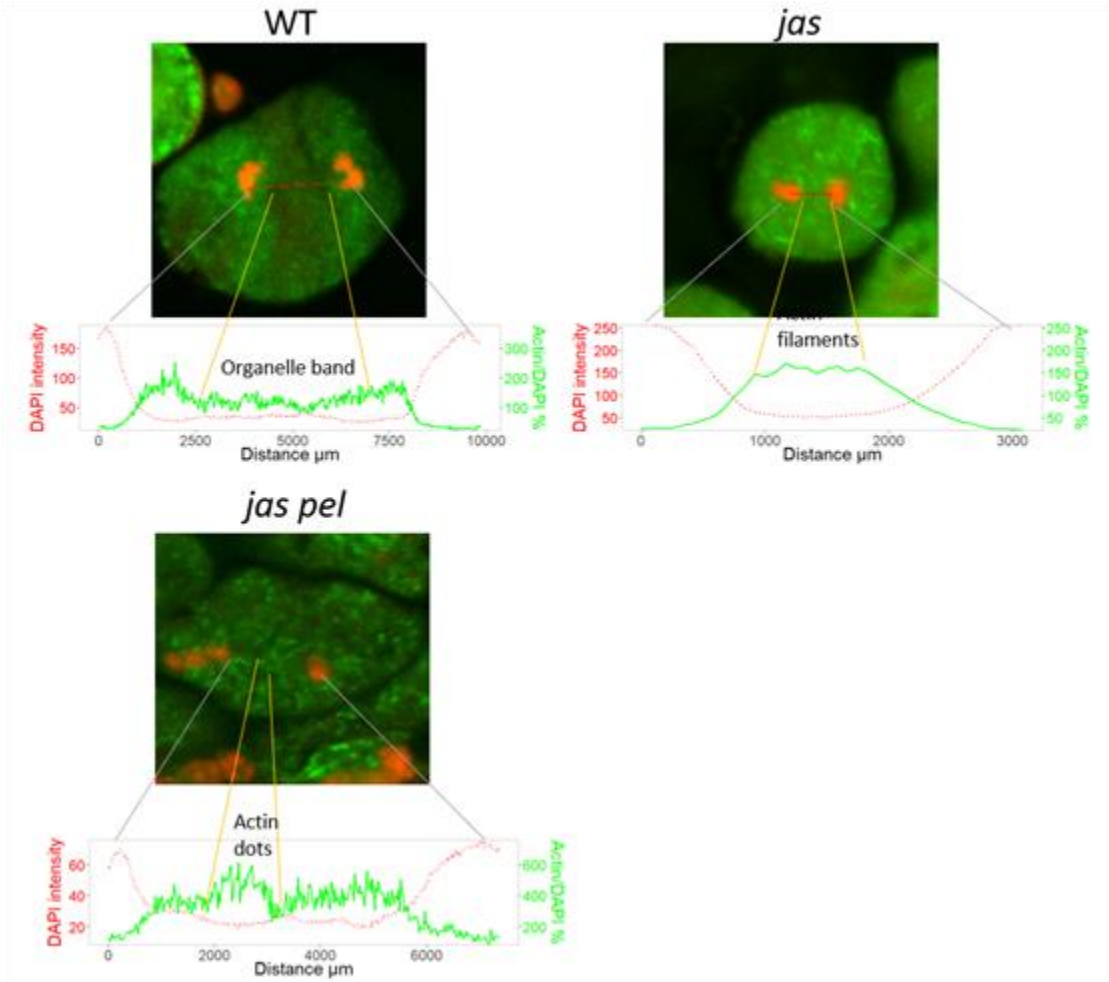

Figure 28. Actin stain during metaphase II in WT, *jas, jas pel*

Red line: λ=405-450 signal intensity measured by ZEN 2.0. Green line: the signal intensity of λ= 488-530 versus the signal intensity of λ=405-450

5 Discussion

5.1 Vesicle trafficking is important in maintaining the organelle band

5.1.1 *pel* maintains the organelle band

In a previous publication, *JAS* was reported to be the key regulator of the organelle band during meiotic division(Brownfield et al., 2015). JAS is located on the organelle band (Brownfield et al., 2015). The presence of JAS maintains the organelle band at metaphase II, while the absence of JAS disrupts the organelle band. *pel* can recover the JAS phenotype and genetically negatively regulate the *jas* phenotype. In this study, PEL is located in the cytoplasm outside of the organelle band and predominantly colocalizes with the vacuole membrane (Figure S5). PEL can partially recover the unreduced gametes produced by *jas* without fully recovering the organelle band.

Vacuoles as an important storage vesicle are recruited to the phragmoplast during mitosis. The phragmoplast organized vesicle trafficking model in mitosis has a dramatic difference from the real case in the *Arabidopsis* male meiotic cell cycle. The mitosis will build a cell wall after the chromosome division, and the vesicles transferred to the mid-zone will be physically fused (Jürgens, 2005; Khoso et al., 2023). But in *Arabidopsis* male meiosis, the organelle band, instead of the cell wall, is formed. The dynamic organelle band needs to be maintained from the telophase I until the end of meiosis. JAS located in the organelle band can stabilize the structure during the cell cycle. While PEL continuously generates a contrast effect to achieve a dynamic balance with JAS. There are many possible ways that PEL could influence, For example, the cytoplasmic streaming force driven by the spindle dynamic and chromosome division (Koc & Storme, 2022) and the organelle trafficking regulator that can increase the dynamic of organelle band as a strategy under stress condition (Koc & Storme, 2022).

5.1.2 *pel* does not fully recover the *jas* phenotype

The recovered organelle band in *jas pel* is different from the organelle band in WT. PEL can inhibit organelle disorder at metaphase II but is not directly involved in regulating the JAS function. The recovery function of the *pel* cannot fully complement the *jas* phenotype in different aspects. i) The DAPI-stained organelle band is not fully recovered since the organelle band in *jas pel* is wider and lacks clear boundaries. ii) The non-DAPI-stained organelle band vesicles are also not fully recovered. The PM marker is not recovered in the *jas pel*, while TGN and vacuole markers show wider signals at the midzone. In meiosis, very little research has been carried on, the study of the difference between the full organelle band and the partial organelle band are

still on going. From this study, partial organelle band have less types of vesicles (TGN and tonoplast derived vesicles) in order. However, the causative regulator of vesicles as well as other structures involved in organelle band formation is still unsure. Research in mitosis might provide some insight for further study. In plant mitosis, a disk-like phragmoplast is built up when the vesicles start to assemble at the midzone (Jürgens, 2005). Then, as the vesicles assemble, the disk-like phragmoplast becomes more condensed and expands from the middle to the periphery area, forming what is called a ring-like phragmoplast (Esseling-Ozdoba et al., 2009). The ring-like phragmoplast can then form cell well by recruiting vesicles containing biosynthesized material. The ring-like phragmoplast is similar to the full organelle band functionally and structurally. Proteins like myosin VIII and PHRAGMOPLAST ORIENTING KINESIN (POK) have been identified to assemble at the division plane (Sinclair et al., 2022). The elimination of these division plane-maintaining proteins will extend the time of the disk-like phragmoplast without forming a ring-like phragmoplast, and lead to cell wall synthesis errors (Kumari et al., 2021; Wu & Bezanilla, 2014). *jas* might perform a similar maintaining role in meiosis. The recovered organelle band in the *jas pel*, which is similar to the disk-like phragmoplast, can partially allow cell division but still can cause nuclear restitution in a low percentage.

5.1.3 *pel* recover *jas* phenotype depends on specific vesicle trafficking pathways

The signal of marker lines under different genetic backgrounds has different locations in meiosis. In WT, almost all the tested markers are located in the organelle band area, indicating that the presence of JAS can stabilize all the vesicles that comprise the organelle band. While in *jas* mutants, most of the vesicles show asymmetric distribution at metaphase II, suggesting that the vesicles are being pushed away from their original location. While in *jas pel* mutants, the asymmetric distribution of different markers is recovered to different levels. TGN marker and vacuole marker are shown to be recovered, while the PM marker is not recovered in *jas pel*. As the result showed in Chapter 4.1.2, no partial or full organelle band is observed after the BFA treatment in *jas pel*. The BFA-inhibited pathways (including TGN and Vacuoles) are necessary to maintain the recovered organelle band in *jas pel*. Although the molecular mechanism regulated by PEL is unclear, the organelle band organization in *jas pel* cannot be successful without the BFA inhibited vesicle trafficking pathways (Figure 29). We are not sure whether the vesicle trafficking maintains quiet in WT, since PEL is located in the cytoplasm in both WT and *jas*. Thus, the arrow of exocytic vesicle trafficking in *jas pel* only suggests that the vacuole vesicles are relocated to the middle zone in *jas pel* compared with *jas*. The in vivo vesicle movement is not essentially as the arrow suggests.

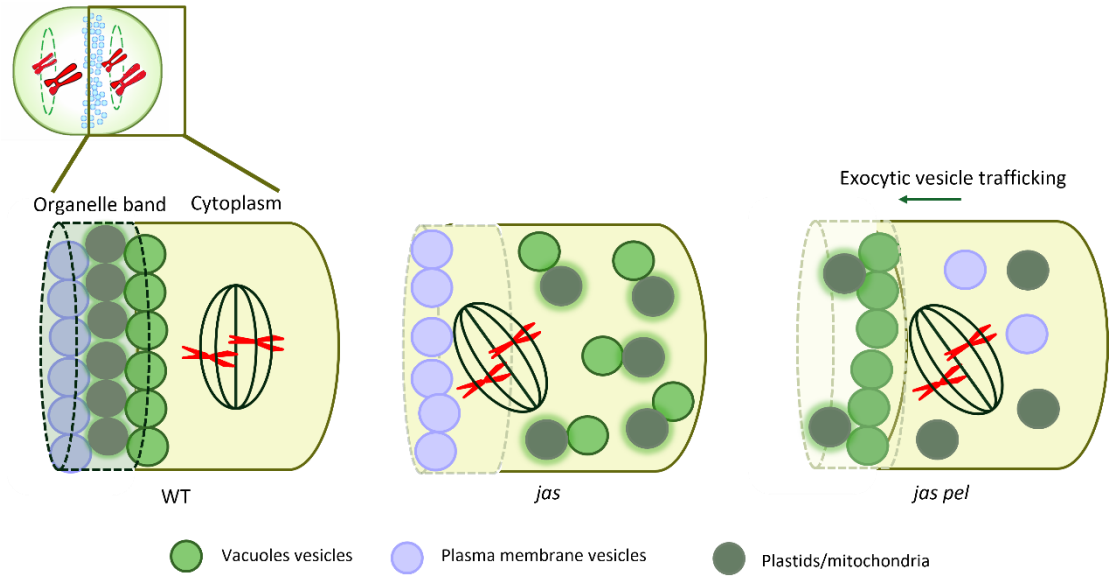

Figure 29. Model of the organelle band organization in WT, *jas, jas pel*

In WT, all the tested vesicle are associated at the middle zone and consists of organelle band to separate spindles. In *jas*, only plasma membrane derived vesicles remains at the middle zone, but cannot separate spindle. The other vesicles are disordered. In *jas pel*, with the help of exocytic vesicle trafficking pathways, the vacuoles derived vesicles are recruited back to the organelle band, and the spindles are separated again.

PEL has co-localization with vacuole membrane marker (or tonoplast) in root cells and meiotic cells (Figure S5), suggesting that PEL is a vacuole-located protein. Vacuoles can be divided into two types: lytic vacuoles and protein storage vacuoles. Lytic vacuoles can store pigments and acids to maintain the homeostasis of the cell, while protein storage vacuoles predominantly form at late embryonic developmental stages to the seed germination stage. The vacuole vesicle trafficking can be inhibited by the BFA treatment (Jiang et al., 2020; Jiang et al., 2021). Polar vacuolar distribution is proved to be essential for accurate asymmetric division of *Arabidopsis* zygotes (Kimata et al., 2016; Kimata et al., 2020). Vacuolar vesicles can traffic through the cytoskeleton during mitosis and meiosis (Kim et al., 2005; Kimata et al., 2016; Kimata et al., 2020). The important function and subcellular feature of vacuoles-derived organelles make it very important to separate spindles during metaphase II.

5.2 The molecular function of PEL and PEL interacting proteins

5.2.1 PEL$^{1295\text{-}1453}$ interacts with a plastid-localized protein

Through a two-hybrid yeast screen, PsbR was found to interact strongly with the C-terminal of PEL. PsbR is associated with the oxygen-evolving complex and is crucial for oxygen production and quinone reoxidation in leaf cells. The PsbR protein is

predominantly located in the chloroplast in leaf protoplasts, and SUMOylation on K51 and K48 sites is necessary to direct PsbR from the cytoplasm to the chloroplast (Zheng et al. 2022). The PEL$^{1295\text{-}1453}$ is also located in the cytoplasm, which gives PsbR a chance to encounter the PEL protein in the cytoplasm. Indeed, when transferring the PsbR and PEL$^{1295\text{-}1453}$ tagged with a fluorescent tag, these two proteins showed an interaction signal on lysosomes in both *Arabidopsis* and *Nicotiana* leaf cells. The chloroplast pigments do not exist in meiosis (Granick, 1961; Marciniec et al., 2019), and the double-layer membrane structure degenerates into single-layer plastids during the seeding growth (Ruppel et al., 2011). The chloroplast genome is shown to be transmitted to the next generation through meiosis (Rose, 2019). Thus, the membrane covering the chloroplast genome can also pass through the meiotic cell cycle. Plastids of *Tinantia erecta*, a species undergoing successive meiotic cytokinesis, are found to be recruited and clustered in triangular areas around the primary cell wall during the second meiotic division (Marciniec et al., 2019). According to the data from this study, I propose that the plastids is associated with vacuoles, and the association is mediated by the PEL-PSBR interaction. In *jas pel*, the interaction is abolished because of the missing of PEL, potentially leading to the partially recovered organelle singal in DAPI staining (Figure 30).

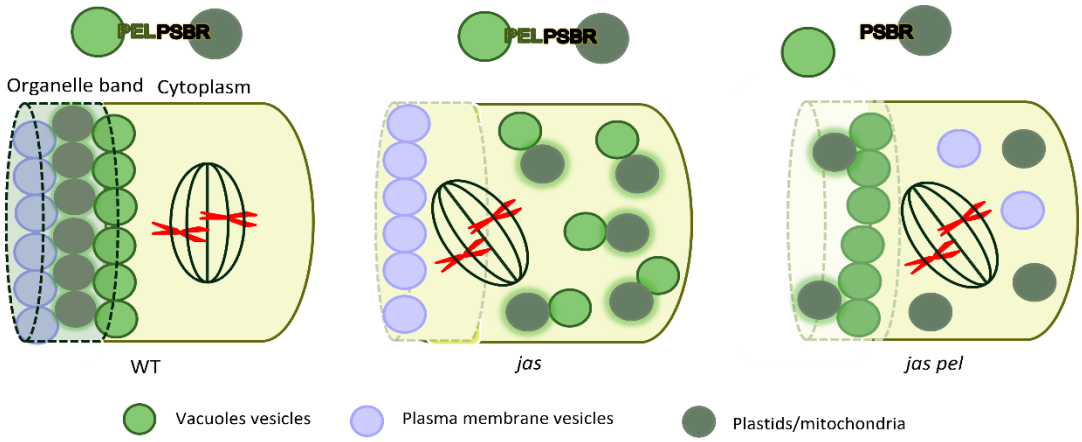

Figure 30. PEL-PSBR interaction mediate vacuoles-plastids association in WT, jas, jas pel

In WT and jas, the PEL-PSBR interaction mediate vacuoles-plastids association. In jas pel, the affinity between vacuoles and plastids is decreased.

PsbR, as a chloroplast-located protein, showed a high transcription level (>500 RPKM) in meiotic stage flower buds. The protein on the thylakoid membrane catalyses light-induced electron transfer. The mutant of *PsbR* does not show an obvious defect phenotype, but reduced light harvesting efficiency (Allahverdiyeva et al., 2013; Suorsa

et al., 2006). PsbR is encoded by the genomic DNA, synthesized outside of chloroplast or plastid. Many other thylakoid proteins are synthesized in the same way. Plastidic type I signal peptidase 1 (Plsp1) is found to help thylakoid proteins, including PsbR, PsbQ, and PsbO, accumulate into plastids (Shipman-Roston et al., 2010). Interestingly, plants that lack Plsp1 (consequently have low levels of PsbR and other thylakoid proteins) were found to have disordered and fused vesicles in the stroma and cotyledons (Inoue et al., 2005; Shipman-Roston et al., 2010), suggesting the plastid membrane proteins are also involved in the vesicle trafficking pathways.

5.2.2 A ubiquitin-like family protein during vacuoles vesicle trafficking and meiotic division

Ubiquitin is a conserved protein in the evolutionary history of eukaryotes. Ubiquitin can form linked chains by attaching the di-glycine motif to another ubiquitin protein at a lysine residue or an N-terminal methionine residue (Kulathu & Komander, 2012; López-Mosqueda & Dikic, 2014). Ubiquitination is a diverse post-translational modification. Proteins can be polyubiquitinated by linking the ubiquitin as a chain, proteins can also be mono-ubiquitinated or multi-monoubiquitinated at different lysine sites (Orr et al., 2021). The canonical function of protein ubiquitination is to initiate proteasome degradation pathways (Ciehanover et al., 1978). Activation of proteasome degradation pathways involves three steps: E1 ubiquitin-activating enzymes recruit ubiquitin, E2 conjugating enzymes accept the ubiquitin from E1, and E3 ligates the ubiquitin and targets substrate proteins. The ubiquitinated (normally polyubiquitinated) protein then undergoes the degradation pathways. However, in the previous results part, UBQL has been proven to be irrelevant to proteasome degradation pathways; I will not discuss it further.

In addition to the degradation pathways, ubiquitin can post-translationally modify the target protein. The UBQL protein in the Rab GTPase pathway can maintain the targeting protein in a soluble state and deliver the target protein to the functional organelles (Kasu et al., 2022; Kawahara et al., 2013; Kuwabara et al., 2015). In mammalian cells, the BAG6 (Bcl-2-associated Athanogene 6) domain interacts with Ubl4a (Ubiquitin-like Protein 4a). The complex binds TA proteins post-translationally, loads them onto the cytosolic ATPase TRC40, and targets ER. In yeast, Get5, as an ortholog of Ubl4a, interacts with Sgt2 via the UBQ domain to recruit tail-anchored (TA) proteins (Chartron et al., 2012; Kuwabara et al., 2015; Simon et al., 2013). Aligning with the knowledge in yeast and human, my result also showed that the UBQL is a positive regulator of the organelle band (Figure 31). Although from the current data, the UBQL is not specifically located at the vacuoles, but the function of UBQL in closely

related with the vacuoles. For example, the VAMP711 marker in *jas pel ubql* is again disrupted at the organelle band, suggesting that trafficking these vesicles needs UBQL to perform its function (Figure S5). The BAG6 protein is also found to influence vesicle trafficking. In human cells, BAG6 recognizes the inactive form of Rab8a but not the active form of Rab8a. The recognition site on Rab8a can also be recognized by the ubiquitin-proteasome degradation pathway. BAG6 prevents the accumulation of inactive Rab8a, which impairs intracellular membrane trafficking (Takahashi et al., 2019) (Figure 24). BAG6 can also interact with other small GTPase proteins (Miyauchi et al., 2023; Takahashi et al., 2019) (Figure 24).

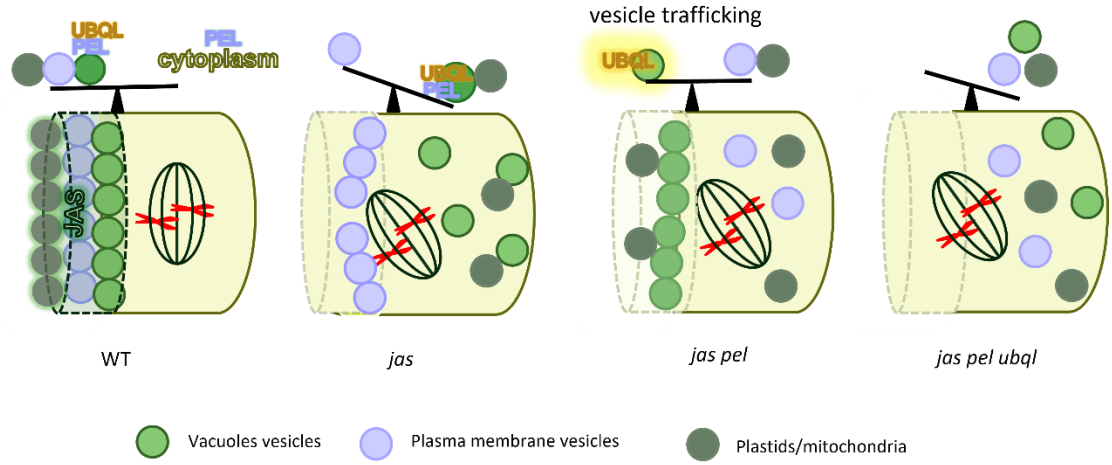

Figure 31. UBQL is a positive regulator of the organelle band.

In WT and *jas*, PEL negatively regulate the UBQL function, and the organelle band is controlled by JAS. In *jas pel*, the inhibitor is removed, UBQL regulate vesicle trafficking of vacuoles to the middle zone, and separate spindles. Like the previous images, UBQL regulation could be activation or inhibition function. UBQL In *jas pel ubql, ubql* is absent, vesicle trafficking cannot be maintained, the spindle distance gets close again.

5.3 Actin maintains spindle separation

In addition to microtubules, actin, as another important cytoskeletal structure, has also been reported to organize vesicles (Schuh, 2011). Actin has a negative function in maintaining the organelle band during meiosis. In this study, actin inhibitor treatment and DN-actin are used to observe the influence of disordered actin filaments on the organelle band. Disassembly of F-actin can partially recover the *jas* phenotype. In oocytes, a dynamic vesicle-actin network is assembled to traffic vesicles to a target area (Schuh, 2011). Vesicles pave their way for movement with actin filaments. By recruiting actin nucleators and connecting the plasma membrane, the actin network is formed at the surface of vesicles and the cell surface, thus moving the vesicle to the

plasma membrane in a locally random but globally directed manner (Schuh, 2011). Meanwhile, the actin-vesicle network is also reported to adjust the spindle position during meiosis (Almonacid et al., 2014; Halet & Carroll, 2007; Sun et al., 2011). During meiosis II in oocytes, the actin-vesicle network is assembled at one side of the nucleus, and the accumulation of actin and vesicles will push the spindle and nucleus to the targeted side of the cell (Almonacid et al., 2014). In *Arabidopsis* male meiosis, actin may generate a similar force to position the spindles. The organelle band pushes the spindle to the cell periphery, yet actin positions the spindles by limiting the area of the organelle band. The correct position of spindles in male meiosis II replies to the balance of the power in two distinct directions. The organelle band partially disrupted by the *jas* mutation breaks the balance between the organelle band and actin, leading to further disrupted organelle band with actin invading the mid-zone of male meiosis. In summary, actin and the organelle band together control the position of spindles in meiosis II.

6 Outlook

The meiotic cell cycle, as a special type of cell cycle, has similarities yet differences compared to mitosis. From this study, we revealed that the organelles involved in exocytotic pathways, including TGN, vacuole, and plastids, are disordered in the *jas* background. However, these organelles can partially be recovered by *jas pel* and prevent the production of unreduced gametes. PEL, as a vacuole-located protein, might have multiple functions. In one way, the PEL C-terminal interacts with a plastid-located protein in vitro, which might explain the partially recovered DAPI-staining signal (representing plastids and mitochondria) in *jas pel*. In another way, the PEL cytoplasmic domain interacts with the UBQL protein on the lipid-liquid phase surface to recruit Rab GTPase to stabilize the filament actin on vesicles. The filament actin was found to enhance the *jas* phenotype; therefore, *pel* destabilize the actin filament and partially recover the *jas* phenotype. In this chapter, models based on current experimental data and published research are suggested. However, further evidence is needed to solidify these ideas.

6.1 The PsbR to maintain the partially recovered organelle band

PEL, as a vacuole-located protein, was found to interact with a plastid-located protein, PsbR. PsbR assists in photosynthesis in chloroplasts in leaf cells, but it is not well studied in meiosis. Since meiotic cells lack photosynthetic pigments and Chloroplast structures, PsbR might perform a different function than in leaf cells. In addition to the chloroplast function, plastids can also store starch, lipids, and proteins during mitosis and transfer the biosynthesized materials to the primary cell wall (Wise, 2006). Vesicles derived from plastids can also traffic to the vacuole to undergo autophagy and recycle materials (Michaeli et al., 2014; Otegui, 2017). However, in dividing cells, large central vacuoles are not formed. Instead, multiple small vesicles called tonoplasts are formed. Plastids are found to be located around the tonoplast (Reisen et al., 2005). How would the plants behave in *psbr* mutant?

In WT plants, JAS can anchor the plastids and mitochondria at the mid-zone to stabilize the organelle band. Vacuoles are located around the organelle band to form a stable yet dynamic structure. In *jas* plants, plastid and mitochondria are not limited to the organelle band, and vacuoles are also disordered. In *jas pel*, PEL prevents the trafficking of vesicles outside of the organelle band, and the vacuole markers are recovered. The interaction between plastid proteins and vacuole proteins can partially recover the plastid location and influence the formation of unreduced gametes. Is

vacuole associated with plastid critical in maintaining the organelle band is another question. Even though the two vesicles are associated together, the meiotic function is so far largely unknown.

6.2 Functional relationship of PEL and UBQL

PEL is a relatively large protein with multiple transmembrane domains. The signal peptide of PEL directs the protein to the secretion pathway after synthesis. On the ER membrane, PEL can encounter UBQL and interact with it through its cytoplasmic domain. UBQL has been reported to be a subunit of the BAG6 complex and can act as a chaperone protein to protect transmembrane proteins (Kawahara et al., 2013). In the discussion part, the model of BAG6 complex from yeast can explain the PEL as a negative regulator of UBQL. However, we do not have any study of the BAG6 complex in plant cell, it is still a question if the same process existed in plant meiosis. The ubiquitin-initiated degradation pathway is very important in the BAG6 complex function. In my study, I have inhibited the ubiquitin-initiated degradation pathway, but do not show any phenotype. Although the positive control proved the function of inhibitors, this result still doesn't match the known knowledge. Since the ubiquitin-initiated degradation pathway is very important in meiosis I, without the pathway, the cell should not be able to pass the first round of meiosis (Cromer et al., 2012; Orr et al., 2021). It is worth exploring more about the relationship between UBQL and ubiquitin-initiated degradation pathway.

In this research, I have identified two important pathways in *jas* plants. The first is the PEL-related vesicle trafficking pathway. The *jas pel* mutant can activate the exocytic vesicle trafficking pathway to assemble vacuoles at the middle zone and separate spindles. PEL acts as a negative regulator when separating the spindles. Meanwhile, the UBQL potentially interacts with PEL and has a counter function with it. As a result, *jas pel ubql* showed a phenotype like *jas*. The UBQL regulated molecular pathway potentially influences the vesicle trafficking (Figure 31). To confirm the actual process in meiosis, the existence of the interaction between UBQL and other BAG6 complex subunits needs to be proved. Additionally, due to the low expression of PEL and UBQL, it is necessary to confirm the interaction of PEL and UBQL in vivo. Further study can reveal the impact of cross-talk between organelles during meiosis.

6.3 Actin filament can move the vesicle outside of the organelle band

The inhibition of actin filaments recovered the *jas* phenotype during meiosis, while the elongation of actin filaments on the vesicles can move the vesicles along the filaments. PEL can inhibit actin polymerization during meiosis, thus preventing vesicles

from moving outside of the organelle band. In WT plants, JAS anchors most of the vesicles at the organelle band area. Actin filaments can only move a few vesicles outside the organelle band, therefore, they do not influence the organelle band. In *jas* mutants, although misoriented, actin filaments can still form and move vesicles all around the cell.

To further explain the possible molecular mechanism, the BAG6 complex (or UBQL-related complex) was also found to be related to vesicle trafficking. In Figure 32The recruitment of the UBQL-related complex with actin filaments to activate vesicle trafficking is illustrated. According to experimental data from yeast, the UBQL-related complex can recruit Rab GTPase to stabilize the actin filaments during polymerization. The stabilized actin acts as a path for vesicle trafficking. In contrast, the UBQL-related complex cannot be recruited to the vesicle surface without the interaction between PEL and UBQL. UBQL activate protease degradation without PEL and degrades Rab GDP (Figure 32). The models shown here are based on data obtained from this experiment combined with the previous model from yeast (Figure 32). The UBQL may have a counter effect of the shown model. The destabilization of actin has been proven to recover the *jas* phenotype, but this destabilization cannot fully complement the *jas* phenotype. More studies are needed to study the UBQL and actin filament function before we make a clear conclusion.

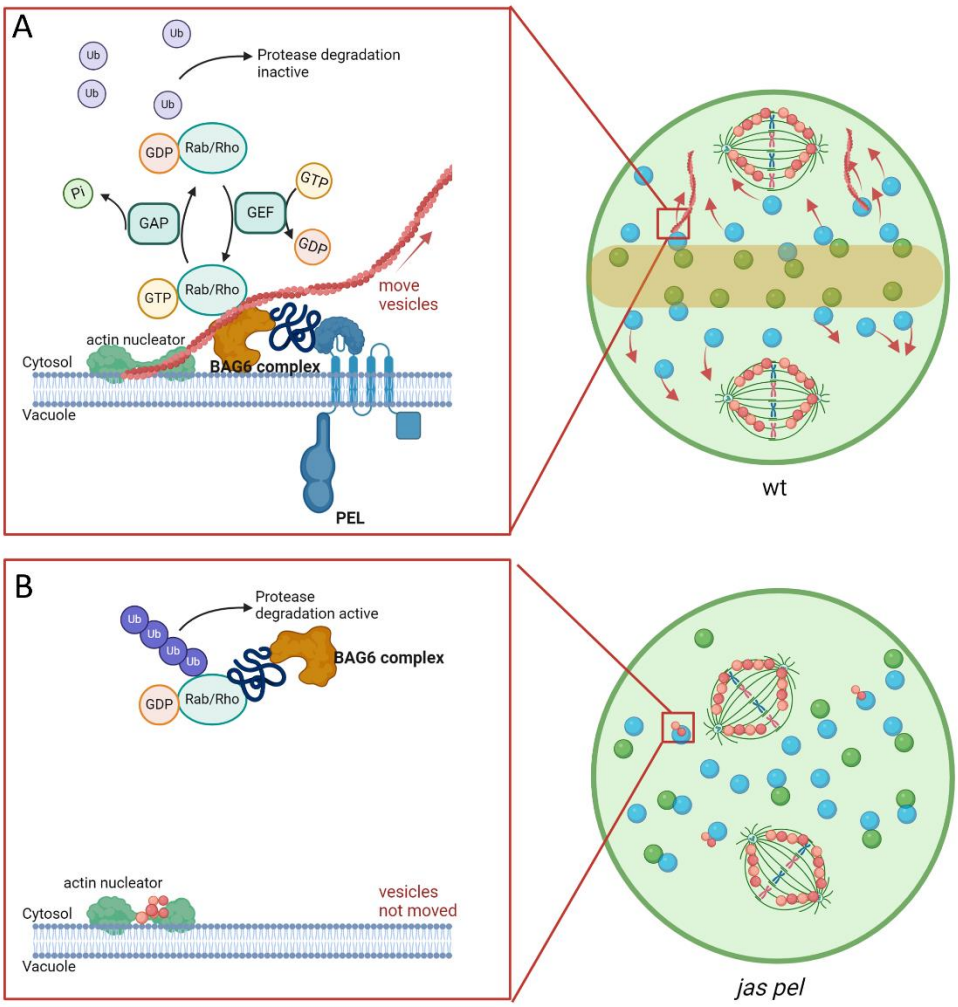

Figure 32. The potential model of actin in vesicle movement during metaphase II

A) In WT, Rab/Rho-GTP was recruited to the vesicle surface by the UBQL related pathway. The Rab/Rho-GTP potentially activates the vesicle trafficking along the actin filament. B) In *jas pel*, without PEL to recruit the system on the surface of vesicles, the vesicle cannot move through the actin filament. It is still not sure whether the UBQL is active in vesicle trafficking or not, the image here only shows one possibility.

7 Summary

The plant meiotic cell cycle is an important process for maintaining the stability of ploidy between generations. The meiotic cell cycle undergoes one round of DNA duplication, followed by two rounds of chromosome division to produce gametes that contain half the DNA material of the parent. Fertilization between male and female gametes maintains stable ploidy between generations. However, when errors occur during the meiotic cell cycle, the chromosomes do not divide normally, leading to unreduced gametes. Unreduced gametes can be caused by disordered organelle bands in dicot plants. The organelle band is a special structure formed after the first division until the end of the second division. The organelle band consists of vesicles derived from different organelles and acts as a physical barrier between the homologous chromosomes after the first division. The *jas* mutant, characterized by meiotic defects, shows a disordered organelle band and nuclear restitution during the second meiotic division.

A *jas* suppressor, *pel*, can recover the phenotype of *jas* without fully recovering the organelle band. *pel* recovered vesicles derived from the BFA and ConK A inhibited vesicle trafficking pathways and partially recovered the vesicle derived from mitochondria and plastids. The recovery function of *pel* depends on BFA and ConK A related vesicle trafficking pathways. The PEL protein is a tonoplast-located protein that does not have known functional domains. Truncation of different functional domains suggests the importance of N terminal signal peptide and C terminal domains. Using the C terminal domain sequence for Y2H screening found a plastid-located protein PsbR. It is still not sure the function of PEL interacts with PsbR, but both vesicles are found to be important in cytokinesis in mitosis. The function of both proteins is rarely studied in meiosis.

In addition to the PsbR protein, a UBQL protein is also reported to interact with PEL. Y2H is applied to confirm the interaction, and the cytoplasmic domain of PEL is confirmed to interact with UBQL. UBQL homologous protein in humans and yeast is involved in the BAG6 complex. The *jas pel* does not respond to proteasome degradation inhibitors, suggesting that the *jas pel* phenotype is not a consequence of proteasome degradation. The recovered vesicle marker in *jas pel* is again disrupted in *jas pel ubql,* indicating *ubql* has a counter effect of *pel*. The BAG6 complex including the UBQL family protein can activate vesicle trafficking through recruiting actin stabilizers like Rab GTPase.

The actin filament is also involved in maintaining the organelle band at metaphase II. Actin network in the cytoplasm can fix the organelle position during the meiotic cell cycle. Both the actin polymerization inhibitor treatment and dominant-negative inhibition of actin filament results showed that inhibiting actin filament can partially recover the JAS phenotype. Here I build a model based on the current knowledge to explain the potential interaction between actin network, PEL induced vesicle trafficking and UBQL related degradation pathways.

8 Zusammenfassung

Der meiotische Zellzyklus der Pflanzen ist ein wichtiger Prozess, um die Stabilität der Ploidie zwischen den Generationen zu erhalten. Im meiotischen Zellzyklus findet eine Runde der DNA-Verdopplung statt, gefolgt von zwei Runden der Chromosomenteilung, um Gameten zu erzeugen, die die Hälfte des DNA-Materials der Eltern enthalten. Nach Befruchtung zwischen männlichen und weiblichen Keimzellen bleibt der Ploidiegrad zwischen den Generationen stabil. Wenn jedoch während des meiotischen Zellzyklus Fehler auftreten, kann es zu nicht-reduzierten Gameten führ. Unreduzierte Gameten können bei dikotylen Pflanzen durch ungeordnete Organellenbänder verursacht werden. Das Organellenband ist eine besondere Struktur, die sich nach der ersten Teilung bis zum Ende der zweiten Teilung bildet. Das Organellenband besteht aus Strukturen, die von verschiedenen Organellen stammen. Dieses Band wirkt als physische Barriere nach der ersten Teilung zwischen den homologen Chromosomen. Die *jas*-Mutante, die durch meiotische Defekte gekennzeichnet ist, zeigt ein gestörtes Organellenband und eine Kernrestitution während der zweiten meiotischen Teilung.

Der *jas*-Suppressor, *pel*, kann den Phänotyp von *jas* wiederherstellen, ohne das Organellenband vollständig wiederherzustellen. *pel* wiederherstellte die Vesikel, die von den durch BFA und ConK A gehemmten Vesikeltransportwegen stammen, und erneuerte teilweise die Vesikel, die von Mitochondrien und Plastiden stammen. Die Wiederherstellungsfunktion von *pel* hängt von BFA- und ConK A-verwandten Vesikeltransportwegen ab. Das PEL-Protein ist ein im Tonoplasten lokalisiertes Protein, das keine bekannten funktionellen Domänen besitzt. Die Trunkierung verschiedener funktioneller Domänen deutet auf die Bedeutung des N-terminalen Signalpeptids und der C-terminalen Domänen hin. Die Verwendung der C-terminalen Domäne für das Y2H-Screening führte zur Entdeckung des Plastid-ansässigen Proteins PsbR. Die Funktion von PEL, das mit PsbR interagiert, ist noch nicht geklärt. Aber es wurde festgestellt, dass beide Vesikel bei der mitotischen Zytokinese eine Rolle spielen. Die meiotische Funktion beider Proteine ist wenig bekannt.

Neben dem PsbR-Protein wird auch von einem UBQL-Protein berichtet, das mit PEL interagiert. Die Interaktion wurde mit Hilfe der Y2H Analyse bestätigt. Die zytoplasmatische Domäne von PEL interagiert nachweislich mit UBQL. *jas pel* reagiert nicht auf Inhibitoren des Proteasom-Abbaus, was darauf hindeutet, dass der *jas pel*-Phänotyp nicht auf den Proteasom-Abbau zurückzuführen ist. Der wiederhergestellte Vesikelmarker in *jas pel* ist in *jas pel ubql* ebenfalls gestört, was darauf hindeutet, dass ubql eine Gegenwirkung von *pel* hat. Der BAG6-Komplex, der das Protein der UBQL-Familie enthält, kann den Vesikeltransport aktivieren, indem er Aktin-Stabilisatoren wie die Rab-GTPase rekrutiert.

Das Aktinfilament ist auch an der Aufrechterhaltung des Organellenbandes in der Metaphase II beteiligt. Das Aktin-Netzwerk im Zytoplasma kann die Position der Organellen während des meiotischen Zellzyklus fixieren. Sowohl die Behandlung mit einem Aktinpolymerisationsinhibitor als auch die dominant-negative Hemmung des Aktinfilaments zeigten, dass die Hemmung des Aktinfilaments den JAS-Phänotyp teilweise wiederherstellen kann. Ein Modell wurde entwickelt, die die mögliche Interaktion zwischen dem Aktinnetzwerk, dem PEL-induzierten Vesikeltransport und den UBQL-bezogenen Abbauwegen erklärt.

9 References

Adams, K. L., & Wendel, J. F. (2005). Polyploidy and genome evolution in plants. *Curr Opin Plant Biol*, *8*(2), 135-141. https://doi.org/10.1016/j.pbi.2005.01.001

Agashe, B., Prasad, C. K., & Siddiqi, I. (2002). Identification and analysis of DYAD: a gene required for meiotic chromosome organisation and female meiotic progression in Arabidopsis. *Development*, *129*(16), 3935-3943. https://doi.org/10.1242/dev.129.16.3935

Alberts B, J. A., Lewis J, et al. (2002). *Molecular Biology of the Cell.* Garland Science.

Allahverdiyeva, Y., Suorsa, M., Rossi, F., Pavesi, A., Kater, M. M., Antonacci, A., Tadini, L., Pribil, M., Schneider, A., Wanner, G., Leister, D., Aro, E.-M., Barbato, R., & Pesaresi, P. (2013). Arabidopsis plants lacking PsbQ and PsbR subunits of the oxygen-evolving complex show altered PSII super-complex organization and short-term adaptive mechanisms. *The Plant Journal*, *75*(4), 671-684. https://doi.org/https://doi.org/10.1111/tpj.12230

Almonacid, M., Terret, M., & Verlhac, M. H. (2014). Actin-based spindle positioning: new insights from female gametes. *J Cell Sci*, *127*(Pt 3), 477-483. https://doi.org/10.1242/jcs.142711

Altschul, S. F., Madden, T. L., Schäffer, A. A., Zhang, J., Zhang, Z., Miller, W., & Lipman, D. J. (1997). Gapped BLAST and PSI-BLAST: a new generation of protein database search programs. *Nucleic Acids Res*, *25*(17), 3389-3402. https://doi.org/10.1093/nar/25.17.3389

Aniento, F., Sánchez de Medina Hernández, V., Dagdas, Y., Rojas-Pierce, M., & Russinova, E. (2021). Molecular mechanisms of endomembrane trafficking in plants. *The Plant Cell*, *34*(1), 146-173. https://doi.org/10.1093/plcell/koab235

Arakel, E. C., & Schwappach, B. (2018). Formation of COPI-coated vesicles at a glance. *J Cell Sci*, *131*(5). https://doi.org/10.1242/jcs.209890

Armstrong, S. J., Franklin, F. C. H., & Jones, G. H. (2003). A meiotic time-course for Arabidopsis thaliana. *Sexual Plant Reproduction*, *16*(3), 141-149. https://doi.org/10.1007/s00497-003-0186-4

Bonifacino, J. S., & Jackson, C. L. (2003). Endosome-Specific Localization and Function of the ARF Activator GNOM. *Cell*, *112*(2), 141-142. https://doi.org/https://doi.org/10.1016/S0092-8674(03)00038-2

Borg, M., Brownfield, L., & Twell, D. (2009). Male gametophyte development: a molecular perspective. *Journal of Experimental Botany*, *60*(5), 1465-1478. https://doi.org/10.1093/jxb/ern355

Boucrot, E., & Kirchhausen, T. (2007). Endosomal recycling controls plasma membrane area during mitosis. *Proc Natl Acad Sci U S A*, *104*(19), 7939-7944. https://doi.org/10.1073/pnas.0702511104

Brown, R. C., Lemmon, B. E., Brown, R. C., & Lemmon, B. E. (1996). Nuclear cytoplasmic domains, microtubules and organelles in microsporocytes of the slipper orchid Cypripedium californicum A. Gray dividing by simultaneous cytokinesis. *Sexual Plant Reproduction*, *9*(3), 145-152. https://doi.org/10.1007/BF02221394

Brownfield, L., Yi, J., Jiang, H., Minina, E. A., Twell, D., & Köhler, C. (2015). Organelles maintain spindle position in plant meiosis. *Nat Commun*, *6*, 6492. https://doi.org/10.1038/ncomms7492

Buzard, G. S., Baker, D., Wolcott, M. J., Norwood, D. A., & Dauphin, L. A. (2012). Multi-platform comparison of ten commercial master mixes for probe-based real-time polymerase chain reaction detection of bioterrorism threat agents for surge preparedness. *Forensic Science*

International, *223*(1), 292-297. https://doi.org/https://doi.org/10.1016/j.forsciint.2012.10.003

Calvo-Baltanás, V., De Jaeger-Braet, J., Cher, W. Y., Schönbeck, N., Chae, E., Schnittger, A., & Wijnker, E. (2022). Knock-down of gene expression throughout meiosis and pollen formation by virus-induced gene silencing in Arabidopsis thaliana. *Plant J*, *111*(1), 19-37. https://doi.org/10.1111/tpj.15733

Carnoy, J. (1887). Les globules polaires de l'Ascaris clavata. *Cellule*, *3*, 247-324.

Chartron, J. W., VanderVelde, D. G., Rao, M., & Clemons, W. M., Jr. (2012). Get5 carboxyl-terminal domain is a novel dimerization motif that tethers an extended Get4/Get5 complex. *J Biol Chem*, *287*(11), 8310-8317. https://doi.org/10.1074/jbc.M111.333252

Ciehanover, A., Hod, Y., & Hershko, A. (1978). A heat-stable polypeptide component of an ATP-dependent proteolytic system from reticulocytes. *Biochem Biophys Res Commun*, *81*(4), 1100-1105. https://doi.org/10.1016/0006-291x(78)91249-4

Clarke, J. M., DeAmbrogio, E., Hare, R. A., & Roumet, P. (2012). CHAPTER 2 - Genetics and Breeding of Durum Wheat. In M. Sissons, J. Abecassis, B. Marchylo, & M. Carcea (Eds.), *Durum Wheat (Second Edition)* (pp. 15-36). AACC International Press. https://doi.org/https://doi.org/10.1016/B978-1-891127-65-6.50007-6

Cromer, L., Heyman, J., Touati, S., Harashima, H., Araou, E., Girard, C., Horlow, C., Wassmann, K., Schnittger, A., De Veylder, L., & Mercier, R. (2012). OSD1 promotes meiotic progression via APC/C inhibition and forms a regulatory network with TDM and CYCA1;2/TAM. *PLoS Genet*, *8*(7), e1002865. https://doi.org/10.1371/journal.pgen.1002865

d'Erfurth, I., Cromer, L., Jolivet, S., Girard, C., Horlow, C., Sun, Y., To, J. P., Berchowitz, L. E., Copenhaver, G. P., & Mercier, R. (2010). The cyclin-A CYCA1;2/TAM is required for the meiosis I to meiosis II transition and cooperates with OSD1 for the prophase to first meiotic division transition. *PLoS Genet*, *6*(6), e1000989. https://doi.org/10.1371/journal.pgen.1000989

d'Erfurth, I., Jolivet, S., Froger, N., Catrice, O., Novatchkova, M., & Mercier, R. (2009). Turning Meiosis into Mitosis. *PLOS Biology*, *7*(6), e1000124. https://doi.org/10.1371/journal.pbio.1000124

d'Erfurth, I., Jolivet, S., Froger, N., Catrice, O., Novatchkova, M., Simon, M., Jenczewski, E., & Mercier, R. (2008). Mutations in AtPS1 (Arabidopsis thaliana parallel spindle 1) lead to the production of diploid pollen grains. *PLoS Genet*, *4*(11), e1000274. https://doi.org/10.1371/journal.pgen.1000274

De Storme, N., & Geelen, D. (2011). The Arabidopsis Mutant jason Produces Unreduced First Division Restitution Male Gametes through a Parallel/Fused Spindle Mechanism in Meiosis II *Plant Physiology*, *155*(3), 1403-1415. https://doi.org/10.1104/pp.110.170415

De Storme, N., & Geelen, D. (2013a). Cytokinesis in plant male meiosis. *Plant Signal Behav*, *8*(3), e23394. https://doi.org/10.4161/psb.23394

De Storme, N., & Geelen, D. (2013b). Sexual polyploidization in plants – cytological mechanisms and molecular regulation. *New Phytologist*, *198*(3), 670-684. https://doi.org/https://doi.org/10.1111/nph.12184

Dinis, A. M., & Mesquita, J. F. (1993). The F-actin distribution during microsporogenesis in Magnolia soulangeana Soul. (Magnoliaceae). *Sexual Plant Reproduction*, *6*(1), 57-63. https://doi.org/10.1007/BF00227584

DORSEY, E. (1936). INDUCED POLYPLOIDY IN WHEAT AND RYE: Chromosome Doubling in Triticum,

Secale and Triticum-Secale Hybrids Produced by Temperature Changes. *Journal of Heredity*, *27*(4), 155-160. https://doi.org/10.1093/oxfordjournals.jhered.a104195

Duan, X., & Sun, S.-C. (2018). Actin cytoskeleton dynamics in mammalian oocyte meiosis†. *Biology of Reproduction*, *100*(1), 15-24. https://doi.org/10.1093/biolre/ioy163

Erilova, A., Brownfield, L., Exner, V., Rosa, M., Twell, D., Scheid, O. M., Hennig, L., & Köhler, C. (2009). Imprinting of the Polycomb Group Gene MEDEA Serves as a Ploidy Sensor in Arabidopsis. *PLOS Genetics*, *5*(9), e1000663. https://doi.org/10.1371/journal.pgen.1000663

Esseling-Ozdoba, A., Kik, R. A., van Lammeren, A. A. M., Kleijn, J. M., & Emons, A. M. C. (2009). Flexibility contra Stiffness: The Phragmoplast as a Physical Barrier for Beads But Not for Vesicles. *Plant Physiology*, *152*(2), 1065-1072. https://doi.org/10.1104/pp.109.150417

Fan, J., & Li, R. (2001). Variable selection via nonconcave penalized likelihood and its oracle properties. *Journal of the American statistical Association*, *96*(456), 1348-1360.

Feldmann, K., & Marks, M. (1987). Agrobacterium-mediated transformation of germinating seeds of Arabidopsis thaliana: A non-tissue culture approach. *MGG Molecular & General Genetics*, *208*, 1-9. https://doi.org/10.1007/BF00330414

Frémont, S., & Echard, A. (2018). Membrane Traffic in the Late Steps of Cytokinesis. *Current Biology*, *28*(8), R458-R470. https://doi.org/https://doi.org/10.1016/j.cub.2018.01.019

Gautreau, A., Oguievetskaia, K., & Ungermann, C. (2014). Function and regulation of the endosomal fusion and fission machineries. *Cold Spring Harb Perspect Biol*, *6*(3). https://doi.org/10.1101/cshperspect.a016832

Geldner, N., Dénervaud-Tendon, V., Hyman, D. L., Mayer, U., Stierhof, Y. D., & Chory, J. (2009). Rapid, combinatorial analysis of membrane compartments in intact plants with a multicolor marker set. *Plant J*, *59*(1), 169-178. https://doi.org/10.1111/j.1365-313X.2009.03851.x

Gibieža, P., & Petrikaitė, V. (2021). The regulation of actin dynamics during cell division and malignancy. *Am J Cancer Res*, *11*(9), 4050-4069.

Gotmare, K. P. M. (2010). Induction of polyploidy in two diploid wild cotton (G. armourianum and G. aridum) species by colchicine treatment. *Electronic Journal of Plant Breeding*, *1*.

Gregan, J., Polakova, S., Zhang, L., Tolić-Nørrelykke, I. M., & Cimini, D. (2011). Merotelic kinetochore attachment: causes and effects. *Trends Cell Biol*, *21*(6), 374-381. https://doi.org/10.1016/j.tcb.2011.01.003

Halet, G., & Carroll, J. (2007). Rac activity is polarized and regulates meiotic spindle stability and anchoring in mammalian oocytes. *Dev Cell*, *12*(2), 309-317. https://doi.org/10.1016/j.devcel.2006.12.010

Hall, B. G. (2013). Building Phylogenetic Trees from Molecular Data with MEGA. *Molecular Biology and Evolution*, *30*(5), 1229-1235. https://doi.org/10.1093/molbev/mst012

Harlan, J. R., & deWet, J. M. J. (1975). On Ö. Winge and a Prayer: The origins of polyploidy. *The Botanical Review*, *41*(4), 361-390. https://doi.org/10.1007/BF02860830

Hawkins, T. J., Kopischke, M., Mentlak, D. A., Duckney, P., Kroon, J. T. M., Bui, M. T., Richardson, A. C., Casey, M., Alexander, A., De Jaeger, G., Kalde, M., Moore, I., Dagdas, Y., Hussey, P. J., & Robatzek, S. (2021). A NET4-RabG3 couple mediate the link between actin and the tonoplast and is essential for normal actin cytoskeletal remodelling in stomatal closure to flg22. *bioRxiv*, 2021.2009.2029.461190. https://doi.org/10.1101/2021.09.29.461190

Headd, J. J., Ban, Y. E., Brown, P., Edelsbrunner, H., Vaidya, M., & Rudolph, J. (2007). Protein-protein interfaces: properties, preferences, and projections. *J Proteome Res*, *6*(7), 2576-2586.

https://doi.org/10.1021/pr070018+

Heckmann, S., Jankowska, M., Schubert, V., Kumke, K., Ma, W., & Houben, A. (2014). Alternative meiotic chromatid segregation in the holocentric plant Luzula elegans. *Nature Communications*, *5*(1), 4979. https://doi.org/10.1038/ncomms5979

Hirose, Y., Suzuki, R., Ohba, T., Hinohara, Y., Matsuhara, H., Yoshida, M., Itabashi, Y., Murakami, H., & Yamamoto, A. (2011). Chiasmata promote monopolar attachment of sister chromatids and their co-segregation toward the proper pole during meiosis I. *PLoS Genet*, *7*(3), e1001329. https://doi.org/10.1371/journal.pgen.1001329

Hitchcock, A. L., Auld, K., Gygi, S. P., & Silver, P. A. (2003). A subset of membrane-associated proteins is ubiquitinated in response to mutations in the endoplasmic reticulum degradation machinery. *Proceedings of the National Academy of Sciences*, *100*(22), 12735-12740. https://doi.org/doi:10.1073/pnas.2135500100

Hong, H., Choi, H. K., & Yoon, T. Y. (2022). Untangling the complexity of membrane protein folding. *Curr Opin Struct Biol*, *72*, 237-247. https://doi.org/10.1016/j.sbi.2021.11.013

Hoshino, H., Yoneda, A., Kumagai, F., & Hasezawa, S. (2003). Roles of actin-depleted zone and preprophase band in determining the division site of higher-plant cells, a tobacco BY-2 cell line expressing GFP-tubulin. *Protoplasma*, *222*(3-4), 157-165. https://doi.org/10.1007/s00709-003-0012-8

Hughes, S. E., & Hawley, R. S. (2020). Meiosis: Location, Location, Location, How Crossovers Ensure Segregation. *Current Biology*, *30*(7), R311-R313. https://doi.org/https://doi.org/10.1016/j.cub.2020.02.020

Inoue , K., Baldwin , A. J., Shipman , R. L., Matsui , K., Theg , S. M., & Ohme-Takagi , M. (2005). Complete maturation of the plastid protein translocation channel requires a type I signal peptidase. *Journal of Cell Biology*, *171*(3), 425-430. https://doi.org/10.1083/jcb.200506171

Jiang, Y.-T., Tang, R.-J., Zhang, Y.-J., Xue, H.-W., Ferjani, A., Luan, S., & Lin, W.-H. (2020). Two tonoplast proton pumps function in Arabidopsis embryo development. *New Phytologist*, *225*(4), 1606-1617. https://doi.org/https://doi.org/10.1111/nph.16231

Jiang, Y.-T., Yang, L.-H., Ferjani, A., & Lin, W.-H. (2021). Multiple functions of the vacuole in plant growth and fruit quality. *Molecular Horticulture*, *1*(1), 4. https://doi.org/10.1186/s43897-021-00008-7

Jürgens, G. (2004). MEMBRANE TRAFFICKING IN PLANTS. *Annual Review of Cell and Developmental Biology*, *20*(Volume 20, 2004), 481-504. https://doi.org/https://doi.org/10.1146/annurev.cellbio.20.082503.103057

Jürgens, G. (2005). CYTOKINESIS IN HIGHER PLANTS. *Annual Review of Plant Biology*, *56*(1), 281-299. https://doi.org/10.1146/annurev.arplant.55.031903.141636

Kasu, Y. A. T., Arva, A., Johnson, J., Sajan, C., Manzano, J., Hennes, A., Haynes, J., & Brower, C. S. (2022). BAG6 prevents the aggregation of neurodegeneration-associated fragments of TDP43. *iScience*, *25*(5), 104273. https://doi.org/10.1016/j.isci.2022.104273

Kawahara, H., Minami, R., & Yokota, N. (2013). BAG6/BAT3: emerging roles in quality control for nascent polypeptides. *The Journal of Biochemistry*, *153*(2), 147-160. https://doi.org/10.1093/jb/mvs149

Khoso, M. A., Zhang, H., Khoso, M. H., Poudel, T. R., Wagan, S., Papiashvili, T., Saha, S., Ali, A., Murtaza, G., Manghwar, H., & Liu, F. (2023). Synergism of vesicle trafficking and cytoskeleton during regulation of plant growth and development: A mechanistic outlook. *Heliyon*, *9*(11),

e21976. https://doi.org/10.1016/j.heliyon.2023.e21976

Kim, H., Park, M., Kim, S. J., & Hwang, I. (2005). Actin filaments play a critical role in vacuolar trafficking at the Golgi complex in plant cells. *Plant Cell*, *17*(3), 888-902. https://doi.org/10.1105/tpc.104.028829

Kimata, Y., Higaki, T., Kawashima, T., Kurihara, D., Sato, Y., Yamada, T., Hasezawa, S., Berger, F., Higashiyama, T., & Ueda, M. (2016). Cytoskeleton dynamics control the first asymmetric cell division in Arabidopsis zygote. *Proceedings of the National Academy of Sciences*, *113*(49), 14157-14162. https://doi.org/doi:10.1073/pnas.1613979113

Kimata, Y., Higaki, T., Kurihara, D., Ando, N., Matsumoto, H., Higashiyama, T., & Ueda, M. (2020). Mitochondrial dynamics and segregation during the asymmetric division of Arabidopsis zygotes. *Quant Plant Biol*, *1*, e3. https://doi.org/10.1017/qpb.2020.4

Koc, A., & Storme, N. (2022). Structural regulation and dynamic behaviour of organelles during plant meiosis. *Frontiers in Cell and Developmental Biology*, *10*, 925789. https://doi.org/10.3389/fcell.2022.925789

Kuwabara, N., Minami, R., Yokota, N., Matsumoto, H., Senda, T., Kawahara, H., & Kato, R. (2015). Structure of a BAG6 (Bcl-2-associated athanogene 6)-Ubl4a (ubiquitin-like protein 4a) complex reveals a novel binding interface that functions in tail-anchored protein biogenesis. *J Biol Chem*, *290*(15), 9387-9398. https://doi.org/10.1074/jbc.M114.631804

Leshem, Y., Seri, L., & Levine, A. (2007). Induction of phosphatidylinositol 3-kinase-mediated endocytosis by salt stress leads to intracellular production of reactive oxygen species and salt tolerance. *The Plant Journal*, *51*(2), 185-197. https://doi.org/https://doi.org/10.1111/j.1365-313X.2007.03134.x

Liu, C., Qi, H., Wang, C., Cong, R., Li, L., & Zhang, G. (2023). Genome-wide analysis of ELOVL family genes in the Pacific oyster genome and functional characterization of CgELOVL2/5 and genomic variations in synthesis of polyunsaturated fatty acids. *Aquaculture*, *571*, 739477. https://doi.org/https://doi.org/10.1016/j.aquaculture.2023.739477

Liu, Z., Qin, J., Tian, X., Xu, S., Wang, Y., Li, H., Wang, X., Peng, H., Yao, Y., Hu, Z., Ni, Z., Xin, M., & Sun, Q. (2018). Global profiling of alternative splicing landscape responsive to drought, heat and their combination in wheat (Triticum aestivum L.). *Plant Biotechnol J*, *16*(3), 714-726. https://doi.org/10.1111/pbi.12822

Lüders, J., & Stearns, T. (2007). Microtubule-organizing centres: a re-evaluation. *Nat Rev Mol Cell Biol*, *8*(2), 161-167. https://doi.org/10.1038/nrm2100

Ma, H. (2005). Molecular genetic analyses of microsporogenesis and microgametogenesis in flowering plants. *Annu Rev Plant Biol*, *56*, 393-434. https://doi.org/10.1146/annurev.arplant.55.031903.141717

Mason, A. S., Nelson, M. N., Yan, G., & Cowling, W. A. (2011). Production of viable male unreduced gametes in Brassica interspecific hybrids is genotype specific and stimulated by cold temperatures. *BMC Plant Biology*, *11*(1), 103. https://doi.org/10.1186/1471-2229-11-103

Matsuoka, Y. (2011). Evolution of polyploid triticum wheats under cultivation: the role of domestication, natural hybridization and allopolyploid speciation in their diversification. *Plant Cell Physiol*, *52*(5), 750-764. https://doi.org/10.1093/pcp/pcr018

Mauch, T., & Schoenwolf, G. (2001). Developmental Biology. Sixth Edition. By Scott F. Gilbert. *American Journal of Medical Genetics*, *99*, 170-171. https://doi.org/10.1002/1096-8628(2000)9999:999<00::AID-AJMG1133>3.0.CO;2-G

Michaeli, S., Honig, A., Levanony, H., Peled-Zehavi, H., & Galili, G. (2014). Arabidopsis ATG8-INTERACTING PROTEIN1 Is Involved in Autophagy-Dependent Vesicular Trafficking of Plastid Proteins to the Vacuole *The Plant Cell*, *26*(10), 4084-4101. https://doi.org/10.1105/tpc.114.129999

Mieulet, D., Jolivet, S., Rivard, M., Cromer, L., Vernet, A., Mayonove, P., Pereira, L., Droc, G., Courtois, B., Guiderdoni, E., & Mercier, R. (2016). Turning rice meiosis into mitosis. *Cell Res*, *26*(11), 1242-1254. https://doi.org/10.1038/cr.2016.117

Mitchison, T., & Kirschner, M. (1984). Dynamic instability of microtubule growth. *Nature*, *312*(5991), 237-242. https://doi.org/10.1038/312237a0

Miyauchi, M., Matsumura, R., & Kawahara, H. (2023). BAG6 supports stress fiber formation by preventing the ubiquitin-mediated degradation of RhoA. *Molecular Biology of the Cell*, *34*(4), ar34. https://doi.org/10.1091/mbc.E22-08-0355

Morgan, C., White, M., Franklin, F. C. H., Zickler, D., Kleckner, N., & Bomblies, K. (2021). Evolution of crossover interference enables stable autopolyploidy by ensuring pairwise partner connections in Arabidopsis arenosa. *Current Biology*, *31*. https://doi.org/10.1016/j.cub.2021.08.028

Moscatelli, A., & Idilli, A. I. (2009). Pollen tube growth: a delicate equilibrium between secretory and endocytic pathways. *J Integr Plant Biol*, *51*(8), 727-739. https://doi.org/10.1111/j.1744-7909.2009.00842.x

Nabais, C., Peneda, C., & Bettencourt-Dias, M. (2020). Evolution of centriole assembly. *Current Biology*, *30*(10), R494-R502. https://doi.org/10.1016/j.cub.2020.02.036

Neto, H., Collins, Louise L., & Gould, Gwyn W. (2011). Vesicle trafficking and membrane remodelling in cytokinesis. *Biochemical Journal*, *437*(1), 13-24. https://doi.org/10.1042/BJ20110153

Niu, L., Tao, Y.-B., Chen, M.-S., Fu, Q., Dong, Y., He, H., & Xu, Z.-F. (2016). Identification and characterization of tetraploid and octoploid Jatropha curcas induced by colchicine. *Caryologia*, *69*(1), 58-66. https://doi.org/10.1080/00087114.2015.1110308

Noguchi, T. (2014). Cell Walls. In T. Noguchi, S. Kawano, H. Tsukaya, S. Matsunaga, A. Sakai, I. Karahara, & Y. Hayashi (Eds.), *Atlas of Plant Cell Structure* (pp. 137-156). Springer Japan. https://doi.org/10.1007/978-4-431-54941-3_7

Orr, J. N., Waugh, R., & Colas, I. (2021). Ubiquitination in Plant Meiosis: Recent Advances and High Throughput Methods. *Front Plant Sci*, *12*, 667314. https://doi.org/10.3389/fpls.2021.667314

Otegui, M. S. (2017). Vacuolar degradation of chloroplast components: autophagy and beyond. *Journal of Experimental Botany*, *69*(4), 741-750. https://doi.org/10.1093/jxb/erx234

Pécrix, Y., Rallo, G., Folzer, H., Cigna, M., Gudin, S., & Le Bris, M. (2011). Polyploidization mechanisms: temperature environment can induce diploid gamete formation in Rosa sp. *J Exp Bot*, *62*(10), 3587-3597. https://doi.org/10.1093/jxb/err052

Piskorz, E. W., Jiang, H., Pecinka, A., & Martin-Luther-Universität, H.-W. (2022). *Elucidating mechanisms of unreduced gamete formation in Arabidopsis thaliana* WorldCat. http://nbn-resolving.de/urn:nbn:de:gbv:3:4-1981185920-883081

Randolph, L. F. (1932). Some Effects of High Temperature on Polyploidy and Other Variations in Maize1. *Proceedings of the National Academy of Sciences*, *18*(3), 222-229. https://doi.org/doi:10.1073/pnas.18.3.222

Reichardt, I., Stierhof, Y. D., Mayer, U., Richter, S., Schwarz, H., Schumacher, K., & Jürgens, G. (2007). Plant cytokinesis requires de novo secretory trafficking but not endocytosis. *Curr Biol*, *17*(23),

2047-2053. https://doi.org/10.1016/j.cub.2007.10.040

Reisen, D., Marty, F., & Leborgne-Castel, N. (2005). New insights into the tonoplast architecture of plant vacuoles and vacuolar dynamics during osmotic stress. *BMC Plant Biol*, *5*, 13. https://doi.org/10.1186/1471-2229-5-13

Romero, S., Le Clainche, C., Didry, D., Egile, C., Pantaloni, D., & Carlier, M. F. (2004). Formin is a processive motor that requires profilin to accelerate actin assembly and associated ATP hydrolysis. *Cell*, *119*(3), 419-429. https://doi.org/10.1016/j.cell.2004.09.039

Rossig, C., Le Lievre, L., Pilkington, S. M., & Brownfield, L. (2021). A simple and rapid method for imaging male meiotic cells in anthers of model and non-model plant species. *Plant Reproduction*, *34*(1), 37-46. https://doi.org/10.1007/s00497-021-00404-5

Šamaj, J., Müller, J., Beck, M., Böhm, N., & Menzel, D. (2006). Vesicular trafficking, cytoskeleton and signalling in root hairs and pollen tubes. *Trends in Plant Science*, *11*(12), 594-600. https://doi.org/10.1016/j.tplants.2006.10.002

Sanchez, A. D., & Feldman, J. L. (2017). Microtubule-organizing centers: from the centrosome to non-centrosomal sites. *Curr Opin Cell Biol*, *44*, 93-101. https://doi.org/10.1016/j.ceb.2016.09.003

Sato, R., & Maeshima, M. (2019). The ER-localized aquaporin SIP2;1 is involved in pollen germination and pollen tube elongation in Arabidopsis thaliana. *Plant Molecular Biology*, *100*(3), 335-349. https://doi.org/10.1007/s11103-019-00865-3

Sattler, M. C., Carvalho, C. R., & Clarindo, W. R. (2016). The polyploidy and its key role in plant breeding. *Planta*, *243*(2), 281-296. https://doi.org/10.1007/s00425-015-2450-x

Schuh, M. (2011). An actin-dependent mechanism for long-range vesicle transport. *Nat Cell Biol*, *13*(12), 1431-1436. https://doi.org/10.1038/ncb2353

Seoighe, C., & Gehring, C. (2004). Genome duplication led to highly selective expansion of the Arabidopsis thaliana proteome. *Trends in Genetics*, *20*(10), 461-464. https://doi.org/https://doi.org/10.1016/j.tig.2004.07.008

Sezer, F., Yüzbaşioğlu, G., Özbilen, A., & Taşkin, K. M. (2016). Genome-wide identification and expression analysis of SWI1 genes in Boechera species. *Comput Biol Chem*, *62*, 75-81. https://doi.org/10.1016/j.compbiolchem.2016.04.004

Shimaoka, T., Ohnishi, M., Sazuka, T., Mitsuhashi, N., Hara-Nishimura, I., Shimazaki, K.-I., Maeshima, M., Yokota, A., Tomizawa, K.-I., & Mimura, T. (2004). Isolation of Intact Vacuoles and Proteomic Analysis of Tonoplast from Suspension-Cultured Cells of Arabidopsis thaliana. *Plant and Cell Physiology*, *45*(6), 672-683. https://doi.org/10.1093/pcp/pch099

Shintani, T., Huang, W. P., Stromhaug, P. E., & Klionsky, D. J. (2002). Mechanism of cargo selection in the cytoplasm to vacuole targeting pathway. *Dev Cell*, *3*(6), 825-837. https://doi.org/10.1016/s1534-5807(02)00373-8

Shipman-Roston, R. L., Ruppel, N. J., Damoc, C., Phinney, B. S., & Inoue, K. (2010). The significance of protein maturation by plastidic type I signal peptidase 1 for thylakoid development in Arabidopsis chloroplasts. *Plant Physiol*, *152*(3), 1297-1308. https://doi.org/10.1104/pp.109.151977

Simon, A. C., Simpson, P. J., Goldstone, R. M., Krysztofinska, E. M., Murray, J. W., High, S., & Isaacson, R. L. (2013). Structure of the Sgt2/Get5 complex provides insights into GET-mediated targeting of tail-anchored membrane proteins. *Proceedings of the National Academy of Sciences*, *110*(4), 1327-1332. https://doi.org/doi:10.1073/pnas.1207518110

Sinclair, R., Hsu, G., Davis, D., Chang, M., Rosquete, M., Iwasa, J. H., & Drakakaki, G. (2022). Plant

cytokinesis and the construction of new cell wall. *FEBS Letters*, *596*(17), 2243-2255. https://doi.org/https://doi.org/10.1002/1873-3468.14426

Singh, M., Goel, S., Meeley, R. B., Dantec, C., Parrinello, H., Michaud, C., Leblanc, O., & Grimanelli, D. (2011). Production of viable gametes without meiosis in maize deficient for an ARGONAUTE protein. *Plant Cell*, *23*(2), 443-458. https://doi.org/10.1105/tpc.110.079020

Singh, M. V., & Weil, P. A. (2002). A method for plasmid purification directly from yeast. *Anal Biochem*, *307*(1), 13-17. https://doi.org/10.1016/s0003-2697(02)00018-0

Smertenko, A., Hewitt, S. L., Jacques, C. N., Kacprzyk, R., Liu, Y., Marcec, M. J., Moyo, L., Ogden, A., Oung, H. M., Schmidt, S., & Serrano-Romero, E. A. (2018). Phragmoplast microtubule dynamics – a game of zones. *Journal of Cell Science*, *131*(2). https://doi.org/10.1242/jcs.203331

Suorsa, M., Sirpiö, S., Allahverdiyeva, Y., Paakkarinen, V., Mamedov, F., Styring, S., & Aro, E.-M. (2006). PsbR, a Missing Link in the Assembly of the Oxygen-evolving Complex of Plant Photosystem II*. *Journal of Biological Chemistry*, *281*(1), 145-150. https://doi.org/https://doi.org/10.1074/jbc.M510600200

Takahashi, T., Minami, S., Tsuchiya, Y., Tajima, K., Sakai, N., Suga, K., Hisanaga, S. i., Ohbayashi, N., Fukuda, M., & Kawahara, H. (2019). Cytoplasmic control of Rab family small GTPases through BAG6. *EMBO reports*, *20*(4), e46794. https://doi.org/https://doi.org/10.15252/embr.201846794

Theillet, F.-X., Kalmar, L., Tompa, P., Han, K.-H., Selenko, P., Dunker, A. K., Daughdrill, G. W., & Uversky, V. N. (2013). The alphabet of intrinsic disorder. *Intrinsically Disordered Proteins*, *1*(1), e24360. https://doi.org/10.4161/idp.24360

Ueda, H., Yokota, E., Kutsuna, N., Shimada, T., Tamura, K., Shimmen, T., Hasezawa, S., Dolja, V. V., & Hara-Nishimura, I. (2010). Myosin-dependent endoplasmic reticulum motility and F-actin organization in plant cells. *Proc Natl Acad Sci U S A*, *107*(15), 6894-6899. https://doi.org/10.1073/pnas.0911482107

Van Damme, D., & Geelen, D. (2008). Demarcation of the cortical division zone in dividing plant cells. *Cell Biology International*, *32*(2), 178-187. https://doi.org/https://doi.org/10.1016/j.cellbi.2007.10.010

Wang, C., Liu, Q., Shen, Y., Hua, Y., Wang, J., Lin, J., Wu, M., Sun, T., Cheng, Z., Mercier, R., & Wang, K. (2019). Clonal seeds from hybrid rice by simultaneous genome engineering of meiosis and fertilization genes. *Nat Biotechnol*, *37*(3), 283-286. https://doi.org/10.1038/s41587-018-0003-0

Wang, X., Xu, M., Gao, C., Zeng, Y., Cui, Y., Shen, W., & Jiang, L. (2020). The roles of endomembrane trafficking in plant abiotic stress responses. *Journal of Integrative Plant Biology*, *62*(1), 55-69. https://doi.org/https://doi.org/10.1111/jipb.12895

Wang, Y., Fuentes, R. R., van Rengs, W. M. J., Effgen, S., Zaidan, M., Franzen, R., Susanto, T., Fernandes, J. B., Mercier, R., & Underwood, C. J. (2024). Harnessing clonal gametes in hybrid crops to engineer polyploid genomes. *Nat Genet*, *56*(6), 1075-1079. https://doi.org/10.1038/s41588-024-01750-6

Wassmann, K. (2013). Sister chromatid segregation in meiosis II: deprotection through phosphorylation. *Cell Cycle*, *12*(9), 1352-1359. https://doi.org/10.4161/cc.24600

Weber, E., Engler, C., Gruetzner, R., Werner, S., & Marillonnet, S. (2011). A modular cloning system for standardized assembly of multigene constructs. *PLoS One*, *6*(2), e16765.

https://doi.org/10.1371/journal.pone.0016765

Weigel, A. V., Chang, C. L., Shtengel, G., Xu, C. S., Hoffman, D. P., Freeman, M., Iyer, N., Aaron, J., Khuon, S., Bogovic, J., Qiu, W., Hess, H. F., & Lippincott-Schwartz, J. (2021). ER-to-Golgi protein delivery through an interwoven, tubular network extending from ER. *Cell*, *184*(9), 2412-2429.e2416. https://doi.org/10.1016/j.cell.2021.03.035

Weigel, D., & Glazebrook, J. (2002). *Arabidopsis : a laboratory manual*. Cold Spring Harbor Laboratory Press Cold Spring Harbor, N.Y.

Wise, R. (2006). The Diversity of Plastid Form and Function. In (Vol. 23, pp. 3-26). https://doi.org/10.1007/978-1-4020-4061-0_1

Wood, T. E., Takebayashi, N., Barker, M. S., Mayrose, I., Greenspoon, P. B., & Rieseberg, L. H. (2009). The frequency of polyploid speciation in vascular plants. *Proc Natl Acad Sci U S A*, *106*(33), 13875-13879. https://doi.org/10.1073/pnas.0811575106

Xu, L., Zheng, S., Witzel, K., Van De Slijke, E., Baekelandt, A., Mylle, E., Van Damme, D., Cheng, J., De Jaeger, G., Inzé, D., & Jiang, H. (2024). Chromatin attachment to the nuclear matrix represses hypocotyl elongation in Arabidopsis thaliana. *Nat Commun*, *15*(1), 1286. https://doi.org/10.1038/s41467-024-45577-5

Yadegari, R., & Drews, G. N. (2004). Female Gametophyte Development. *The Plant Cell*, *16*(suppl_1), S133-S141. https://doi.org/10.1105/tpc.018192

Yang, C., Hamamura, Y., Sofroni, K., Böwer, F., Stolze, S. C., Nakagami, H., & Schnittger, A. (2019). SWITCH 1/DYAD is a WINGS APART-LIKE antagonist that maintains sister chromatid cohesion in meiosis. *Nat Commun*, *10*(1), 1755. https://doi.org/10.1038/s41467-019-09759-w

Yi, J., Kradolfer, D., Brownfield, L., Ma, Y., Piskorz, E., Köhler, C., & Jiang, H. (2023). Meiocyte size is a determining factor for unreduced gamete formation in Arabidopsis thaliana. *New Phytologist*, *237*(4), 1179-1187. https://doi.org/https://doi.org/10.1111/nph.18473

Yu, K., Feng, M., Yang, G., Sun, L., Qin, Z., Cao, J., Wen, J., Li, H., Zhou, Y., Chen, X., Peng, H., Yao, Y., Hu, Z., Guo, W., Sun, Q., Ni, Z., Adams, K., & Xin, M. (2020). Changes in Alternative Splicing in Response to Domestication and Polyploidization in Wheat *Plant Physiology*, *184*(4), 1955-1968. https://doi.org/10.1104/pp.20.00773

Zeeh, J. C., Zeghouf, M., Grauffel, C., Guibert, B., Martin, E., Dejaegere, A., & Cherfils, J. (2006). Dual specificity of the interfacial inhibitor brefeldin a for arf proteins and sec7 domains. *J Biol Chem*, *281*(17), 11805-11814. https://doi.org/10.1074/jbc.M600149200

Zhang, X., Henriques, R., Lin, S.-S., Niu, Q.-W., & Chua, N.-H. (2006). Agrobacterium-mediated transformation of Arabidopsis thaliana using the floral dip method. *Nature Protocols*, *1*(2), 641-646. https://doi.org/10.1038/nprot.2006.97

Zheng, X.-T., Wang, C., Lin, W., Lin, C., Han, D., Xie, Q., Lai, J., & Yang, C. (2022). Importation of chloroplast proteins under heat stress is facilitated by their SUMO conjugations. *New Phytologist*, *235*(1), 173-187. https://doi.org/https://doi.org/10.1111/nph.18121

Zhou, X., Mo, X., Gui, M., Wu, X., Jiang, Y., Ma, L., Shi, Z., Luo, Y., & Tang, W. (2015). Cytological, molecular mechanisms and temperature stress regulating production of diploid male gametes in Dianthus caryophyllus L. *Plant Physiol Biochem*, *97*, 255-263. https://doi.org/10.1016/j.plaphy.2015.10.003

Zickler, D., & Kleckner, N. (2015). Recombination, Pairing, and Synapsis of Homologs during Meiosis. *Cold Spring Harb Perspect Biol*, *7*(6). https://doi.org/10.1101/cshperspect.a016626

10 Appendix

Appendix 1: Abbreviation

Abbreviation	Full Name
WT	Wild Type
A. tumefaciens	*Agrobacterium tumefaciens*
N. benthamiana	*Nicotiana benthamiana*
osd1	*omission of secondary division mutation*
MiMe	*Mitosis instead of Meiosis*
rec8	*meiotic recombination protein 8*
spo11-1	*meiosis-specific protein SPO11*
(swi1)/dyad	*switch1/dyad*
Jas	*jason*
ER	Endoplasmic reticulum
Golgi	Golgi apparatus
PM	Plasma Membrane
CPO I	Coat Protein Complex I
COP II	Coat Protein Complex II
BFA	Brefeldin A
ARFs	Adenosine Ribosylation Factors
TGN	Trans-Golgi Network
ConK A	Concanamycin A
PI3K	Phosphatidylinositol 3-kinase
PI3P	Phosphatidylinositol 3-phosphate
Pel	*pellous*
PIP1;4	Plasma membrane Intrinsic Protein 1;4
SYP32	Syntaxin of plants31
VAMP711	VESICLE ASSOCIATED MEMBRANE PROTEIN 711
VTI12	Vesicle transport v-SNARE 12
DMSO	Dimethyl sulfoxide
MS	Murashige and Skoog medium
Wort	Wortmannin
Hrs	hours
BiFC	Bimolecular fluorescence complementation
DAPI	4’,6-diamidino-2-phenylindole
UBQL	Ubiqutin-like super family protein 1
PsbR	Photosystem II subunit R
SUMO	SUMOylation
TOC	Translocon on the Outer Chloroplast membrane
TIC	Translocon on the Inner Chloroplast membrane

Appendix 2: Supplement figures

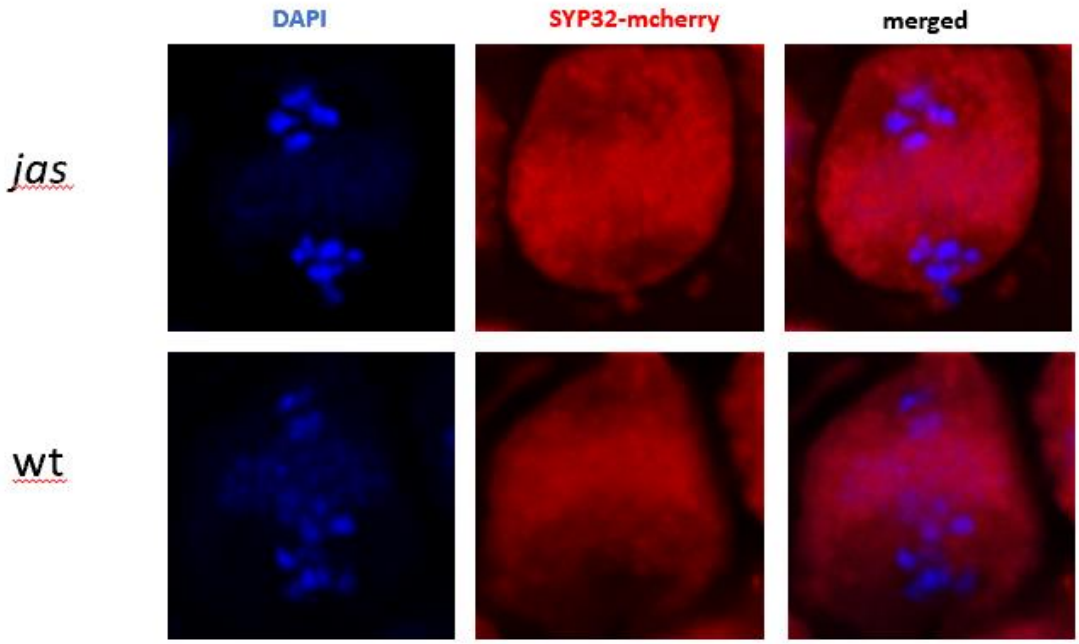

Figure S1. Golgi marker SYP32-mcherry in WT and *jas* background.

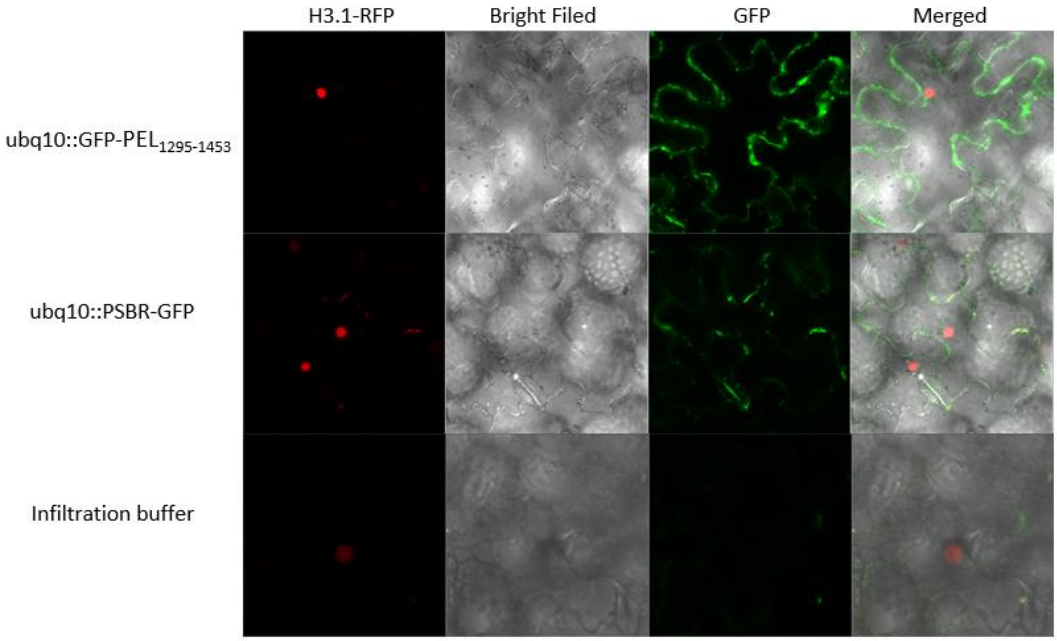

Figure S2. Testing of the expression of PEL and UBQL.

Ubq10 is an overexpression promoter in vegetative and meiosis. Overexpression of PEL is mainly located at the cytoplasm. Overexpression of PsbR mainly at the cytoplasm.

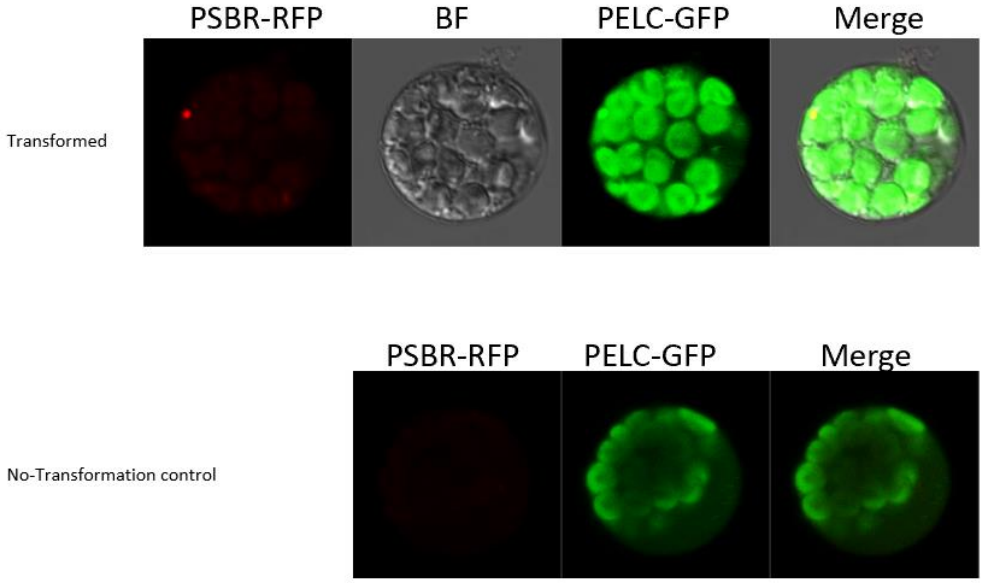

Figure S3. localization of PEL$^{1295\text{-}1453}$ and PsbR in *Arabidopsis* protoplast

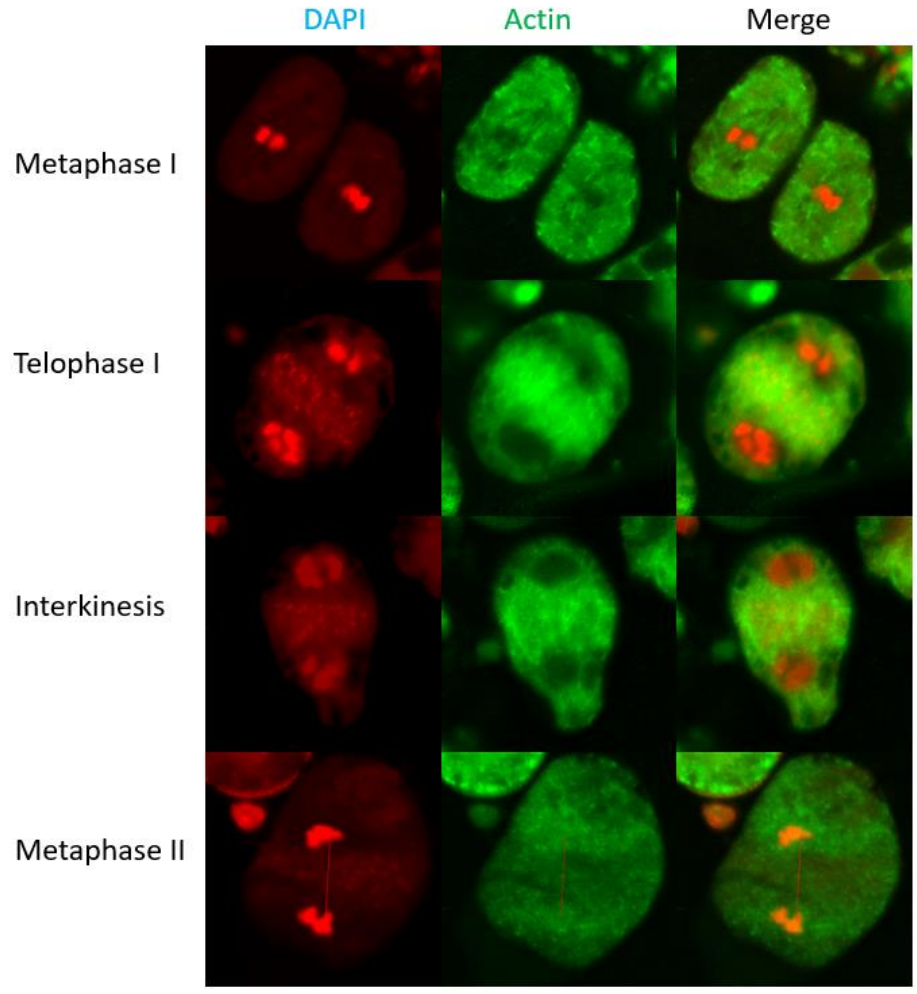

Figure S4. Actin structure during male meiosis.

Red color represents DAPI signal. Green signal represents actin filament structure.

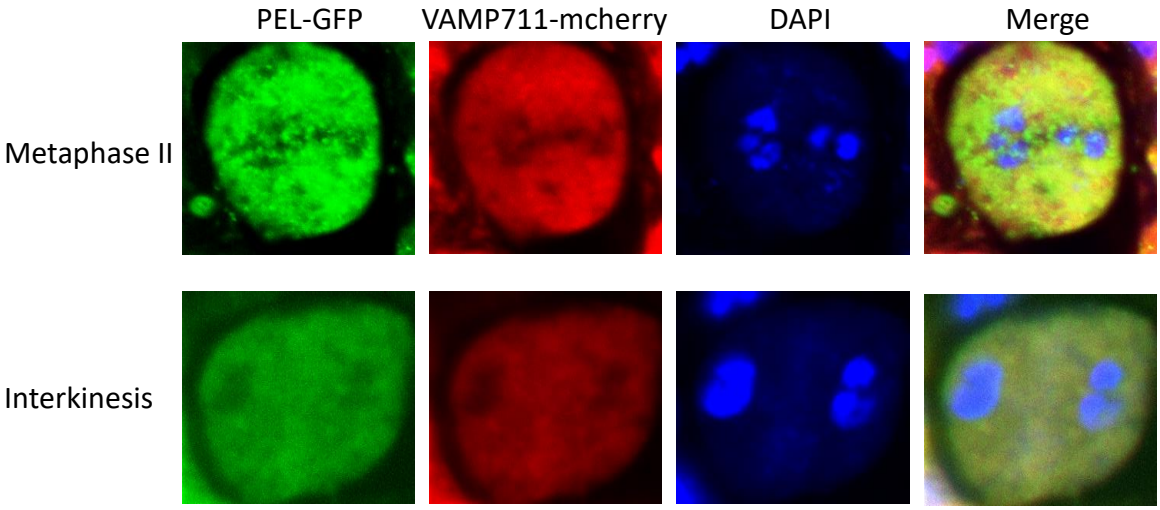

Figure S5. PEL-GFP collocated with VAMP711-mcherry signal in meiotic *jas pel* cells.

Appendix 3: Supplement tables

Table S1. Primer used in this study

Number	Primer sequence	Description
YM11	cttgtacagctcgtccatgc	GFP Rv
YM54	ATTTTGCCGATTTCGGAAC	LB for Salk genotyping
YM71	TAGCATCTGAATTTCATAACCAATCTCGATACAC	LB for Sail genotyping
YM72	ATTAACAAGGCCATTACGGCCATGGCTCGATTTCAATTTTGC	PEL-bait Y2H constructs
YM73	AACTGATTGGCCGAGGCGGCCCCCGACTGCCAAAACAGCTC	
YM74	AACTGATTGGCCGAGGCGGCCCGACTGCCAAAACAGCTC	
YM81	ggGGTACCGTAAACCATAATCTTCATGATTAATCC	Genomic *UBQL* insert into entry vector
YM82	ggGTCGACCAAATTTTCGATCAAAACCAAAATTG	
YM98	ccccttacATAAATCCGG	*pel* grnotyping
YM99	cttaccttaggacaagttgag	
YM100	cagaaggagtccaccttac	Y2H plasmid sequencing
YM103	AAGCGTGACATAACTAATTAC	
YM131	agacttcgtctgtgatgacgGAGGATCTCGGCGGCGTT	
YM132	ctagaactagtggatccccCGACTGCCAAAACAGCTCATAATC	$PEL_{75-1450}$ insert into entry vector
YM133	aat tcc tgc agg gcc att agt ATGGCTCGATTTCAATTTTGCTGC	*PEL* insert into Pray vectors of Y2H
YM134	tac tta cca tgg ggc cga ggt CGACTGCCAAAACAGCTCATAATC	
YM135	GAATTCATGGCCGATGCTGATGAC	*ACT8* insert into entry vector
YM136	TCTAGATTAGAAGCATTTTCTGTGGACAATG	
YM139	CGTTGGCTACCCGTGATATT	Terminal vector sequencing
YM140	CTATTCGGCTATGACTGGGC	
YM143	GGAATCACTTAATGAGGTGTTGG	*PEL* sequencing
YM145	TGGAATGaaaGCTGCAGGGATCCACGAGACAA	*DN-ACT8* site mutation
YM146	CTGCAGCtttCATTCCAACAAATGATGGCTGG	
YM149	cgatgtcgatgataaattgatgatg	*DMC1* sequencing 1000 fw
YM151	cgcggccgccccttggtaccTTGGAATCCGCGAAAATGTT	*PEL* promoter insert into entry vector
YM152	tcgctacaagataccgaattcGTCATCACAGACGAAGTCTACTAAGGTT	
YM155	cgcggccgccccttggtacGTTTCGATATGGCTCACG	*DMC1* promoter insert into entry vector
YM156	gcttatcgataccgtcgaccCTGGCTCGTTTCTTCAGC	
YM158	ttgaagacaaAGGTATGGCGATTCTGTACGC	*VAMP711-mCherry* constructs
YM159	ttgaagacaaAGACGTAACGATCCTGAGA	
YM160	ttgaagacaaGTCTTTCACGTTAAACGCAC	
YM161	ttgaagacaaCGAATTAAATGCAAGATGGTAGAGTAG	
YM162	ttgaagacaaAGGTATGTCCGTGGAGAGGCTTGACCAATCAAGTGACAGAATCAGGGAG	
YM163	TCAAGTGACAGAATCAGGGAGAGTAGACGACTAATGCTGGAGACAGAAG	*VTI12-mcherry* constructs
YM164	ttgaagacaaCGAATTAATGAGAAAGCTTGTATGAGATG	
YM165	ttgaagacaaAGGTATGGAAGGCAAAGAAGAAGAT	*PIP1;4-mCherry* constructs
YM166	ttgaagacaaACAGTGTAGACGAGAACGAAT	
YM167	ttgaagacaaCTGTGTTCTCCGCCACCGACG	
YM168	ttgaagacaaCGAACTAACTCTTGCTCTTGAAAGGAAT	

YM169	AGCGAGTCAGTGAGCGAG	Marker line constructs checking
YM170	AATAGGCGTATCACGAGGC	
YM227	gtgagcaagggcgagg	*mCherry* checking
YM228	gtacagctcgtccatgcc	
YM236	aat tcc tgc agg gcc att agt ATGGAAGATCAACCCATTAACCAGTGC	*UBQL* insert in to Bait plasmid of Y2H
YM237	tac tta cca tgg ggc cga ggt TAGACCTTGATCATCTTTTAGCCGGC	
YM316	aaattcctgcagggccattcgaatgaaatttgttggagttgatgatttac	*PEL* cytopmasmid domain insert into Bait plasmid
YM317	Tacttaccatggggccgaggtatcctggtggcccacagg	

Table S2. Seeds used in this study

GVO ID	Plant ID	Name	Selection-marker
ACB00	22	Col-0	no
ACB02	25	*jas -/-*	no
ACB02	27	*jas -/-; pel* (site mutation)-/-	no
ACB00	28	*pel* (site mutation)-/-	no
ACB01/02	44	*jas-/-; ubq-like-1-/+; pel-/-* F2	no
ACB01/02	45	*jas-/-; pel-/-; ubq-like-/-* F2	no
ACB01/02	46	*jas3-/-; ubqlike1-/- F2*	no
ACB01/02	47	*jas3-/-; ubqlike1-/-; pel-/+* F2	no
ACB01/02	48	*jas3* ubqlike-2* F2	no
ACB01/02	49	*jas3; pel* ubqlike-2* F3	no
ACB01/02	50	*jas3*pel (TDNA*) F2	no
ACB-EP-G17	51	*PEL-GFP* in WT	hyg
ACB-EP-G16	52	*PEL-GFP* in *jas;pel*	hyg
ACB-EP-G24	53	*PEL-CTD in jas3;pel* T0	hyg
ACB-MY-008	54	*PUBC-UBQL-GFP* in wt	PPT
ACB02	57	jas3 -/-	no
ACB02	58	*jas-/- pel -/-* (site mutation)	no
ACB-EP-G16	59	*PEL-GFP* in jas3;pel	hyg
ACB-EP-G24	76	*PELCTD-GFP* IN *jas3 pel*-1	hyg
ACB-EP-G24	77	*PELCTD-GFP* IN *jas3 pel*—2	hyg
ACB-EP-G24	78	*PEL CTD-GFP* IN *jas3 pel*—3	hyg
ACB-EP-G24	79	*PEL NTD-GFP* IN *jas3 pel*—4	hyg
ACN01/02	83	*jas -/-; ubql-/-*	no
ACB01/02	84	*jas -/-; ubq-/-; pel-/-*	no
ACB01	85	*PEL tDNA -/-*	no
ACB01	86	*ubql- 2 -/-*	no
ACB01	87	*ubql-1 -/-*	no
ACB-MY-092	106	PM marker	kan
ACB-MY-107	107	TGN marker	kan
ACB-MY-108	108	NIP1 marker	no
ACB-MY-110	110	tonoplast marker in jas3 -/-	Kan
ACB-MY-111	111	TGN marker in jas3 -/-	kan
ACB-MY-029	112	Perixosome marker in jas3 -/-	Kan
ACB-MY-113	113	Golgi marker in jas3 -/-	kan
ACB-MY-031	118	*UBQL-GFP* in *jas ubql*	hyg
ACB-MY-032	119	*UBQL-GFP* in *ubql*	hyg
ACB-MY-136	136	PM marker in *jas-/-*	kan

ACB-MY-138	138	PM marker in *jas pel*	hyg
ACB-MY-139	139	TGN marker in *jas pel*	hyg
ACB-MY-140	140	vamp marker in *jas pel*	hyg
ACB-MY-141	141	*DN-ACT8* in *jas*	hyg
ACB-MY-154	154	*PEL NTD-GFP* In *jas pel*	hyg
ACB-MY-155	155	PM marker in *jas pel ubq*	hyg
ACB-MY-156	156	TGN marker in *jas pel ubq*	hyg
ACB-MY-157	157	Vacuole marker in *jas pel ubq*	hyg

Note: kan represents 50 μg/ml kanamycin for plants selection. Ppt represents 20 mg/l phosphinothricin for plant selection. Hyg represents 50 μg/mL hygromycin for plant selection.

Table S3. Plasmid used in this study

No.	Modification	Background	Plant resistant	Bacteria resistant
YM01	MSC insert JAS	TSK108	No	kan
YM13	no	PH7FWG2	Hyg	spe
YM14	no	TSK108	No	no
YM18	no	PGWB401	Kan	spe
YM19	no	PGWB440	Kan	spe
YM20	no	PGWB450	Kan	spe
YM21	no	pgwb404	Kan	spe
YM22	no	PGWB501	Hyg	spe
YM23	no	PGWB504	Hyg	spe
YM24	no	PGWB453	Kan	spe
YM25	no	PGWB553	Hyg	spe
YM26	H2B	TSK108	No	Kan
YM27	ym26	YM10	Ppt	ppt
YM28	lifeact	TSK108	No	kan
YM29	prom:PUBC	ym28	No	kan
YM31	no	PBT3-N	No	kan
YM34	prom:ubqlike1 -gUBQLIKE1	TSK108	No	kan
YM35	prom:pubc-lifeact	PGWB453	Kan	spe
YM36	prom:pubc-lifeact	PGWB404	Kan	spe
YM37	no	PBT3-N ste	No	kan
YM38	no	PubG-Fe65	No	kan
YM39	no	Post1-Nub1	No	kan
YM40	no	pPR3-N	No	amp
YM41	prom:peL	tsk108	No	kan
YM42	YM34	PGWB404	Kan	spe
YM43	pel-CDS	BT3-n	No	kan
YM44	ubq-cds	pr3-n	No	kan
YM45	ntd-pel	tsk108	No	kan
YM46	ubq-cds	BT3-n	No	kan
YM47	act8-cds	TSK108	No	kan
YM48	E272-K272	YM47	No	kan
YM49	E272-K272	YM47	No	kan
YM50	pro,:pel-	TSK108	no	

	pelNTD			
YM51	no	pAPP y2h	No	kan
YM52	NO	PGWB507	Hyg	
YM53	NO	PGWB513	Hyg	
YM54	Prom::dmc1	tsk108	No	kan
YM55	YM50	PGWB504	Hyg	spe
YM56	YM48	PGWB513	Hyg	spe
YM57	YM48	PGWB501	Hyg	spe
YM58	YM48	PGWB507	Hyg	spe
YM59	PEL-C	BT3-n	Yeast	kan
YM95	pel cds	tsk108	No	kan
YM96	UBQL cds	tsk108	No	kan
YM97	UBQL cds	tsk108	No	kan
YM106	PSBR cds	TSK108	No	KAN
YM107	BTPEL	bt3-n	No	kan
YM108	BT PELC	bt3-n	No	kan
YM109	pel cds protoplast expression	YM13	Hyg	spe
YM110	pelc	TSK108	No	kan
YM111	PSBR cds protoplas expression	LH660	Ppt	spe
YM114	PSBR cds	PR3-N	No	AMP
YM117	PELC cds	LH660	Ppt	spe
YM118	PELC cds	LH655	Ppt	spe
YM122	PELC cds	tsk108	No	kan
YM123	psbr cds	LH655	Ppt	spe
YM124	PSBR	LH854	Ppt	spe
YM125	PSBR	LH866	Ppt	spe
YM126	PSBR	LH837	Ppt	spe
YM127	PSBR	LH838	Ppt	spe
YM128	PELC	LH854	Ppt	spe
YM129	PELC	LH866	Ppt	spe
YM130	PELC	LH837	Ppt	spe
YM131	PELC	LH838	Ppt	spe
YM132	CYTOPLASMIC PEL	BT3-N	No	kan
YM133	NO	LH655	Ppt	spe
YM134	ym121	PGWB553	Hyg	spe
YM135	ym123	LH661	Ppt	spe

Note: kan represents 50 μg/ml kanamycin for agrobacterium and colony selection. Spe represents 50 μg/ml spectinomycin for colony selection. Amp represents 100 μg/ml Ampicillin for colony selection. Ppt represents 20 mg/l phosphinothricin for agrobacterium selection. Hyg represents 50 μg/mL hygromycin for agrobacterium selection.

Appendix 4: Script for analysis

Script 1. Chi-square test using R

```
library(openxlsx)
usedata <- read.xlsx("FILE-NAME.xlsx", sheet = 1, rowNames = TRUE) # input data
X2="(-)"
p.value="(-)"
for (i in 2:6) {

  usedata1 <- rbind(usedata[1,], usedata[i,])

  usedatachisq1 <- chisq.test(usedata1)
  X2 <- c(X2, round(usedatachisq1$statistic, 2))
  p.value <- c(p.value, round(usedatachisq1$p.value, 2))
} # cycle to do Chi-square test
usedata2 <- cbind(usedata,X2,p.value) #add usedata to usedata2
write.xlsx(usedata2, "OUTPUT-NAME.xlsx", rowNames = TRUE, colNames = TRUE) #overwrite
the excel file. will delet other sheet.
```

Script 2. Generating bar plot with alluvial plot using R

```
install.packages("ggplot2")
install.packages("ggalluvial")
install.packages("alluvial")
install.packages("ggpubr")
install.packages("reshape2")
library(ggplot2)
library(ggalluvial)
library(alluvia)
control+shift+H #change direction to excel.
library(openxlsx)
usedata <- read.xlsx("BiFC.xlsx", sheet = 1, rowNames = TRUE) # input data
reshape2::melt(usedata,id.vars="group") -> usedata2 # formating the data that can be used
for ggplot2
ggplot(usedata2,aes(x = group, y = value, fill = variable, alluvium = variable)) +
 geom_alluvium(aes(fill = variable, colour = variable), alpha = 0.5) +
 geom_bar(stat = "identity", aes(fill = variable), width = 3/5) +
 theme_classic() +
 theme(axis.text.x = element_text(angle = 45,
                          vjust = 1,hjust = 1)) +
 theme(legend.title = element_blank(),
     axis.ticks.x = element_blank()) +
 scale_y_continuous(expand = c(0,0)) +
 labs(x=" ",y="percentage")
```

Script 3. Generating line plot using R.

```
library(ggplot2)
library(openxlsx)
usedata <- read.xlsx("test.xlsx", sheet = 1)

p <- ggplot(data = usedata) +
 geom_line(aes(x = Distance1, y = DN.actin.DAPI), size = 1, color = "red") +
 geom_line(aes(x = Distance1, y = ratio1 * 20), size = 1, color = "green") +
 theme(axis.text = element_text (size = 18)) +
 theme(axis.title.x = element_text(vjust = 2, size = 22)) +
 theme(axis.title.y = element_text(vjust = 2, size = 22)) +
 labs(
  x = "Distance µm",              # Set the x-axis title here
  y = "DAPI intensity"   # Set the y-axis title here
 ) +
 scale_y_continuous(
  sec.axis = sec_axis(~ . / 20, name = "Actin/DAPI signal"),
  expand = expansion(mult = c(0, 0))
 ) +
 theme(
  panel.background = element_rect(fill = "transparent",
                                  color = "gray")
```

11 Curriculum Vitae

Yingrui Ma

ORCHID: 0000-0002-2287-5321

Education

- Ph.D Biology (Dr.rer.nat) 07.2021-present

  Leibniz Institute of Plant Genetics and Crop Plant Research (IPK)
  PhD thesis: Dissecting the mechanism of organelle band organization during male meiotic cell cycle in *Arabidopsis thaliana*

- MSc Biotechnology 09.2017-08.2018

  University of Edinburgh, School of Biological Science

  Graduated with merit.

  Graduation thesis: Fission yeast *Bub1* recruit *Mad3* protein via TPR dimerization in spindle assembly checkpoint

- Visiting Student 09.2016-03.2017

  University of Edinburgh, School of Biological Science

- BSc Biotechnology 09.2013-07.2017

  Ningbo University, School of Marine Science

  Graduated at the average score of 84.5/100

  Graduation thesis: Induced Expression and Bioinformatic Analysis of Geranyl Pyrophosphate Synthase Gene (GPS) in *Dunaliella viridis*

Publication

Piskorz EW, Xu L, Ma Y, Jiang H. Doubled-haploid induction generates extensive differential DNA methylation in Arabidopsis. J Exp Bot. 2023;74(3):835-847. Http://doi:10.1093/jxb/erac397

Yi, J., Kradolfer, D., Brownfield, L., Ma, Y., Piskorz, E., Köhler, C., & Jiang, H. (2023). Meiocyte size is a determining factor for unreduced gamete formation in Arabidopsis thaliana. The New phytologist, 237(4), 1179–1187. https://doi.org/10.1111/nph.18473

Leontiou, I., London, N., May, K. M., Ma, Y., Grzesiak, L., Medina-Pritchard, B., Amin, P., Jeyaprakash, A. A., Biggins, S., & Hardwick, K. G. (2019). The Bub1-TPR Domain Interacts Directly with Mad3 to Generate Robust Spindle Checkpoint Arrest. Current Biology : CB,29(14), 2407–2414.e7. https://doi.org/10.1016/j.cub.2019.06.011

MA Yingrui, GONG Yifu, ZHOU Jing, LIU Hao, ZHU Shuaiqi, WANG Heyu. Induced Expression and Bioinformatic Analysis of Geranyl Pyrophosphate Synthase Gene (GPS) in *Dunaliella viridis*. Journal of Nuclear Agricultural Sciences, 2017, 31(2): 248-254. https://doi.org/10.11869/j.issn.100-8551.2017.02.0248

Articles related with my PhD thesis are in preparation.

Experience

- Biomedical Lab, National University of Singapore 09.2019-06.2020

  Research Assistant

  Lab skills: DNA cloning, Plasmid construction and transformation, Yeast cell culture, Yeast mating and spore tetra-dissecting, Chromosome immunoprecipitation, fluorescence Microscopy.

  Admin experience: Organized weekly lab safety meeting; Monitoring the expense of lab funding and on charge of lab purchasing; Training new lab members based on the University safety training material; Generating and recording lab documents like experiment risk assessment and technique manual sheet.

- Unilever R&D Department (Shanghai) 10.2018-08.2019

  Personal and home care consumer insight and claim specialist
  Work experience: Conducted consumer and clinical test for personal and home care new products.

- Wellcome Trust Cell Biology Research Centre, Edinburgh 03.2018-08.2018

  Laboratory student

  Research experience: Studied Fission Yeast spindle checkpoint protein assembly mechanism. Employed in vitro protein expression system and physical methods to understand the interaction model of two important checkpoint activation protein.

  Publication: “The Bub1-TPR Domain Interacts Directly with Mad3 to Generate Robust Spindle Checkpoint Arrest” PMID: 31257143

12 Eidesstattliche Erklärung/Declaration under Oath

Ich erkläre an Eides statt, dass ich die Arbeit selbstständig und ohne fremde Hilfe verfasst, keine anderen als die von mir angegebenen Quellen und Hilfsmittel benutzt und die den benutzten Werken wörtlich oder inhaltlich entnommenen Stellen als solche kenntlich gemacht habe.

I declare under penalty of perjury that this thesis is my own work entirely and has been written without any help from other people. I used only the sources mentioned and included all the citations correctly both in word or content.

_____ _____

Datum / Date Unterschrift des Antragstellers /
Signature of the applicant

13 Erklärung über bestehende Vorstrafen und anhängige Ermittlungsverfahren/Declaration concerning Criminal Record and Pending Investigations

Hiermit erkläre ich, dass ich weder vorbestraft bin noch dass gegen mich Ermittlungsverfahren anhängig sind. / *I hereby declare that I have no criminal record and that no preliminary investigations are pending against me.*

_____ _____

Datum / Date

Unterschrift des Antragstellers / *Signature of the applicant*